Spray drying for the preparation of innovative nanocoatings and inhalable nanocarriers

Dissertation

zur

Erlangung des Doktorgrades

der Naturwissenschaften

(Dr.rer.nat.)

dem

Fachbereich Pharmazie der

Philipps-Universität Marburg

vorgelegt von

Elias Baghdan

aus **Damaskus, Syrien**

Marburg/Lahn **2018**

Erstgutachter: **Prof. Dr. Udo Bakowsky**

Zweitgutachter: **Prof. Dr. Frank Runkel**

Eingereicht am **01.10.2018**

Tag der mündlichen Prüfung am **12.11.2018**

Hochschulkennziffer: 1180

E I D E S S T A T T L I C H E E R K L Ä R U N G

Ich versichere, dass ich meine Dissertation

„**Spray drying for the preparation of innovative nanocoatings and inhalable nanocarriers**“

selbständig ohne unerlaubte Hilfe angefertigt und mich dabei keiner anderen als der von mir ausdrücklich bezeichneten Quellen bedient habe. Alle vollständig oder sinngemäß übernommenen Zitate sind als solche gekennzeichnet.

Die Dissertation wurde in der jetzigen oder einer ähnlichen Form noch bei keiner anderen Hochschule eingereicht und hat noch keinen sonstigen Prüfungszwecken gedient.

Marburg, den 01.10.2018

.....

Elias Baghdan

Die vorliegende Arbeit entstand auf Anregung und unter Leitung von

Herrn Prof. Dr. Udo Bakowsky

am Institut für Pharmazeutische Technologie und Biopharmazie
der Philipps-Universität Marburg

TABLE OF CONTENTS

Chapter I: Introduction 1

1.1 Background 2
1.2 Spray drying parameters 3
1.3 Characterizing spray dried particles 4
1.4 Applications of spray drying 6
1.4.1 Pulmonary applications 6
1.4.2 Nano-in-Microparticles (NiMps) 7
1.4.2.1 Preparation of NiMps 7
1.4.2.2 Characterization of NiMps 8
1.4.3 Nano spray drying 11
1.5 Aims and scope 14

Chapter II: Materials and methods 15

2.1 Materials 16
2.1.1 List of materials and devices 16
2.1.2 Solvents 20
2.1.3 Cell culture 21
2.1.3.1 Human lung epithelial carcinoma cells (A549) 21
2.1.3.2 Mouse fibroblasts (L929) 21
2.1.4 Bacterial strains 21
2.2 Methods 22
2.2.1 Nano-in-Microparticles for pulmonary applications 22
2.2.1.1 Preparation of nanoparticles 22
2.2.1.2 Particle size distribution and ζ-potential 23
2.2.1.3 Scanning electron microscopy 23
2.2.1.4 Activated partial thromboplastin time (aPTT) test 23
2.2.1.5 Hemolysis assay 23
2.2.1.6 *In vitro* cytotoxicity and irradiation experiments 24
2.2.1.7 Visualization with confocal laser scanning microscope 24
2.2.1.8 Preparation of Nano-in-Microparticles 25
2.2.1.9 Redispersibility 25
2.2.1.10 Correlative light and electron microscopy 25
2.2.1.11 Aerodynamic properties 26
2.2.1.12 Langmuir film balance 26
2.2.2 Nano spray drying for coating of medical implants 28
2.2.2.1 Preliminary experiments 28
2.2.2.2 Visualization 30
2.2.2.3 Scanning electron microscopy 30
2.2.2.4 Preparation of antibacterial and biocompatible nanocoatings 30
2.2.2.5 Morphology and surface structure 31
2.2.2.6 *In vitro* drug release studies 32
2.2.2.7 Nanocoating degradation 32

2.2.2.8 Amount of drug per cm^2 nanocoating 32
2.2.2.9 Agar diffusion test 32
2.2.2.10 Bacterial viability assay 33
2.2.2.11 *In vitro* biocompatibility 34
2.2.3 Statistical analysis 34

Chapter III: Results and discussion 35
3.1 Nano-in-Microparticles for pulmonary applications 36
3.1.1 Physicochemical properties of the nanoparticles 36
3.1.2 Hemocompatibility 37
3.1.3 Photodynamic activity 38
3.1.4 Physicochemical properties of the Nano-in-Microparticles 42
3.1.5 Aerodynamic properties and lung compatibility 44
3.2 Nano spray drying for coating of medical implants 48
3.2.1 Preliminary experiments 48
3.2.2 Antibacterial and biocompatible nanocoatings 54
3.2.2.1 Morphology and surface properties 54
3.2.2.2 *In vitro* drug release studies 57
3.2.2.3 Nanocoating degradation 60
3.2.2.4 Antibacterial activity 62
3.2.2.5 *In vitro* biocompatibility 66
3.2.3 Coating of coronary stents 69

Chapter IV: Summary and outlook 71
4.1 Summary and outlook 72
4.2 Zusammenfassung und Ausblick 76

Chapter V: Appendix 80
5.1 References 81
5.2 Lists 93
5.2.1 List of abbreviations 93
5.2.2 List of figures 95
5.2.3 List of tables 97
5.3 Research output 98
5.4 Presentations 99
5.4.1 Oral presentations 99
5.4.2 Poster presentations 99
5.5 Awards 99
5.6 Curriculum Vitae 100
5.7 Danksagung 101

CHAPTER I: Introduction

1.1 Background

Spray drying is defined as the conversion of liquid feed into dried particles through spraying the atomized feed into a warmer drying gas [1, 2]. The discovery of spray drying goes back to the late 19th century. Over the years, this technique has been subjected to lots of modifications and improvements. From World War II era until our current time, spray drying gained remarkable capabilities and exhibited wide range of applications utilizing the great research and technology advancements [2].

Spray drying is a single-step technique in which the sprayed product goes through three main stages (i.e. atomization, drying and separation). In the first stage, the liquid feed will be transformed into fine droplets. Different forms of liquid feeds can be sprayed e.g. solutions, emulsions, and suspensions [1, 3]. Atomization devices are available in many types e.g. rotatory atomizers, hydraulic nozzles, pneumatic nozzles and ultrasonic nozzles [2].

Second stage is drying, wherein the sprayed droplets are subjected to a stream of warmer drying gas. Air is typically used as the drying gas. At the end of the drying process, air will be filtered and exit the spray dryer without being reused (open-cycle system). However, when working with explosive solvents or oxygen sensitive substances, an inert drying gas must be used (e.g. nitrogen). In this case, the drying gas will circulate and re-enter the spray dryer after passing through special accessory that will extract the solvents from the gas stream (closed-cycle system) [3, 4].

Sprayed droplets can be mixed with the drying gas using either co-current flow, counter-current flow or a combination of both [2, 4]. Each type has its own advantages and drawbacks. For instance, in case of using counter-current flow, the sprayed product will be more efficiently dried; however, this type is not suitable for thermolabile substances [3].

The final stage is when the dried particles separated from the gas stream and collected in the product container. This stage takes place inside the separation device e.g. the cyclone [2]. The functional principle of the cyclone has been previously described in detail [1].

1.2 Spray drying parameters

One of the spray drying main advantages is the possibility to adjust several process parameters (e.g. inlet temperature, drying gas flow rate and feed rate) to produce dried particles with desirable physicochemical properties depending on the intended application (e.g. morphology, particle size, aerodynamic behavior and residual moisture content) [2-9].

Table 1 Spray drying process parameters. Reproduced from [4] with permission.

Parameter / **Dependence**	**Aspirator rate** ↑	**Air humidity** ↑	**Inlet temperature** ↑	**Spray air flow** ↑	**Feed rate** ↑	**Solvent instead of water**	**Concentration** ↑
Outlet temperature	↑↑ less heat losses based on total inlet of energy	↑ more energy stored in humidity	↑↑↑ direct proportion	↓ more cool air to be heated up	↓↓ more solvent to be evaporated	↑↑↑ less heat of energy of solvent	↑↑ less water to be evaporated
Particle size	-	-	-	↓↓↓ more energy for fluid dispersion	(↑) more fluid to disperse	(↓) less surface tension	↑↑↑ more remaining product
Final humidity of product	↑↑ lower partial pressure of evaporated water	↑↑ higher partial pressure of drying air	↓↓ lower relative humidity in air	-	↑↑ more water leads to higher particle pressure	↓↓↓ no water in feed leads to very dry product	↓ less water evaporated, lower partial pressure
Yield	↑↑ better separation rate in cyclone	(↓) more humidity can lead to sticking product	(↑) eventually dryer product prevent sticking	-	(↓↑) depends on application	↑↑ no hygroscopic behavior leads to easier dying	↑ bigger particles lead to higher separation

An interesting study was previously reported by Paluch et al., wherein they investigated the impact of several parameters like feed concentration and solvent composition on the physicochemical properties of the spray dried microparticles, especially the morphology. Moreover, they introduced a new morphology classification system based on four major criteria, namely shape, surface properties, visual morphology and interior of the particles [8].

The influence of spray drying process parameters on the powder yield was studied by Maury et al. For this reason, they designed a new improved cyclone with enhanced separation efficiency. Their findings emphasized the significant role of the cyclone in obtaining higher powder yield taking into consideration other important process parameters like inlet temperature [10].

Recently, several studies reported the optimization of spray drying parameters based on advanced statistical designs instead of "trial-and-error" method. This new approach will offer systematic development and improvement of spray drying products instead of depending on coincidence and luck [11-15]. For instance, Amaro et al. utilized design of experiments (DOE) to determine the significance level of several process parameters influencing the properties of the produced microparticles. By performing 2^4 full factorial design (i.e. studying four factors at two levels), they aimed to prepare sugar-based respirable formulation with improved characteristics [13].

1.3 Characterizing spray dried particles

Depending on the intended application, various characterization methods have been utilized to investigate the physicochemical properties of spray dried particles. The most common characterization methods that are relevant to this work are summarized in **Table 2**.

Table 2 Literature review of the most common characterizations of spray dried particles.

Properties	**Methods**	**References**
Particle size	Laser diffraction	[8, 11-13, 15-25]
Morphology	Scanning electron microscopy	[8, 11-13, 15, 17-28]
Aerodynamic properties	Glass twin impinger Multi-stage liquid impinger Andersen cascade impactor Next generation impactor	[12, 17] [19, 20] [16, 17, 26] [13, 21, 22, 25]
Flowability	Carr's index and Hausner ratio	[12, 14, 15, 18, 19, 25]
Residual moisture content	Karl Fischer titration Thermogravimetric analysis	[9, 10, 16] [11-15, 19, 21]
Thermal behavior	Differential scanning calorimetry	[8-10, 12, 15, 19, 20, 22, 25, 28]
Amorphous/ crystalline	X-ray powder diffraction	[8, 9, 12, 16, 20, 22, 25, 28]
Specific surface area	Gas adsorption	[8, 13, 18, 22, 27]

1.4 Applications of spray drying

Spray drying has a widespread variety of applications ranging from chemical industry e.g. ceramic materials, detergents and pigments [1] to food industry e.g. flavors and milk products [1, 29] and pharmaceutical applications e.g. improving the bioavailability of drugs with poor aqueous solubility and preparing microparticles with controlled release properties [30, 31]. In the following subchapters, it will be focused on the applications of spray drying dealing with pulmonary drug delivery and nano spray drying.

1.4.1 Pulmonary applications

In the field of drug delivery, spray drying has been utilized to prepare drug carriers capable of delivering various active ingredients to their site of action via several routes of administration [3]. The pulmonary route has gained increasing attention because of the numerous advantages it offers e.g. being non-invasive route, large surface area (~ 100 m^2), rapid onset of action, and lower concentrations of drug-metabolizing enzymes [32-34]. Therefore, pulmonary drug delivery has been used for the treatment of local diseases like asthma, chronic obstructive pulmonary disease, and cystic fibrosis as well as systemic delivery of many therapeutics [35, 36]. However, in order to achieve successful therapy, formulations intended for pulmonary applications must fulfil certain requirements and overcome the biological barriers of the lung e.g. mucociliary clearance, mucus penetration, macrophage uptake and interaction with pulmonary surfactant [33, 37, 38].

In this regard, spray drying has the advantage over other drying techniques in terms of several adjustable process parameters capable of producing dried particles with appropriate physicochemical properties suitable for pulmonary drug delivery [39, 40]. Moreover, parameters related to feed solution (e.g. solvent type and excipients) have been extensively investigated to produce particles with improved properties e.g. better aerosolization and controlled drug release [17, 21, 26, 40]. Amino acids, especially L-leucine, have been commonly used to enhance the dispersibility of inhalable dry powders [19, 41-43].

All of these reasons make spray drying such an efficient technique for the preparation of dry powders intended for pulmonary delivery of various therapeutic agents e.g. antibiotics [20], proteins [44], peptides [45], hormones [46] and nucleic acids [47].

1.4.2 Nano-in-Microparticles (NiMps)

1.4.2.1 Preparation of NiMps

Day after day, inhalable nanoscale drug carriers have been showing promising potentials in the field of pulmonary drug delivery [48, 49]. Among these nanocarriers are, for example, liposomes, solid lipid nanoparticles and polymeric nanoparticles [49-51]. Various strategies have been developed to transform nanocarriers into inhalable formulations that can be administered using dry powder inhalers, metered-dose inhalers, or nebulizers [52-54].

In the last decade, Nano-in-Microparticles (NiMps) emerged as an interesting drug carrier with superior aerodynamic properties and higher deposition in the lungs. NiMps are microparticles consisting of two main components: nanoparticles and a matrix excipient that will serve as a wall material to embed the nanoparticles and stabilize them during the atomization process used to produce a more stable dry powder form [55, 56].

Although spray drying is the most common preparation method of NiMps [55, 57], other atomization techniques e.g. spray freeze drying [54, 58] and supercritical assisted atomization [59] were also reported. Furthermore, ultrasonic atomization and electrospraying are interesting approaches that can also be employed [55].

The first component of NiMps (i.e. nanoparticles) can be produced via various methods e.g. solvent evaporation technique [60], modified solvent displacement technique [61], ionotropic gelation [62] and high pressure homogenization [63].

Biocompatible polymeric nanoparticles have gained increasing interest in this field [54, 57, 59]. For instance, PLGA-based NiMps have been extensively utilized to encapsulate numerous drugs intended for pulmonary applications e.g. rifampicin [64], curcumin [65], sildenafil [60], clarithromycin [66], dexamethasone [67] and siRNA [68].

Grenha et al. developed NiMps by spray drying chitosan nanoparticles with lactose or mannitol as matrix excipients and different nanoparticles:matrix mass ratios were tested. Furthermore, the potential of NiMps for pulmonary delivery of peptides and proteins was investigated using insulin as a model therapeutic protein [62, 69, 70].

Due to it is critical role in stabilizing the nanoparticles, choosing the second component of NiMps (i.e. matrix excipient) is one of the most important parameters in preparing NiMps. Physicochemical properties of the matrix (e.g. crystallinity and water solubility) and nanoparticles:matrix mass ratio will significantly influence the morphology, redispersibility and aerodynamic properties of NiMps [56, 61, 71, 72].

The most frequently used matrix excipients are sugars (e.g. mannitol [68, 72-74], trehalose [71] and lactose [75]), biocompatible polymers (e.g. chitosan [63, 65]), and amino acids (e.g. arginine and L-leucine [64]).

Despite the several advantages of using matrix excipient, previous study reported the preparation of excipient-free PLGA-based NiMps [60]. Using the Nano Spray Dryer B-90, Beck-Broichsitter et al. transformed PLGA nanoparticles into composite particles without adding any additional excipient to the formulation. Interestingly, the produced particles exhibited aerodynamic behavior suitable for pulmonary applications. Moreover, the prepared NiMps have a good redispersibility in aqueous media and were able to disintegrate into the original nanoparticles without significant increase in mean particle size.

It is worthwhile to mention that NiMps have been recently used for other applications beside pulmonary drug delivery. Elbaz et al. prepared NiMps intended for the oral delivery of propolis extract loaded nanoparticles against liver and colon cancer [76]. Different types of propolis loaded nanoparticles were dispersed in chitosan solution and spray dried using Nano Spray Dryer B-90.

1.4.2.2 Characterization of NiMps

Redispersibility

Once NiMps are deposited in the lung, they should rapidly disintegrate and release the original nanoparticles intact and fully functional [56, 72]. Therefore, NiMps should exhibit good redispersibility in lung lining fluid to achieve an effective therapy and evade macrophage clearance [61, 77].

As mentioned previously, type of matrix excipient and nanoparticles:matrix mass ratio have significant impact on the redispersibility of NiMps. Additionally, Wang et al. discussed further important parameters [56]. Several types of nanoparticles and excipients with different properties were investigated. They found that the hydrophilicity of the nanoparticles is directly proportional to the amount of excipient required to stabilize them. They also reported that PLGA-based NiMps prepared with amorphous excipients (e.g. trehalose) exhibited better redispersibility in comparison to those prepared with crystalline excipients (e.g. mannitol).

In most studies, NiMps have been redispersed in aqueous media (e.g. pure water or buffer) sometimes with aid of mechanical forces e.g. shaking or ultrasound. The quality of the redispersed nanoparticles was determined mainly based on particle size and morphology measurements. Usually, no significant change in the physiochemical properties of the

redispersed nanoparticles has been observed. Few studies reported significant increase in the particle size after spray drying. This change; however, was still considered to be in the acceptable ranges [60, 61, 64, 69, 70, 73, 77, 78].

However, most of redispersibility experiments have been performed under conditions that do not take the realistic *in vivo* environment into consideration [71, 72]. To address this issue, Ruge et al. investigated the disintegration behavior of NiMps upon deposition onto model mucus layer under different conditions (i.e. static conditions or agitation). Using fluorescence microscopy, it was found that even when the matrix excipient (i.e. trehalose) was completely dissolved, without sufficient shear forces the nanoparticles did not disintegrate from NiMps and remained in their nanoaggregate form [71]. In another study, Torge et al. evaluated the redispersibility of PLGA-based NiMps by measuring the particle size of the redispersed nanoparticles in a simulated lung fluid using dynamic light scattering (DLS). Furthermore, they performed surface roughness measurements to study the disintegration behavior of NiMps on agarose gel pads thereby imitating lung conditions in terms of relative humidity and temperature. The rate of disintegration and redispersible fraction were directly proportional to the matrix excipient content (i.e. mannitol). This latter played a significant role in stabilizing the nanoparticles and preserving their original properties [72].

Morphology

Morphology and surface structure of NiMps are also important properties that have been investigated to develop more efficient NiMps and offer better understanding of the process parameters and their significance. Scanning electron microscopy (SEM) is the most used method to study the morphology of NiMps and observe their composite structure (**Figure 1**). Usually, DLS measurements are used to support SEM findings and evaluate the intactness of redispersed nanoparticles by observing significant variations in the particle size before and after spray drying [60, 61, 71-73, 79-81].

Fluorescence microscopy has been employed to visualize the detailed structure of NiMps and the distribution of the nanoparticles within the matrix excipient. This is usually performed by labelling the nanoparticles and the matrix excipient with two different fluorophores [62, 67, 72, 82].

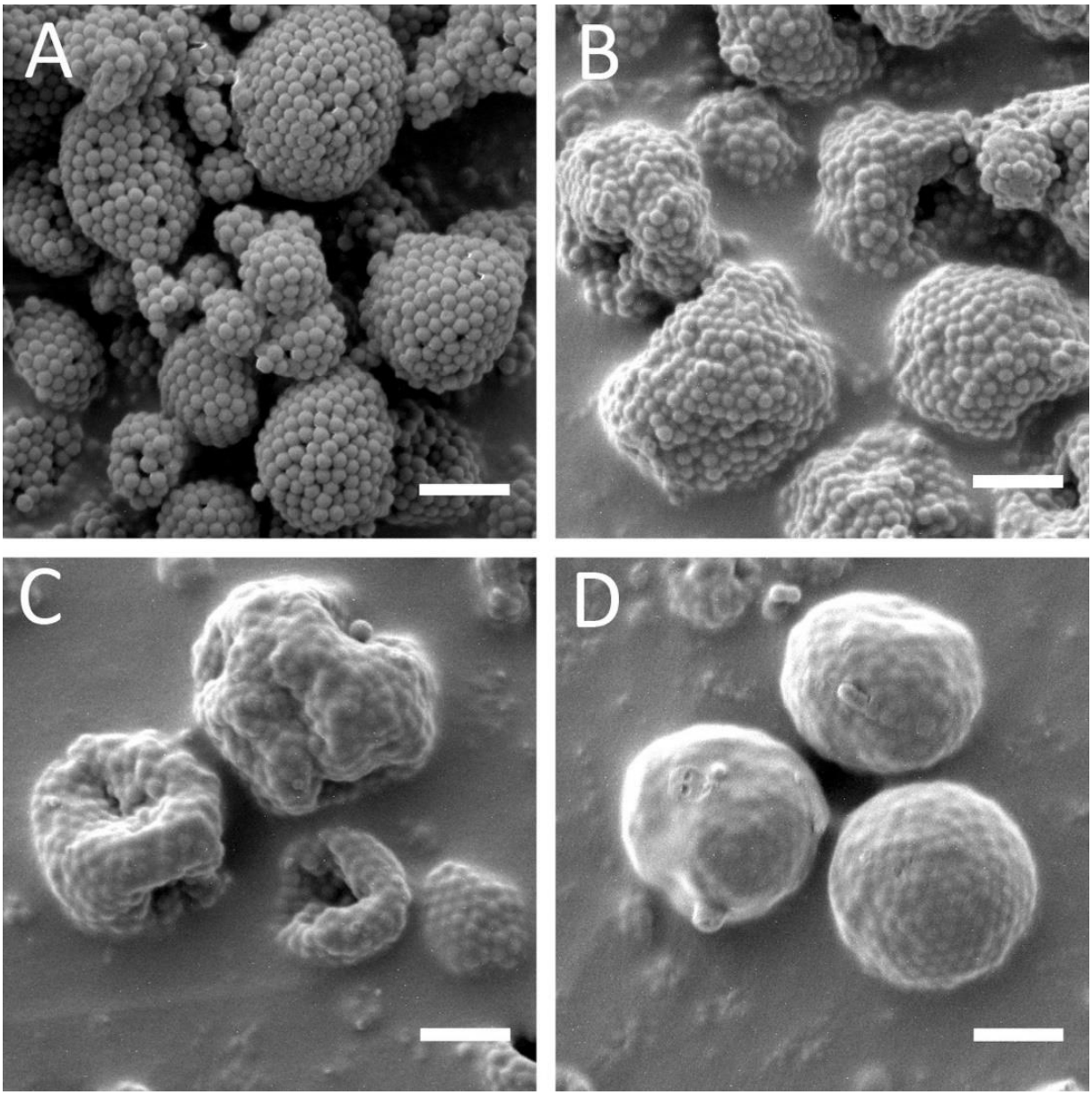

Figure 1 SEM micrographs showing the influence of nanoparticles:matrix mass ratio on the morphology of NiMps which were prepared by spray drying polystyrene nanoparticles with different amounts of trehalose (A: 0%, B: 0.1%, C: 0.2% and D: 0.4%). Scale bars represent 1 µm. Reproduced from [71] with permission.

Recently, correlative light and electron microscopy (CLEM) was developed as a new characterization method that utilizes the benefits of two well-known technologies i.e. SEM and fluorescence microscopy. Thus, offering a detailed morphology and colorful images of the examined sample [83, 84]. However, this method has not been exploited yet as a characterization method to study the morphology of NiMps. Later in this work, this method will be explained in detail pointing out its main advantages.

1.4.3 Nano spray drying

Just a few years ago, nano spray drying technique has emerged. Equipped with several cutting-edge technologies, the Nano Spray Dryer B-90 (**Figure 2**) was introduced by BÜCHI Labortechnik AG paving the way for numerous innovative applications, especially in the field of pulmonary drug delivery and preparation of drug nanocrystals [3, 60, 72, 85-92].

This spray dryer is a laboratory-scale device that has the ability to produce particles in the submicron range due to its unique spray head technology which has a spray mesh that can vibrate at ultrasonic frequency (60 kHz) to generate ultra-fine droplets [85, 88, 93]. These droplets will be dried into solid particles in the drying chamber by a laminar gas flow. Subsequently, the dried particles will get a negative charge and be deflected towards the electrostatic particle collector due to an electric field generated between the star-shaped electrode and the particle collector [86, 88]. Detailed description of the functional principle of the Nano Spray Dryer B-90 is comprehensively described in previous studies [85, 86, 88, 90].

Figure 2 The Nano Spray Dryer B-90 with an illustration showing the functional principle of the spray mesh. Reproduced from [89] with permission.

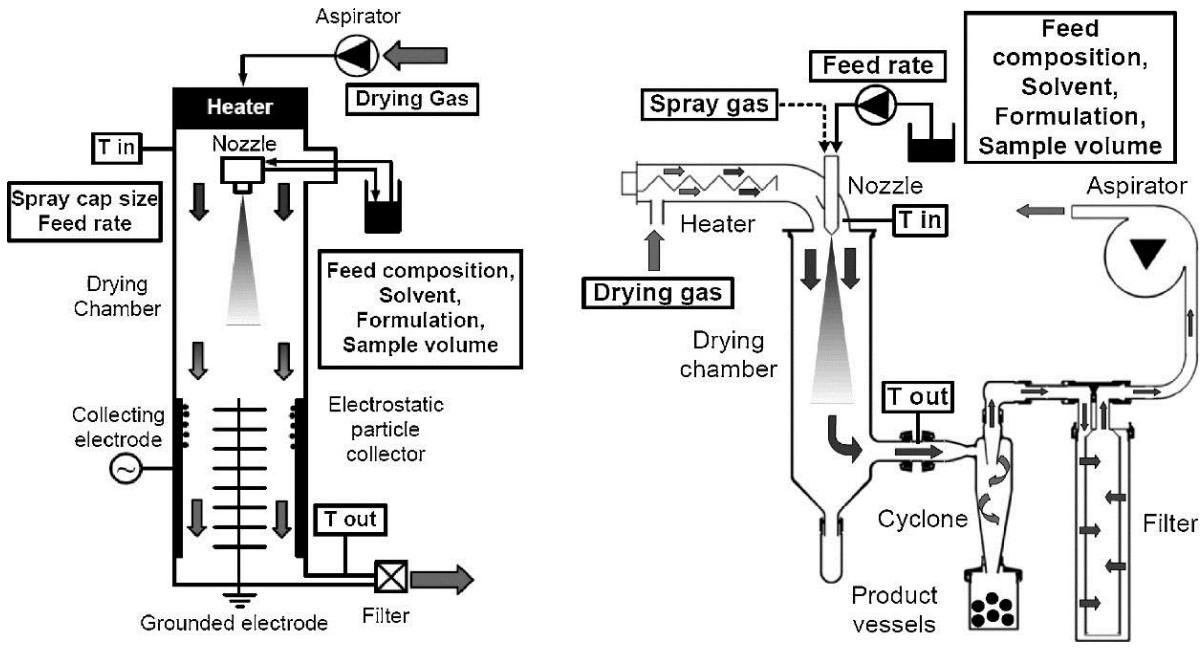

Figure 3 Diagram showing the difference in the functional principle between the Nano Spray Dryer B-90 (left) and the Mini Spray Dryer B-290 (right) from BÜCHI Labortechnik AG. The main process parameters are also presented. Reproduced from [87] with permission.

Table 3 Comparison between the Nano Spray Dryer B-90 and the Mini Spray Dryer B-290 from BÜCHI Labortechnik AG. Reproduced from [94] with permission.

	Nano Spray Dryer B-90	**Mini Spray Dryer B-290**
Main benefit	for small quantities, finest particles, highest yields	for traditional spray drying, established process
Max. inlet temperature	120 °C	220 °C
Water evaporation	max. 0.2 kg/h	1.0 kg/h, higher for solvents
Nozzle type	piezoelectric driven vibrating mesh	two-fluid nozzle
Particle size	300 nm – 5 µm	2 – 25 µm
Particle separation	electrostatic particle collector	cyclone
Typical yield	up to 90%	typically around 60%
Min. sample volume	1 ml	30 ml
Max. sample viscosity	10 cps (diluted samples)	300 cps (viscous samples and juices possible)
Scale-up	limited by spray head and electrical particle collector	possible to scale-up to kg- and tons-scale

Nano spray drying has several advantages over conventional spray drying in terms of ability to produce nanoparticles by generating far smaller droplets with narrower size distribution, gentle drying conditions due to laminar flow of the drying gas, smaller sample quantities are required, and higher powder yields are achievable [3, 85, 86, 88, 90]. However, there are still some limitations associated with nano spray drying that need to be addressed, e.g. upscaling difficulties and inability to spray highly viscous solutions [3, 88, 95].

Recently, an interesting attempt to expand the capabilities of nano spray drying was reported. Beck-Broichsitter et al. introduced a new approach to modify the spray mesh of the Nano Spray Dryer B-90 using polymeric coating. They have succeeded to reduce the size of the generated droplets which lead to the formation of even smaller dried particles with narrower size distribution [96].

1.5 Aims and scope

This work was focused on innovative utilizations of spray drying in two interesting fields.

The first field was pulmonary drug delivery, where the aim was to develop a photosensitizer loaded formulation in the form of a dry powder for inhalation, which together with bronchoscopic photodynamic therapy would offer an effective treatment against lung cancer. The means to accomplish this objective laid within the answers of the following questions:

1. Which photosensitizer should be chosen? Could nanoencapsulation enhance its phototoxic effect against tumor cells? Which nanoparticle preparation method would be suitable?
2. What would be the physicochemical properties of the produced nanoparticles? What about their *in vitro* phototoxicity?
3. Would it be feasible to transform these nanoparticles into an inhalable formulation via spray drying? Which matrix excipient would be appropriate to produce Nano-in-Microparticles with suitable aerodynamic properties?
4. Which characterization method would give a better understanding of the structure of the Nano-in-Microparticles?
5. Would the Nano-in-Microparticles be able to disintegrate into the original nanoparticles upon redispersion? To what extent would they be compatible with pulmonary surfactant?

The second field was coating and surface modification of medical implants, where the key objective was to introduce nano spray drying as a novel coating technique with promising potentials. To achieve this goal, the following questions needed to be answered:

1. Would it be possible to manage particle production and implant coating in a single step?
2. Which process parameters will have a major influence on particle size distribution and surface coverage? Should these parameters first be optimized on a model material?
3. How to implement this coating technique in the surface modification of actual medical implants like dental implants and coronary stents? Would it generate the same results?
4. Could this method be employed in producing biocompatible nanocoatings with potent antibacterial activity? Which characterizations should be carried out to investigate their full potentials and study their characteristics?

CHAPTER II: Materials and methods

2.1 Materials

2.1.1 List of materials and devices

Materials	Source
12-well plates, Nunclon™ Delta	Thermo Fischer Scientific GmbH Dreieich, Germany
24-well plates, Standard, F	Sarstedt AG & Co. KG Nümbrecht, Germany
5 ml glass vials	Schott AG Müllheim, Germany
5 ml screw cap tubes	Sarstedt AG & Co. KG Nümbrecht, Germany
96-well plates, Nunclon™ Delta	Thermo Fischer Scientific GmbH Dreieich, Germany
96-well plates, UV-Star®, half area	Greiner Bio One International GmbH Frickenhausen, Germany
A549 cells	ATCC® Manassas, USA
Alveofact®	Lyomark Pharma GmbH Oberhaching, Germany
Antibiotic/antimycotic solution	Capricorn Scientific GmbH Ebsdorfergrund, Germany
BD™ Mueller Hinton II agar plates	BD GmbH Heidelberg, Germany
Centrifuge, 5418	Eppendorf AG Hamburg, Germany
Clear disposable folded capillary cell, DTS1060	Malvern Panalytical GmbH Herrenberg, Germany
CLSM, LSM 700	Carl Zeiss Microscopy GmbH Jena, Germany

CLSM, LSM 710 NLO	Carl Zeiss Microscopy GmbH Jena, Germany
CO_2 incubator, In-VitroCell ES NU-5841E	NuAire, Inc. Plymouth, MN, USA
Coagulation analyzer, Coatron® M1	Teco Gmbh Neufahrn, Germany
Conductive adhesive carbon tabs	Agar Scientific Ltd Stansted, United Kingdom
Coronary stent, Camouflage® coronary stent system	eucatech AG Rheinfelden, Germany
Coumarin 6, laser grade, 98%	Acros Organics Geel, Belgium
Cover slips, Ø 15 mm	Gerhard Menzel B.V. & Co. KG Braunschweig, Germany
Critical flow controller, TPK	Copley Scientific AG Therwil, Switzerland
Curcumin, ≥ 80%	Sigma-Aldrich Chemie GmbH Taufkirchen, Germany
DAPI	Sigma-Aldrich Chemie GmbH Taufkirchen, Germany
Dental implants, AR Fixture, R-Type, Regular	Biotem Co., Ltd South Korea
Digital image acquisition system DISS 5	Point Electronic GmbH Halle, Germany
di-Sodium hydrogen phosphate dehydrate, ≥ 99%	Merck KGaA Darmstadt, Germany
D-Mannitol, ≥ 98%	Sigma-Aldrich Chemie GmbH Taufkirchen, Germany
DMEM	Capricorn Scientific GmbH Ebsdorfergrund, Germany
Dry powder inhaler, Handihaler®	Boehringer Ingelheim Ingelheim, Germany

Escherichia coli DH5α, DSM 6897	DSMZ Braunschweig, Germany
Fetal bovine serum	Sigma-Aldrich Chemie GmbH Taufkirchen, Germany
Film balance, teflon trough	Riegler & Kirstein GmbH Potsdam, Germany
Flow meter, DFM 2000	Copley Scientific AG Therwil, Switzerland
Fluorescence light source, U-HGLGPS	Olympus Deutschland GmbH Hamburg, Germany
FluorSave™ reagent	Calbiochem Corp San Diego, California, USA
GIBCO® Trypan blue stain 0.4%	Life Technologies, Inc. Grand Island, New York, USA
High capacity pump, HCP5	Copley Scientific AG Therwil, Switzerland
Inert Loop B-295	BÜCHI Labortechnik AG Flawil, Switzerland
Inverted microscope, CKX53	Olympus Deutschland GmbH Hamburg, Germany
L929 cells	ATCC® Manassas, USA
Low power LED irradiating device, prototype	Lumundus GmbH Eisenach, Germany
Magnetic stirrer, IKA RT 15	IKA Werke GmbH & Co. KG Staufen, Germany
MHB	Sigma-Aldrich Chemie GmbH Taufkirchen, Germany
Microplate reader, FLUOstar® OPTIMA	BMG Labtech Ortenberg, Germany
Microplate spectrophotometer, Multiskan™ GO	Thermo Fisher Scientific Waltham, Massachusetts, USA

Mini Spray Dryer B-290	BÜCHI Labortechnik AG Flawil, Switzerland
MTT dye	Sigma-Aldrich Chemie GmbH Taufkirchen, Germany
Nano Spray Dryer B-90	BÜCHI Labortechnik AG Flawil, Switzerland
NGI	Copley Scientific AG Therwil, Switzerland
Norfloxacin, ≥ 98%	Sigma-Aldrich Chemie GmbH Taufkirchen, Germany
Orbital shaker, Compact Shaker KS 15 A	Edmund Bühler GmbH Bodelshausen, Germany
Orbital shaker, KS4000 IC	IKA Werke GmbH & Co. KG Staufen, Germany
PLGA, Resomer® RG 503 H	Evonik Nutrition & Care GmbH Essen, Germany
Polyethylene capsules, size 3	RPC Formatec Mellrichstadt, Germany
Potassium chloride, ≥ 99.5%	Merck KGaA Darmstadt, Germany
Potassium dihydrogen phosphate, ≥ 99.5%	Merck KGaA Darmstadt, Germany
PVA, Mowiol® 4-88	Kuraray Europe GmbH Frankfurt, Germany
Rhodamine B, for fluorescence	Sigma-Aldrich Chemie GmbH Taufkirchen, Germany
Rotary-Pumped Sputter Coater, Q150R ES	Quorum Technologies Ltd East Grinstead, UK
Roti®-Histofix 4%, phosphate-buffered formaldehyde solution 4%	Carl Roth GmbH + Co. KG Karlsruhe, Germany
SEM, EVO HD15	Carl Zeiss Microscopy GmbH Jena, Germany

SEM, Hitachi S-510	Hitachi High-Technologies Europe GmbH Krefeld, Germany
Sodium acetate, ≥ 98.5%	Carl Roth GmbH + Co. KG Karlsruhe, Germany
Sodium chloride, > 99.8%	Carl Roth GmbH + Co. KG Karlsruhe, Germany
Sputter coater, Edwards S150	Edwards Vacuum Crawley, UK
Sputter coater, Gatan Alto 2500	Gatan GmbH München, Germany
Stereomicroscope, Stemi 2000-C	Carl Zeiss Microscopy GmbH Jena, Germany
Superspeed Centrifuge, Sorvall RC6 Plus™	Thermo Fisher Scientific Waltham, Massachusetts, USA
TEClot aPTT-S Kit	Teco GmbH Neufahrn, Germany
Titanium foil, 0.25 mm thick, annealed	Alfa Aesar Karlsruhe, Germany
Trypsin-EDTA, (0.5%) in DPBS (10x)	Capricorn Scientific GmbH Ebsdorfergrund, Germany
Ultra-pure chitosan chloride, Protasan™ UP CL 113	FMC BioPolymer AS Sandvika, Norway
Ultrasound bath, Elmasonic P	Elma Schmidbauer GmbH Singen, Germany
Zetasizer Nano ZS	Malvern Panalytical GmbH Herrenberg, Germany

2.1.2 Solvents

All solvents were of analytical or HPLC grade and were used as received. Ultrapure water from PURELAB® flex 4 equipped with a Point-of-Use biofilter (ELGA LabWater, UK) was used for all experiments.

2.1.3 Cell culture

All cell lines were purchased from American Type Culture Collection (ATCC®). The cells were cultivated in monolayers and passaged upon reaching 80% confluency.

2.1.3.1 Human lung epithelial carcinoma cells (A549)

A549 cells were maintained at 37 ºC and 5 % CO_2 under humid conditions and were cultured in DMEM medium supplemented with 10% fetal bovine serum.

2.1.3.2 Mouse fibroblasts (L929)

L929 cells were maintained at 37 ºC and 8.5% CO_2 under humid conditions and were cultured in DMEM medium supplemented with 10% fetal bovine serum and 10 µl/ml antibiotic/antimycotic solution (amphotericin B, penicillin and streptomycin).

2.1.4 Bacterial strains

Escherichia coli DH5α (DSM 6897, DSMZ) were cultured in MHB and stored at -80 °C. One day prior to the bacterial experiments, the bacteria were thawed and then incubated overnight at 37°C under gentle shaking (100 rpm) using an orbital shaker (Compact Shaker KS 15 A, Edmund Bühler GmbH).

2.2 Methods

2.2.1 Nano-in-Microparticles for pulmonary applications

2.2.1.1 Preparation of nanoparticles

Curcumin loaded PLGA nanoparticles (PLGA.CUR.NPs) were prepared according to the nanoprecipitation method with slight modifications [97]. Briefly, 200 mg PLGA and 5 mg curcumin were dissolved in 10 ml acetone (organic phase). A beaker filled with a 40 ml of 0.5% PVA solution (aqueous phase) was placed on a magnetic stirrer (IKA RT 15, IKA Werke) at medium stirring speed (400 rpm). The organic phase was injected into the aqueous phase and the mixture was left stirring under light-protected conditions until complete evaporation of acetone. Afterwards, the final volume was adjusted to 50 ml using water and the nanoparticles were stored at 4 °C until further characterization. Unloaded nanoparticles (PLGA.NPs) were also prepared following the same procedure except that the organic phase consisted only of PLGA. Scheme of nanoparticles preparation is illustrated in **Figure 4**. To determine the amount of free curcumin, freshly prepared nanoparticles were centrifuged at 2,000 g for 2 min (Centrifuge 5418, Eppendorf AG). The supernatant was carefully collected and the resulting pellet which contained the large free curcumin crystals was completely dissolved in ethanol. The amount of free curcumin was then quantified using a microplate spectrophotometer (Multiskan™ GO, Thermo Scientific) by measuring the absorbance at λ = 420 nm.

Encapsulation efficiency (EE%) was calculated according to the following equation:

$$\text{EE\%} = \frac{\text{Total amount of curcumin} - \text{Amount of free curcumin (mg)}}{\text{Total amount of curcumin (mg)}} * 100$$

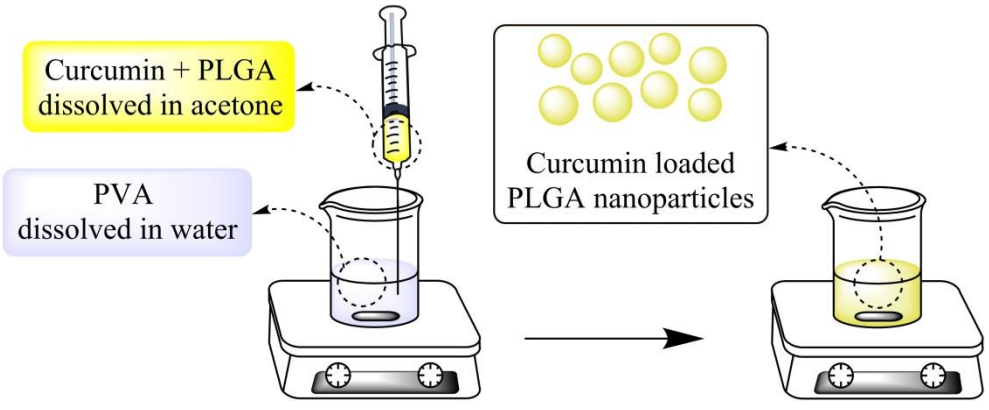

Figure 4 Scheme of preparation of curcumin loaded PLGA nanoparticles according to the nanoprecipitation method.

2.2.1.2 Particle size distribution and ζ-potential

Dynamic light scattering (DLS) and laser Doppler velocimetry (LDV) were performed using Zetasizer Nano ZS (Malvern Panalytical GmbH) to determine the particle size and ζ-potential respectively. The samples were diluted 1:100 with phosphate-buffered saline (PBS, pH 7.4) and then placed in a clear disposable folded capillary cell (DTS1060, Malvern Panalytical GmbH). Prior to measurements, temperature of the samples was equilibrated to 25 °C. This instrument is equipped with Non-Invasive BackScatter (NIBS) technology that uses a detection angle of 173°. Measurement duration and number of sub-runs were automatically adjusted by the instrument [98].

2.2.1.3 Scanning electron microscopy

The morphology and particle size of the nanoparticles were investigated using scanning electron microscopy (SEM). The sample was pipetted onto a silica wafer and left to dry. Afterwards, the sample was sputtered with gold at a current of 20 mA for 50 s (Q150R ES, Quorum Technologies Ltd). The sample holder was then placed in the SEM (EVO HD15, Carl Zeiss Microscopy GmbH) and images were taken with an acceleration voltage of 5 kV and a secondary electron detector. Particle size analysis of the SEM micrographs was performed by measuring the diameter of a representative number of particles (n = 250) using ImageJ software (version 1.47, National Institutes of Health).

2.2.1.4 Activated partial thromboplastin time (aPTT) test

aPTT test was performed to determine the effect of the nanoparticles on blood coagulation. Fresh blood was drawn into citrate tubes followed by centrifugation at 1500 *g* for 10 min to separate the plasma fraction. The aPTT test was performed in a Coatron M1 coagulation analyzer (Teco Gmbh) using the TEClot aPTT-S Kit as per the manufacturer's protocol with slight modifications [99]. Briefly, 25 µl of plasma was mixed with 25 µl of either PLGA.NPs or PLGA.CUR.NPs. 25 µl of aPTT reagent was added to the mixture to activate coagulation factors followed by the addition of prewarmed 0.025 M calcium chloride. Coagulation was confirmed spectrophotometrically, and the time was recorded in seconds.

2.2.1.5 Hemolysis assay

To investigate the hemolytic potential of the nanoparticles, human erythrocytes were isolated from fresh blood as described previously [100]. Briefly, fresh blood was drawn into tubes containing EDTA followed by centrifugation of the whole blood. The obtained red blood cell pellet was washed thrice with PBS (pH 7.4) and diluted (1:50) with PBS. The erythrocytes

were incubated together with the nanoparticles for 1 h at 37 °C in V-bottom microtiter plates in an orbital shaker (KS4000 IC, IKA Werke GmbH & Co. KG). The plates were then centrifuged, and the absorbance of the collected supernatant was determined at λ = 540 nm using a plate reader (FLUOstar® OPTIMA, BMG Labtech). PBS (pH 7.4) and 1% Triton X-100® were used as controls and the absorbance values of Triton X-100® were considered as 100% hemolysis.

2.2.1.6 *In vitro* cytotoxicity and irradiation experiments

A prototype low power LED device (Lumundus GmbH) was used as light source to irradiate the cells. Detailed device description was previously mentioned elsewhere [101]. A549 cells were seeded onto 96-well plates (Nunclon™ Delta, Thermo Fischer Scientific GmbH) at a seeding density of 10,000 cells/0.35 cm^2 (per well). After 24 h, the cells were incubated for 4 h with several concentrations of PLGA.CUR.NPs (i.e. 1.56 - 100 µM of curcumin) and equivalent volumes of PLGA.NPs. Subsequently, the samples were removed, and fresh medium was added. The cells were irradiated at λ = 457 nm with different radiation fluence levels (i.e. 33.03 and 66.06 J/cm^2) and were incubated overnight for 24 h. Unirradiated microtiter plate (dark) and untreated cells (blank) were used as controls. After the incubation time, the medium was removed, and the cells were incubated for 4 h with fresh medium containing dissolved MTT (1:10, 0.2 mg/ml). The remaining medium was then aspirated and 200 µl of DMSO were added to each well to dissolve the resulting formazan crystals. The absorbance was measured at λ = 570 nm (FLUOstar® OPTIMA). Viability of blank cells was considered as 100%.

2.2.1.7 Visualization with confocal laser scanning microscope

For the visualization experiments, 90,000 cells/3.5 cm^2 (per well) were seeded onto 12-well plates (Nunclon™ Delta, Thermo Fischer Scientific GmbH) containing cover slips (Ø 15 mm). After 24 h, the cells were incubated with PLGA.CUR.NPs containing 100 µM curcumin or an equivalent volume of PLGA.NPs. After 4 h, the supernatant was removed and replaced with fresh medium and the plates were irradiated at a radiation fluence of 33.03 J/cm^2. Unirradiated cells (dark) were used as a control. The cells were then washed with PBS containing Ca^{2+} and Mg^{2+} (pH 7.4) and fixed with 4% formaldehyde solution for 20 min. For counterstaining the cell nucleus, the cells were incubated with DAPI (0.1 µg/ml) for 20 min. Finally, the cells were washed with PBS (pH 7.4) and the cover slips were mounted onto glass slides and sealed using FluorSave™ (Calbiochem Corp, La Jolla, USA).

Subsequently, the cellular uptake of the nanoparticles and their photoresponse were visualized using confocal laser scanning microscope (CLSM) (Zeiss Axio Observer Z1 equipped with an LSM 700 confocal unit, Carl Zeiss Microscopy GmbH). All micrographs were recorded with a similar detector gain and pinhole size.

2.2.1.8 Preparation of Nano-in-Microparticles

The nanoparticles were centrifuged at 13,000 rpm (20,064 *g*) for 60 min at 4 °C (Sorvall RC6 Plus™ Superspeed Centrifuge, Rotor F21-8x50y, Thermo Scientific). The supernatant was carefully collected, and the pellet was redispersed in a solution of mannitol (matrix substance) and rhodamine B (0.1 wt% of mannitol) with a mass ratio of 30:70 (nanoparticles:matrix) and the solid concentration was adjusted to 1% (w/v) with water. Nano-in-Microparticles (NiMps) were prepared by spray drying the mixture of nanoparticles and mannitol using the Min Spray Dryer B-290 (BÜCHI Labortechnik AG) equipped with two-fluid nozzle as previously described [61]. The process parameters were set as follows: inlet temperature 65 °C, aspirator 100%, pump rate 7%, spray gas flow 536 l/h, nozzle cleaner 1, outlet temperature ≤ 41 °C. The spray dried product was collected with high performance cyclone and the yield% was calculated using the following equation:

$$\text{Yield\%} = \frac{\text{Amount of the collected spray dried product (mg)}}{\text{Total amount of constituents used for preparation (mg)}} * 100$$

2.2.1.9 Redispersibility

NiMps should be readily dispersible in aqueous media and disintegrate into the original nanoparticles. Therefore, a specific amount of the spray dried powder was weighed and redispersed in water with a final concentration of 1 mg/ml. The sample was vortexed for 30 s and then placed in an ultrasound bath for 60 s at room temperature. Subsequently, particle size distribution of the redispersed sample was investigated using DLS [71].

2.2.1.10 Correlative light and electron microscopy

Correlative light and electron microscopy (CLEM) is a microscopy technique, based on the combination of electron and light microscopy. The Shuttle & Find setup (Carl Zeiss Microscopy GmbH) offers a modular system of standardized hardware and software for a straightforward relocation of any region of interest (ROI), both in the CLSM (LSM 710 NLO, Carl Zeiss Microscopy GmbH) and SEM (EVO HD15). The general procedure was described earlier [84]. Due to the calibration of the Shuttle & Find specimen holder, each image was

saved with its coordinates allowing relocating the reference point. No additional manipulation of the sample was necessary. The light microscopy was performed first, owing to possible interference between the electron beam and the fluorophores [83]. The microparticles were placed on a high precision coverslip (22x22 mm, 0.17 mm thickness) and loose particles were removed with a stream of air. For the electron microscope, the sample was then sputtered with a gold layer of ~30 nm using a current of 20 mA for 100 s (Q150R ES). Images were taken with an acceleration voltage of 5 kV and a secondary electron detector. The "Shuttle and Find" function in the ZEN 2 (blue edition) software combines both microscope images together into one overlaying image.

2.2.1.11 Aerodynamic properties

Next generation impactor (NGI) (Copley Scientific AG) was used to determine the aerodynamic properties of NiMps. Polyethylene capsule (size 3) was filled with approx. 20 mg of the spray dried powder. Handihaler® (Boehringer Ingelheim) was used as dry powder inhaler. All NGI cups were coated with an anti-bouncing agent (Brij® 35/glycerol). Prior to experiment, the air flow rate was adjusted using flow meter (DFM 2000, Copley Scientific AG), critical flow controller (TPK, Copley Scientific AG) and high capacity pump (HCP5, Copley Scientific AG). To perform the test, one filled capsule was placed in the Handihaler® then punctured. The pump was then turned on and the powder was aerosolized at a flow rate of 60 l/min for 4 s. Afterwards, water was used to rinse the induction port, pre-separator and the cups of the impactor. To calculate mass median aerodynamic diameter (MMAD), geometric standard deviation (GSD) and fine particle fraction (FPF), the amount of particles in each stages was quantified by measuring the fluorescence (λ_{ex} = 540 nm, λ_{em} = 610 nm) using a plate reader (FLUOstar® OPTIMA) [72].

2.2.1.12 Langmuir film balance

Langmuir film balance was utilized as *in vitro* model to investigate the biophysical properties of pulmonary surfactant upon contact with the nanoparticles. Using the naturally-derived pulmonary surfactant; Alveofact®, alveoli specific surface pressures could be generated. The surface pressure (π) is the difference between the surface tension of pure water (γ_0) and the measured surface tension (γ).

$$\pi = \gamma_0 - \gamma$$

Surface pressure measurements in the film balance (Riegler & Kirstein GmbH; Teflon trough 100 ml total volume and total area of 171 cm^2) were performed according to Wilhelmy-

method [102]. Alveofact® was dissolved in cyclohexane to a final concentration of 1 mg/ml. PBS (pH 7.4, filtered through 0.2 μm syringe filter) was used as the subphase (i.e. the aqueous medium on which the monolayer will spread). All experiments were performed at 25°C. 5 min after spreading Alveofact® on the surface, the monolayer was formed. The monolayer was compressed, and the total surface area was reduced to generate two different surface pressures (i.e. 25 mN/m and 42 mN/m). Afterwards, the monolayer was left to stabilize for 15 min. PLGA.CUR.NPs were then injected under the monolayer into the subphase. The π-t (pressure-time) isotherms were recorded by a control unit (Riegler & Kirstein).

2.2.2 Nano spray drying for coating of medical implants

2.2.2.1 Preliminary experiments

Nano Spray Dryer B-90 (BÜCHI Labortechnik AG) was used to produce nanoparticles which will coat the medical implants. In this study, the electrostatic particle collector was utilized in a different approach. The implants were fixed on the electrostatic collector using conductive adhesive carbon tabs (Agar Scientific Ltd). Thus, the implant surface will gain the same charge of the particle collector since they are made of titanium which is a conductive metal. Therefore, the dried particles will deposit also on the implant surface forming a homogenous layer of nanoparticles. The scheme of particle production and coating of the implants is illustrated in **Figure 5**.

To prove the feasibility of this technique, three model substances were tested. The first substance chosen was chitosan which is a semi-synthetic polymer obtained from the deacetylation of the natural polymer chitin. Chitosan has a variety of biomedical applications, e.g. tissue engineering and wound healing [27, 103, 104]. The second model substance was PLGA which is a biodegradable and biocompatible synthetic polymer that has been exploited in the field of drug delivery and controlled release formulations [105-107]. Finally, curcumin was chosen as a model substance for hydrophobic natural compounds. Curcumin has antioxidant and anti-inflammatory activities and has proven its efficacy against cancer and several chronic diseases [101, 108-110].

0.1% solution of each was prepared with the suitable solvent or solvents mixture. For the purpose of visual inspection, 1% rhodamine B and 1% coumarin 6 were added to the solutions of chitosan and PLGA, respectively. Spray cap of 4.0 µm mesh diameter (45° angular position) and tall set-up of the Nano Spray Dryer B-90 were used for all formulations. The combination of Nano Spray Dryer B-90 with the Inert Loop B-295 (BÜCHI Labortechnik AG) enabled operating the device in closed loop mode which allowed the safe use of organic solvents. Oxygen levels were kept below 4%. Spray drying parameters were chosen depending on the properties of the sprayed substance taking into consideration previous studies [111]. A summary of the experimental parameters is presented in **Table 4**.

Preliminary experiments were performed on titanium plates to determine the appropriate amount of sprayed sample and the optimal position of the implant inside the particle collector. The titanium plates (1.5x1.5 cm) were cut from a titanium foil (0.25 mm thick, annealed, 99.5% (metals basis); Alfa Aesar). Prior to use, they were thoroughly cleaned using several solvents with the aid of ultrasound bath (Elmasonic P, Elma Schmidbauer GmbH).

Three different positions were chosen to fix the titanium plates on the particle collector (Top, Middle and Bottom) with approx. 6 cm distance between each of them. Subsequently, the optimized parameters were applied on dental implants (Internal submerged system, AR Fixture, R-Type, Regular Ø 4.0 mm, length: 11.5 mm, Biotem Co., Ltd.) which were placed approx. 12 cm towards the bottom of the particle collector.

Table 4 Summary of spray drying parameters

	Chitosan	**PLGA**	**Curcumin**
Solvent	H_2O	ACN:H_2O (95:5) + 0.005% NaOAc	ACE:ETOH (1:1)
Drying gas	Compressed air	N_2/ CO_2	N_2/ CO_2
Gas flow [l/min]	100	100	100
Spray rate [%]	100	50	50
Inlet temperature [°C]	120	55	75
Outlet temperature [°C]	40 - 46	28 - 34	35 - 41
Feed rate [ml/h]	41.98	54.30	26.39

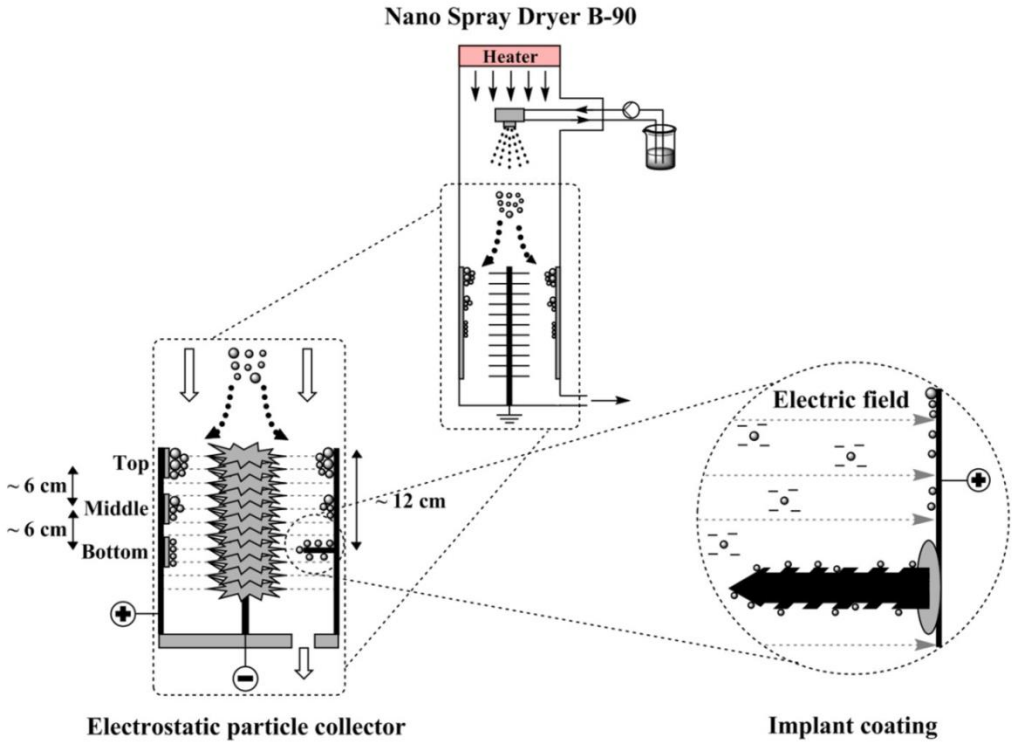

Figure 5 Illustration of the functional principle of the Nano Spray Dryer B-90 and the coating of the implants.

2.2.2.2 Visualization

To confirm the homogenous coating of the dental implants, initial visual inspections of the implants before and after spray drying were performed using a stereomicroscope (Zeiss Stemi 2000-C, Carl Zeiss). Afterwards, CLSM was used to examine the coating uniformity of the implants using an Axio Observer Z1 inverted microscope equipped with an LSM700 confocal unit (Carl Zeiss).

2.2.2.3 Scanning electron microscopy

Morphology and surface structure studies were done using a Hitachi S-510 SEM (Hitachi High-Technologies Europe GmbH). The titanium plates and the dental implants were fixed on aluminum pin stubs. The samples were sputter-coated with a platinum layer (10 mA for 2 min) using a Gatan Alto 2500 sputter coater (Gatan GmbH) and were examined at an accelerating voltage of 5 kV and 30 µA emission current. The micrographs were recorded digitally using DISS 5 digital image acquisition system (Point Electronic GmbH) [112]. Afterwards, particle size distribution was determined by analyzing SEM micrographs using ImageJ software (version 1.51q, National Institutes of Health, USA). Mean particle size was obtained by measuring the diameter of at least 100 particles.

2.2.2.4 Preparation of antibacterial and biocompatible nanocoatings

Small titanium discs (Ti-discs) with definite surface area (1 cm^2) were cut from a titanium foil (0.25 mm thick, annealed, 99.5% (metals basis); Alfa Aesar). Prior to use, the discs were thoroughly cleaned using several solvents with the aid of ultrasound bath (Elmasonic P, Elma Schmidbauer GmbH). Nano Spray Dryer B-90 (BÜCHI Labortechnik AG) was used to produce nanoparticles which will coat the Ti-discs as previously mentioned (**2.2.2.1**). The spay drying parameters were kept constant for all formulations: spray cap of 4.0 µm mesh diameter (45° angular position), gas flow 100 l/min, spray rate 50%, inlet temperature 70 °C. Nano Spray Dryer B-90 was operated in the closed loop mode using nitrogen as drying gas. The feed solution was prepared by dissolving norfloxacin (NFX) and PLGA in a solvent mixture (acetonitrile and water (95:5) containing 0.005% w/v sodium acetate). Three nanocoatings (PLGA 2.5% NFX, PLGA 5% NFX and PLGA 10% NFX) with different theoretical norfloxacin loadings (2.5, 5 and 10% wt. of PLGA) were prepared. Unloaded nanocoatings (PLGA 0% NFX) were also prepared following the aforementioned procedure but without adding norfloxacin. The effect of the disc position on the produced nanocoatings was also investigated. Therefore, three different levels inside the particle collector were

chosen (i.e. Top, Middle and Bottom) with approx. 6 cm distance between each of them. The coating process of the Ti-discs is illustrated in **Figure 6**.

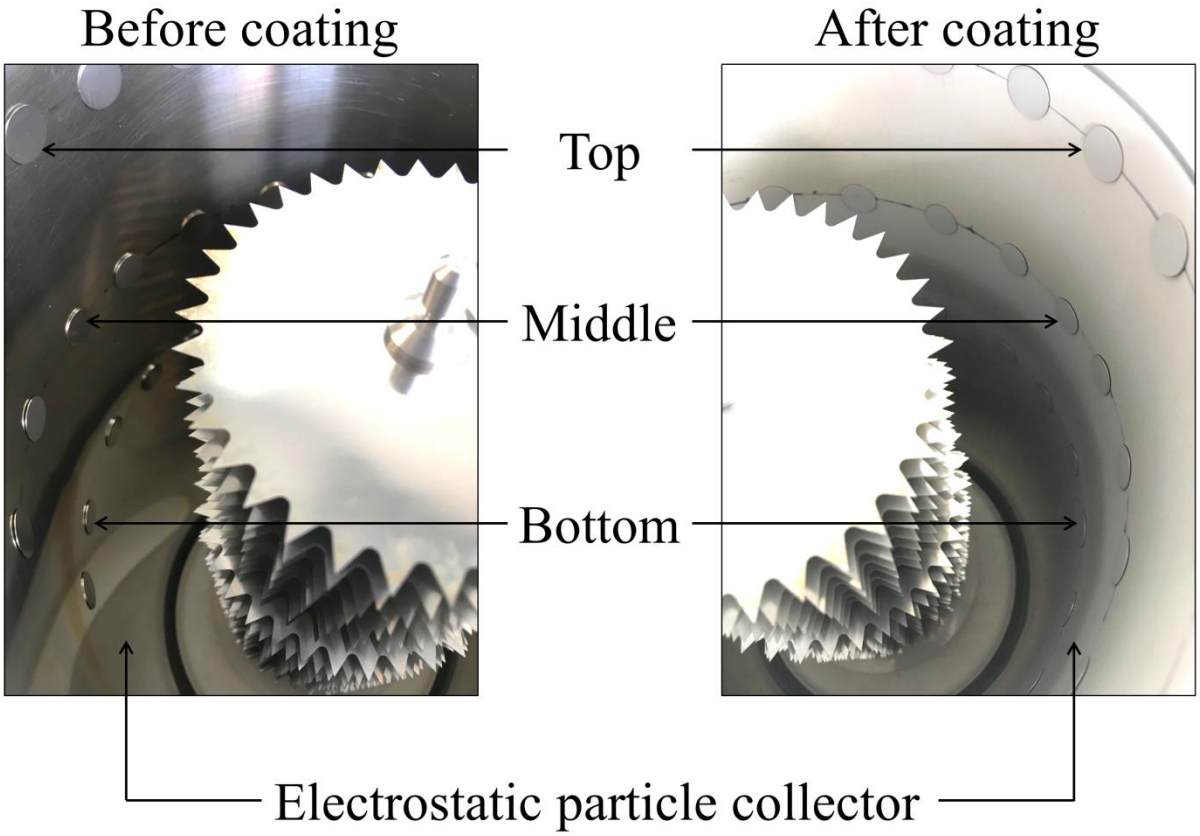

Figure 6 Close-up images from inside the electrostatic particle collector of the Nano Spray Dryer B-90 illustrating the coating process of the titanium discs. The star-shaped electrode can be observed as well as the titanium discs which were placed at three different positions inside the particle collector (i.e. Top, Middle and Bottom).

2.2.2.5 Morphology and surface structure

The Morphology and surface structure of the nanocoatings were studied using SEM (Hitachi S-510, Hitachi-High Technologies Europe GmbH). The Ti-discs were fixed on aluminum pin stubs and sputter-coated with a gold layer (30 mA for 1 min) using Edwards S150 Sputter Coater (Edwards Vacuum). The samples were examined at an accelerating voltage of 5 kV. The micrographs were recorded digitally using DISS 5 digital image acquisition system (Point Electronic GmbH). Afterwards, mean particle size was determined by analyzing SEM micrographs using ImageJ software (version 1.47v, National Institutes of Health).

2.2.2.6 *In vitro* drug release studies

Norfloxacin release studies were performed over a period of 15 days under static conditions. The coated Ti-discs were placed in 5 ml glass vials (Schott AG) filled with 1 ml PBS (filter-sterilized, pH 7.4) at 37 °C under light protection. After specific time intervals, 200 µl samples were withdrawn and replaced with equivalent volumes of fresh PBS. To avoid temperature variations, PBS was also stored at 37 °C under the same conditions. The concentration of norfloxacin was quantified by measuring the absorbance at λ = 270 nm using a microplate spectrophotometer (Multiskan™ GO, Thermo Scientific).

2.2.2.7 Nanocoating degradation

Degradation of nanocoatings under physiological conditions (in terms of pH and temperature) was investigated by placing coated Ti-discs in 5 ml tubes (Sarstedt AG & Co. KG) filled with 1 ml PBS (filter-sterilized, pH 7.4). After 15 days incubation at 37 °C, the discs were carefully taken out and dipped thrice in ultrapure water to remove residual PBS. The Ti-discs were then left to dry at room temperature under a fume hood. Subsequently, the morphology of the nanocoatings were studied using SEM following the same procedure mentioned previously (**2.2.2.5**).

2.2.2.8 Amount of drug per cm^2 nanocoating

The nanocoatings were completely dissolved by placing coated Ti-discs in 24-well plates (Standard, F, Sarstedt AG & Co. KG) filled with 1 ml acetonitrile:0.1 M NaOH (1:1) per well. The 24-well plates were then gently shaken (150 rpm for 60 min) using an orbital shaker (KS4000 IC, IKA Werke GmbH & Co. KG) at room temperature and under light protection. Subsequently, the concentration of norfloxacin was quantified by measuring the absorbance at λ = 274 nm using a microplate spectrophotometer (Multiskan™ GO, Thermo Scientific).

2.2.2.9 Agar diffusion test

The overnight culture of *E. coli* was used to prepare a bacterial culture with an optical density (OD_{600}) of 0.025, which was incubated at 37 °C under gentle shaking (200 rpm) using an orbital shaker (Compact Shaker KS 15 A, Edmund Bühler GmbH). To reduce further growth, the bacteria were cooled in an ice bath after reaching an OD_{600} over 0.400. Subsequently, 100 µl of the bacterial culture were plated on BD™ Mueller Hinton II agar plates (BD GmbH). The Ti-discs were then placed in the center of the agar plates (one disc per agar plate (**Figure 7**)). Afterwards, the agar plates were incubated at 37 °C and ~ 90% RH (In-VitroCell ES NU-5841E, NuAire, Inc.). After 24 h, the antibacterial activity of the

nanocoatings was evaluated by measuring the diameter of the zones of inhibition formed around the Ti-discs [113]. Each sample was analyzed in triplicates.

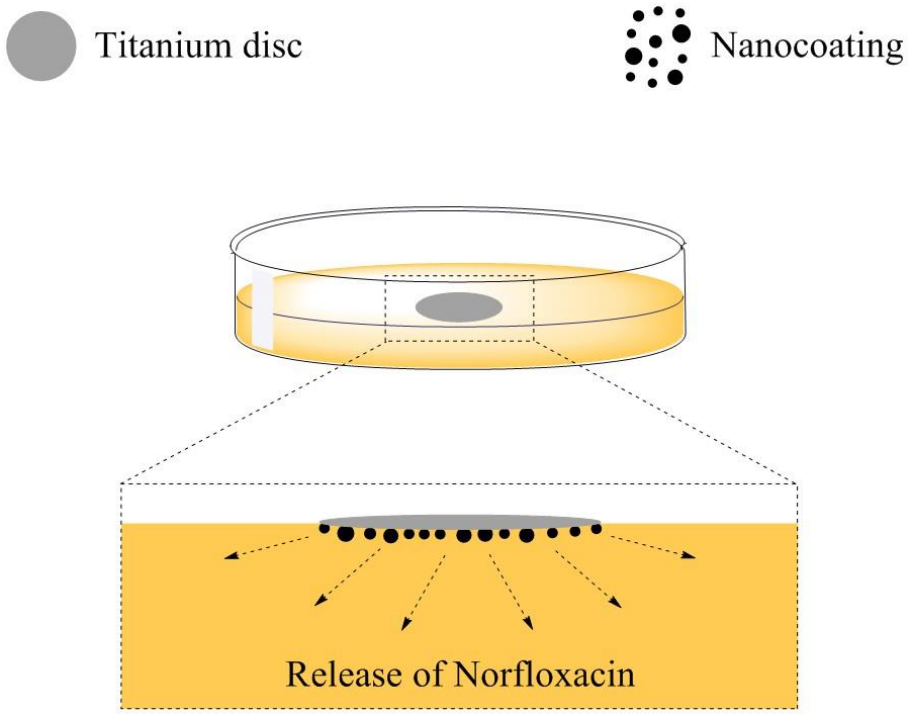

Figure 7 Illustration of the agar diffusion test performed with coated titanium discs and Mueller Hinton agar plates.

2.2.2.10 Bacterial viability assay

Antibacterial activity of the nanocoatings was evaluated according to a procedure mentioned elsewhere with some modifications [114]. The overnight culture of *E. coli* was used to prepare a bacterial culture with an OD_{600} of 0.2. 1 ml of this culture was added to 24-well plates (Standard, F, Sarstedt AG & Co. KG) containing the Ti-discs. The 24-well plates were incubated under static conditions at 37 °C and ~ 90% RH (In-VitroCell ES NU-5841E, NuAire, Inc.). After 24 h, the Ti-discs were taken out and immersed thrice in PBS (filter-sterilized, pH 7.4) to remove non-adherent bacterial cells. The Ti-discs were then transferred into new 24-well plates. To detach the bacteria from the surface of the Ti-discs, 1 ml trypsin-EDTA (5 mg/ml) was added and the samples were gently shaken (100 rpm) at room temperature for 20 min using an orbital shaker (Compact Shaker KS 15 A, Edmund Bühler GmbH). In order to evaluate the bacterial viability (CFU/cm^2), different dilutions (1:10 - 1:1,000,000) of the samples were plated on BD™ Mueller Hinton II agar plates (BD GmbH)

and the colonies were counted after 24 h incubation at 37°C and ~ 90% RH (In-VitroCell ES NU-5841E, NuAire, Inc.). The samples were analyzed in three independent experiments.

2.2.2.11 *In vitro* biocompatibility

L929 cells were seeded onto 12-well plates (Standard, F, Sarstedt AG & Co. KG) containing Ti-discs at a seeding density of $1x10^5$ cells/ 3.65 cm² (per well). After predetermined time intervals (i.e. 24 h and 96 h), the Ti-discs were transferred into new 12-well plates and washed thrice with PBS containing Ca^{2+} and Mg^{2+} (filter-sterilized, pH 7.4), to remove non-adherent cells. For visualizing the cells adhered to the surface of the Ti-discs, the cells were fixed with 4% formaldehyde solution for 20 min after which the cell nucleus was counterstained with DAPI (0.1 µg/ml) for 20 min [99]. Finally, the Ti-discs were mounted onto microscope slides and examined under an inverted microscope (CKX53, Olympus Deutschland GmbH) equipped with light guide-coupled illumination system (U-HGLGPS, Olympus Deutschland GmbH) as fluorescence light source.

Cell counting experiments were performed according to a procedure mentioned elsewhere with some modifications [115]. L929 cells were cultured as mentioned above. After predetermined time intervals (i.e. 24 h and 96 h), the Ti-discs were transferred into 24-well plates (Standard, F, Sarstedt AG & Co. KG) and washed twice with PBS without Ca^{2+} or Mg^{2+} (filter-sterilized, pH 7.4), to remove non-adherent cells. Afterwards, the Ti-discs were incubated with EBSS without Ca^{2+} or Mg^{2+} for 10 min at 37 °C. The cells were detached from the surface of the Ti-discs using trypsin-EDTA (0.05%). After 10 min incubation at 37 °C, DMEM medium (supplemented with 10 % fetal bovine serum) was used to gently wash down the cells from the Ti-discs. Finally, 100 µl of the cell suspension were mixed with trypan blue solution (1:1) and the viable cells were directly quantified by pipetting 10 µl of this mixture into cell counting slide (R1-SLI, Olympus Deutschland GmbH) specially designed for the automated cell counter (Cell Counter model R1, Olympus Deutschland GmbH). Each sample was analyzed in three independent measurements.

2.2.3 Statistical analysis

All measurements were performed in triplicates and the values are presented as mean ± standard deviation, unless otherwise stated. Two-tailed Student's t-test was performed to identify statistical significance differences. Probability values of $p < 0.05$ were considered significant.

CHAPTER III: Results and discussion

3.1 Nano-in-Microparticles for pulmonary applications

3.1.1 Physicochemical properties of the nanoparticles

Photodynamic therapy (PDT) is amongst the most rapidly developing therapeutic strategies against cancer. With its high safety profile and minimally invasive nature, PDT offers several advantages over conventional treatments, which are normally associated with systemic toxicity and undesirable side effects [116, 117]. Bronchoscopic PDT is one of the methods used in the endoluminal treatment of lung cancer. It involves the administration of a photoactive substance (i.e. photosensitizer) followed by illumination of the tumor mass with light of a specific wavelength using a flexible fiberoptic bronchoscope. This technique offers the advantage of selective cytotoxicity towards tumor cells with minimum damage to the surrounding healthy tissues [118].

Nevertheless, many photosensitizers suffer from several limitations and drawbacks related to off-target toxicity, low water solubility or poor bioavailability. Therefore, researchers have been focusing on developing more efficient and selective nanoformulations with controlled release properties [119-121].

In this work, curcumin was chosen as naturally occurring photosensitizer with diverse applications in the field of PDT [122]. Nanoprecipitation method was used to produce curcumin loaded nanoparticles, which is a well-established method for preparing PLGA nanoparticles with a narrow size distribution and controllable particle size [123].

Preliminary experiments were performed to improve the preparation method by optimizing the parameters which had significant effect on particle size, dispersity, and encapsulation efficiency (e.g. concentration of PLGA, concentration of PVA and curcumin loading). DLS and LDV measurements did not indicate any significant effect of curcumin encapsulation on particle size, polydispersity index (PdI) or ζ-potential ($p > 0.05$). Both unloaded and loaded nanoparticles had a similar hydrodynamic diameter with monodisperse size distribution ($PdI \leq 0.1$) and a negative surface charge (**Table 5**).

PLGA nanoparticles have been previously reported to have the ability to efficiently encapsulate curcumin [97]. Spectrophotometric quantification revealed that 2.5% loading of curcumin (%wt of the polymer) is the most appropriate concentration leading to relatively high encapsulation efficiency (**Table 5**). Moreover, when higher curcumin concentrations were used (≥ 5%), a yellowish-orange ring appeared on the inside of the beaker. The width of the formed ring increased proportionately with increasing the concentration of curcumin due

to higher amounts of free curcumin that were precipitating on the beaker while evaporating the solvent.

Table 5 Particle size distribution, ζ-potential and encapsulation efficiency (EE).

Formulation	Z-Average [nm]	PdI	ζ-potential [mV]	EE [%]
PLGA.NPs	176.47 ± 13.74	0.10 ± 0.02	-5.07 ± 0.52	-
PLGA.CUR.NPs	181.20 ± 11.52	0.08 ± 0.02	-4.63 ± 0.13	94.38 ± 0.64

The values are presented as mean ± standard deviation.

SEM micrographs of PLGA.CUR.NPs showed that the nanoparticles were spherical and had a homogenous size distribution with few larger particles which were not detected with DLS (**Figure 12A**). Average particle size was around 160 nm which is slightly smaller than the size obtained from DLS measurements. This difference in particle size can be attributed to sample preparation and measurement principle since DLS measurements are performed while the nanoparticles are still suspended in a dispersant (e.g. water or buffer), whereas in case of SEM, the samples are left to dry first [124].

3.1.2 Hemocompatibility

While being transported to the tumor site, the nanoparticles could come in contact with the cellular and non-cellular components of blood. Therefore, their hemocompatibility must be investigated. Hemolysis assay revealed the influence of nanoparticles on the integrity of erythrocytes. Both unloaded and loaded nanoparticles showed minor hemolytic potential (**Figure 8**). Furthermore, aPTT test was performed to study the interaction of nanoparticles with intrinsic coagulation factors. Upon addition of nanoparticles, an increase by approx. 9 s in the coagulation time was noticed, yet, without serious consequences (**Figure 8**). aPTT values above 70 s are considered to be critical which indicate a spontaneous bleeding [125]. Unloaded and loaded nanoparticles exhibited similar hemocompatibility in both of aPTT test and hemolysis assay with no significant difference between the observed effects ($p > 0.05$). Negative surface charge of PLGA nanoparticles is one of the key factors that granted them good hemocompatibility showing no toxic interactions with blood constituents [126].

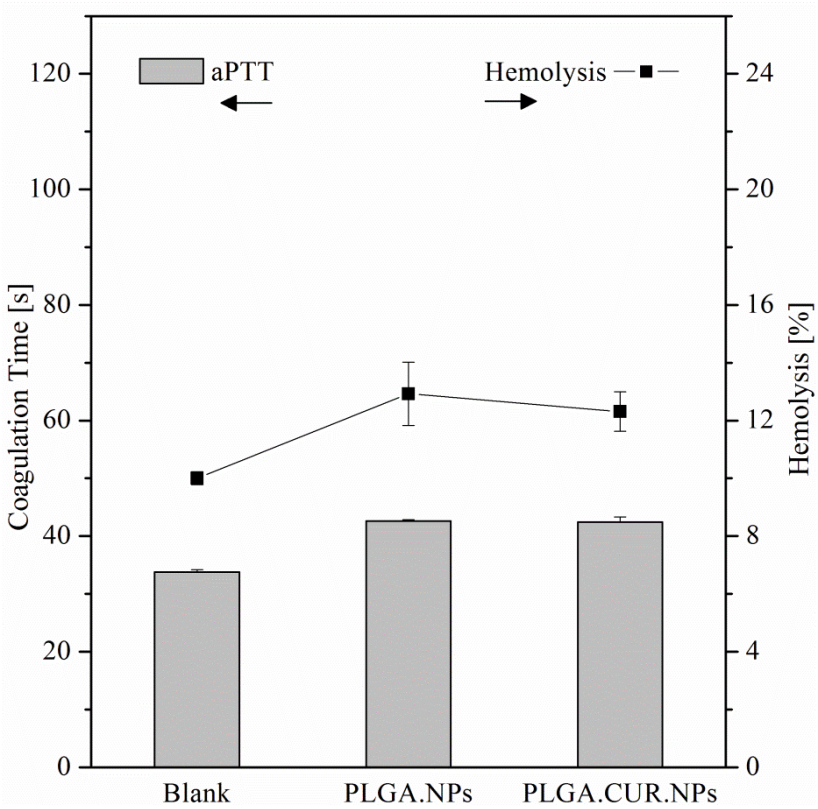

Figure 8 Hemocompatibility experiments of unloaded nanoparticles (PLGA.NPs) and curcumin loaded nanoparticles (PLGA.CUR.NPs). Blank represents untreated erythrocytes in hemolysis assay and blood plasma in aPTT test.

3.1.3 Photodynamic activity

The successful application of curcumin nanoformulations against cancer is well documented [108]. Moreover, the combination of curcumin and PDT is a well-proven strategy offering higher selectivity towards tumor cells and more localized treatment omitting the need of higher doses or longer incubation times [101, 110]. In this study, the photoactivity of the nanoparticles was evaluated by measuring their ability to destroy cancer cells upon exposure to light of a specific wavelength. As seen in **Figure 9**, PLGA.CUR.NPs exhibited minimal cytotoxicity when the cells were not irradiated (dark). Upon irradiation using an LED device, a significant decrease in the cellular viability was observed for both radiation fluence levels. The nanoparticles showed a dose-dependent photocytotoxicity and the effective response was noticed above certain curcumin dose (>12.5 µM). The half-maximal inhibitory concentration (IC_{50}) for curcumin was calculated from the fitted dose-response curves (**Figure 10**). IC_{50} values were 27.38 µM for 33.03 J/cm^2 and 17.14 µM for 66.06 J/cm^2. PLGA.NPs were

used as a control and did not exhibit any significant photocytotoxicity regardless of the dose or the radiation fluence (**Figure 9**).

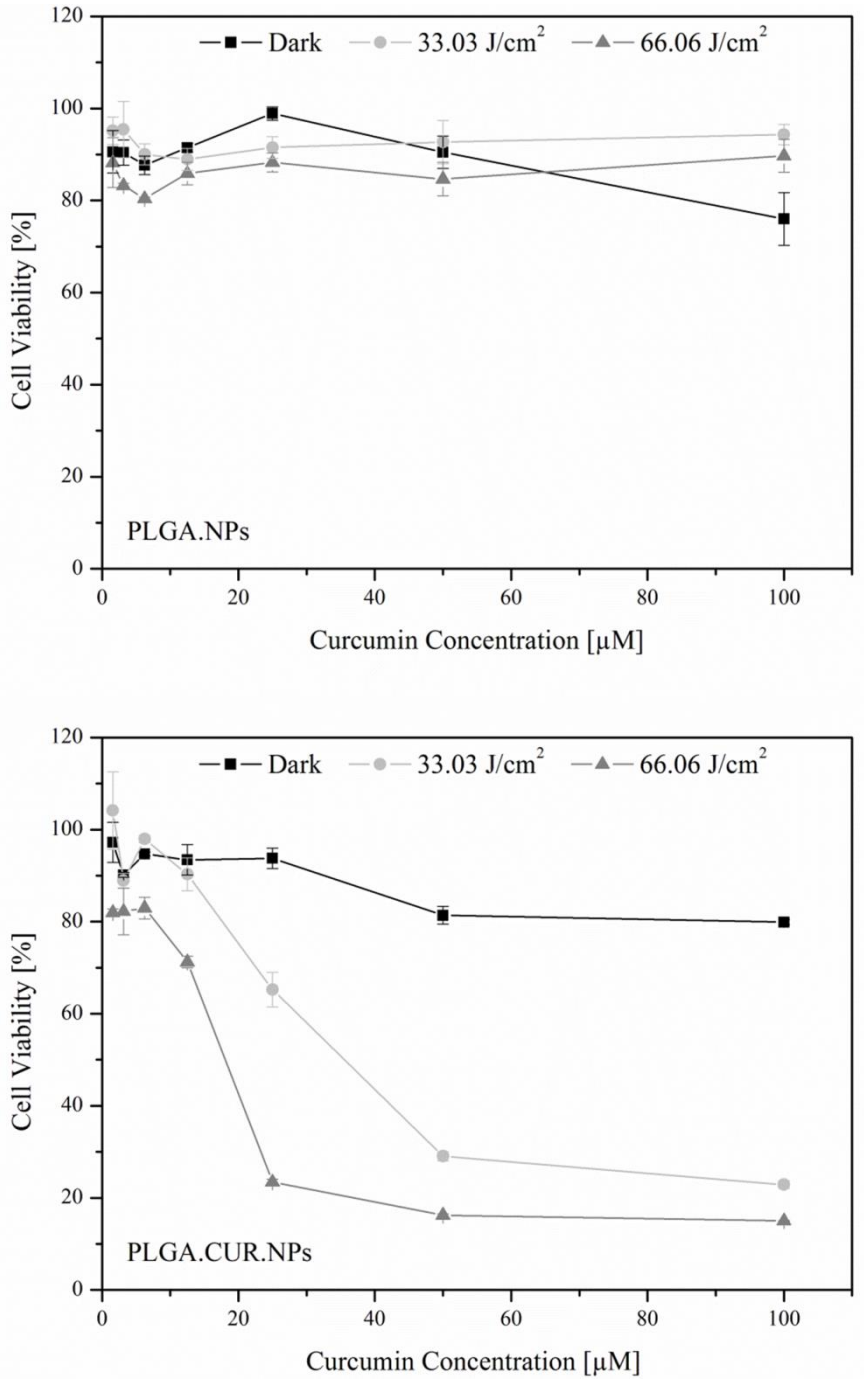

Figure 9 Evaluation of the photocytotoxicity of unloaded nanoparticles (PLGA.NPs) and curcumin loaded nanoparticles (PLGA.CUR.NPs) in A549 cells. Two different radiation fluence levels were tested (i.e. 33.03 and 66.06 J/cm^2) at $\lambda = 457$ nm. Dark represents unirradiated cells. In case of PLGA.NPs, the x-axis values represent the corresponding curcumin concentrations in PLGA.CUR.NPs when equivalent volumes of PLGA.NPs are used.

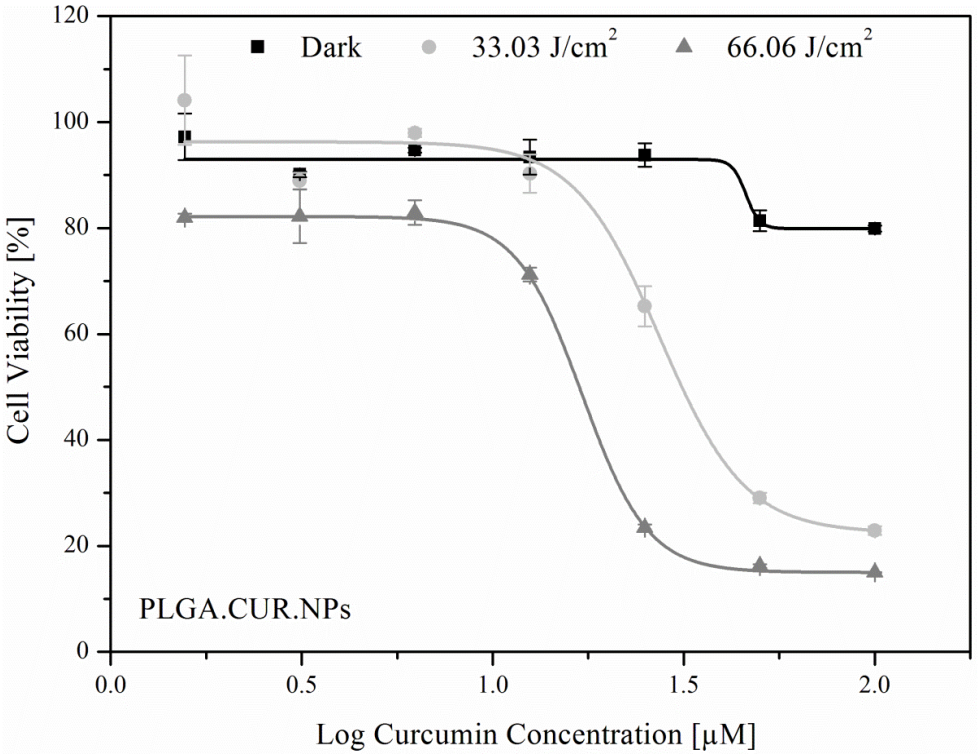

Figure 10 Fitted dose-response photocytotoxicity curves of curcumin loaded nanoparticles (PLGA.CUR.NPs) in A549 cells (**Figure 9**). Two different radiation fluence levels were tested (i.e. 33.03 and 66.06 J/cm^2) at λ = 457 nm. Dark represents unirradiated cells.

A key factor for an effective PDT is the sufficient cellular uptake of the photosensitizer by the target tumor cells [127]. Therefore, CLSM was used to visualize the intracellular localization of curcumin after incubating the nanoparticles with A549 cells for 4 h. High fluorescence intensity was observed confirming the successful uptake of PLGA.CUR.NPs with curcumin mostly localized near the cell nucleus (**Figure 11B**). Upon irradiation, more intensive and distributed fluorescence was observed (**Figure 11D**) in comparison with unirradiated cells indicating further release of curcumin from the nanoparticles [110].

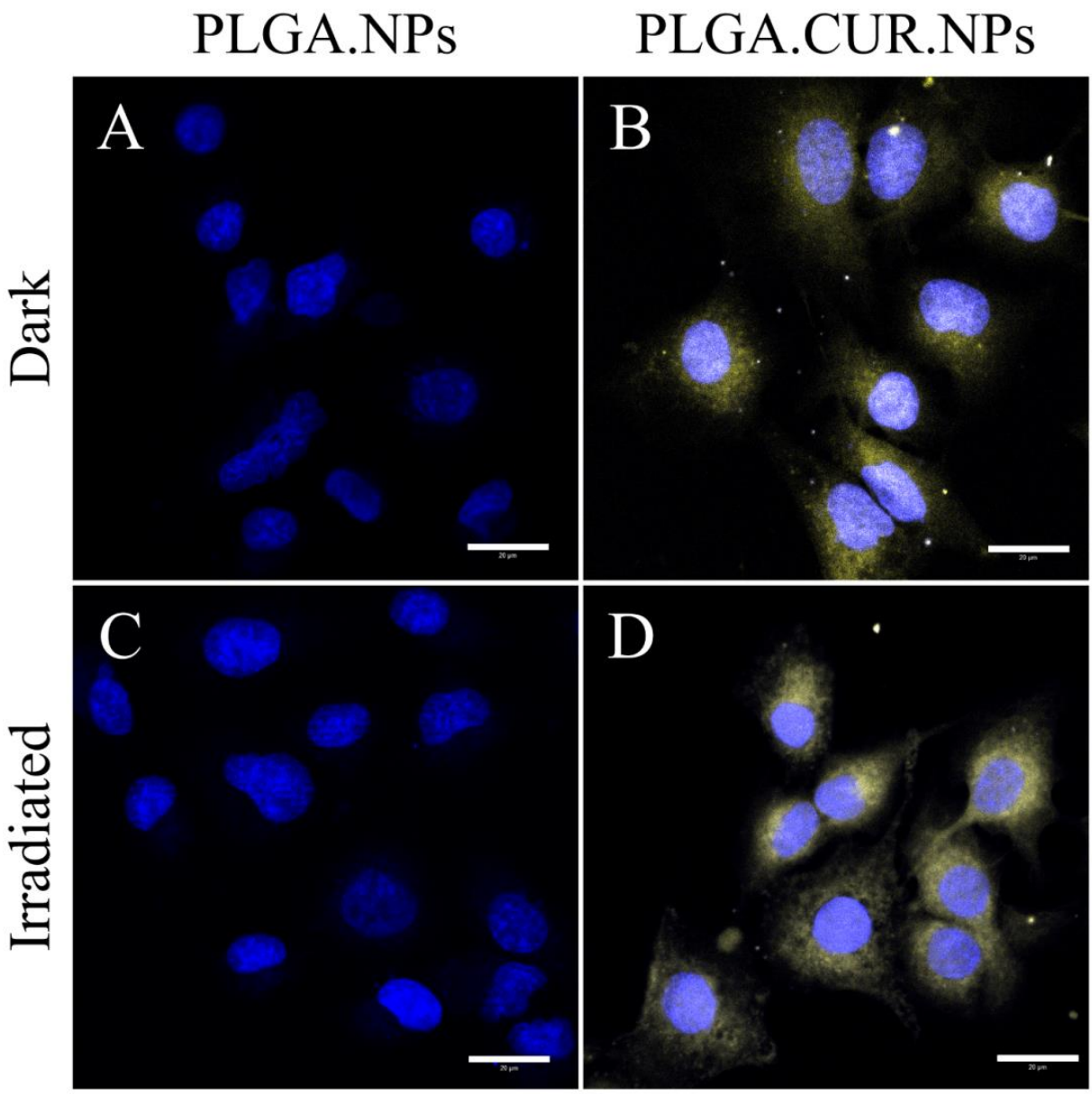

Figure 11 CLSM images of A549 cells incubated with unloaded nanoparticles (PLGA.NPs) and curcumin loaded nanoparticles (PLGA.CUR.NPs). Radiation fluence used was 33.03 J/cm^2 at λ = 457 nm. Dark represents unirradiated cells. The cell nucleus (blue) was counterstained with DAPI. Scale bars represent 20 µm.

3.1.4 Physicochemical properties of the Nano-in-Microparticles

A suitable route of administration must be chosen, so that the photosensitizer reaches its target tissue and accumulates in therapeutic concentrations. Although PDT has been effectively applied against several types of lung cancer [128], intravenous administration is still the route of choice for most of the clinically approved photosensitizers with only a few reports about pulmonary drug delivery in this field [129]. This issue raises the need of photosensitizer loaded nanoformulations which could exploit the numerous advantages of the lungs such as: being non-invasive route of administration, a lower administered dose and minimum systemic exposure of drug intended for local application [34].

In this regard, the photosensitizer loaded nanoformulation which was previously prepared in **2.2.1.1** (i.e. PLGA.CUR.NPs) was spray dried with a sugar matrix (mannitol) to be transformed into a dry powder for inhalation in the form of Nano-in-Microparticles (NiMps). The spray drying parameters were optimized to achieve high powder yield and enhanced aerodynamic properties, taking into consideration the physical properties of PLGA, especially the glass transition temperature. After collecting the spray dried product, yield% was calculated and found to be 54.80 ± 4.21 %. This is considered a very good product yield which can be related to the use of high-performance cyclone which facilitated the recovery of a high amount of the spray dried product [13]. Mannitol was chosen as matrix excipient due to its suitability for pulmonary applications and it has been already used in FDA approved pharmaceutical preparations (e.g. Exubera®) [130]. Moreover, mannitol has a high aqueous solubility which is essential for the disintegration of the microparticles to release the nanoparticles once they are deposited in the lungs. Other matrix excipients have been also used in the preparation of inhalable formulations based on curcumin loaded PLGA nanoparticles [65]. However, using polycationic polymers like chitosan as matrix substance will lead to electrostatic interactions with the anionic lipids in the lung surfactant and critically influencing their surface activity [131, 132].

Redispersibility of NiMps was evaluated by redispersing the sprayed powder in water. DLS measurements of the redispersed nanoparticles revealed a particle size of 233.41 ± 24.22 nm and PdI of 0.23 ± 0.03. This increase in particle size and PdI could be due to slight aggregation caused by shear forces during the atomization step [61]. Even after storage for almost five months, NiMps were readily dispersible, confirming the benefit of spray drying in improving long-term stability of the nanoparticles. Furthermore, mannitol plays a vital role in increasing the space between the nanoparticles which will reduce particle-particle interactions and improve the disintegration of the microparticles [56].

SEM micrographs of NiMps (**Figure 12B and C**) showed raisin-like particles with wrinkled morphology and relatively broad particle size distribution ranging from 0.5 to 4 µm. The particle size and morphology of NiMps are mainly determined by the mass ratio of nanoparticles to mannitol. Increasing the nanoparticles content will lead to the formation of less spherical and more collapsed particles [72].

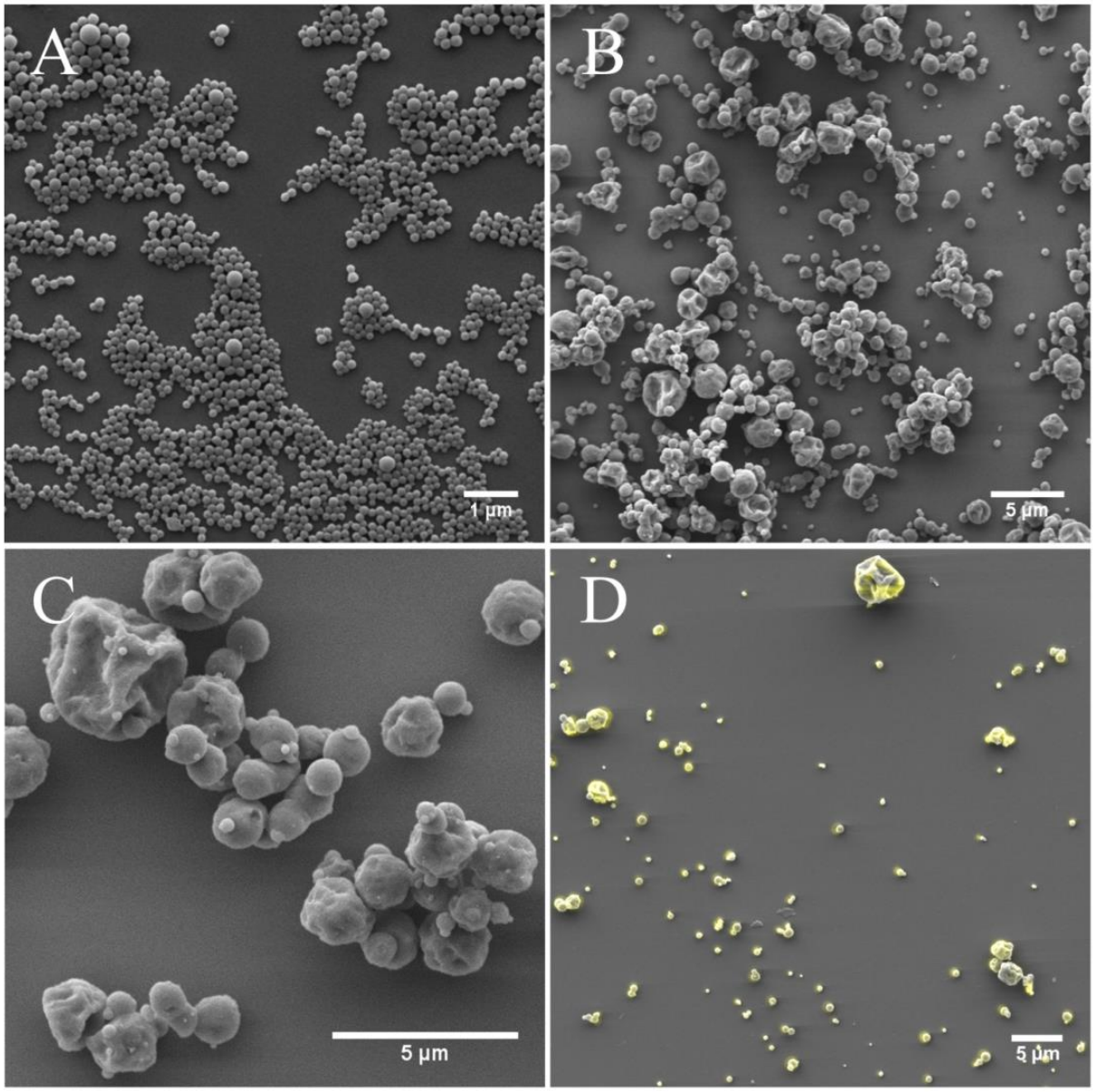

Figure 12 SEM micrographs showing the morphology of A: curcumin loaded PLGA nanoparticles, B and C: Nano-in-Microparticles. D: CLEM image consisting of SEM micrograph of Nano-in-Microparticles merged with the fluorescence signal (yellow) of curcumin loaded nanoparticles from CLSM.

Additional details about NiMps structure were obtained from CLEM imaging which served as a confirmation of the nanoparticle distribution within the microparticles (**Figure 12D**). Moreover, using CLSM, it was also possible to confirm the ability of mannitol to embed nanoparticles homogenously by analyzing each fluorescence channel separately since the nanoparticles were loaded with curcumin and mannitol was labeled with rhodamine B (**Figure 13**). Previous studies reported similar results with mannitol and different types of nanoparticles [62, 72].

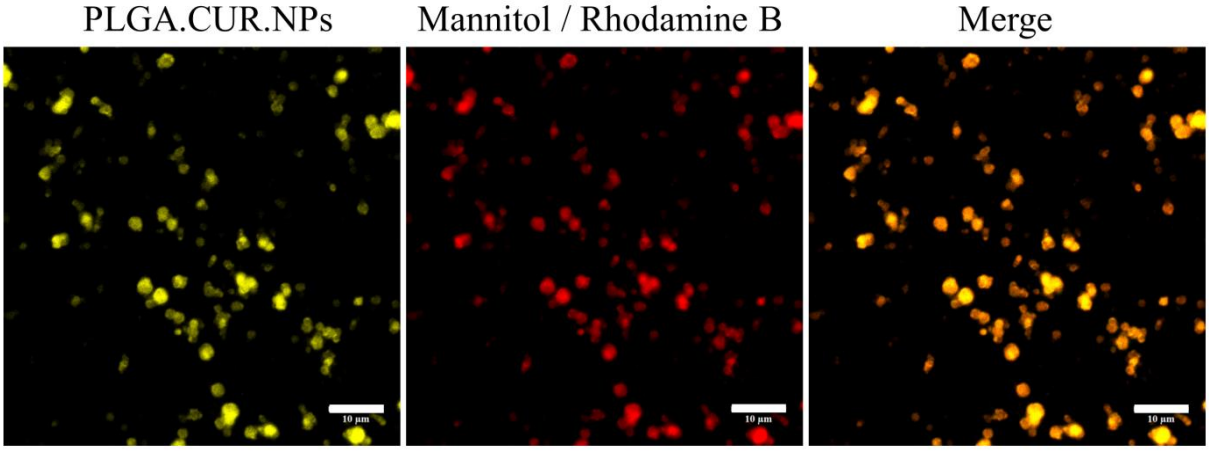

Figure 13 CLSM images showing the morphology of the Nano-in-Microparticles and the homogenous distribution of curcumin loaded nanoparticles (PLGA.CUR.NPs) within the matrix substance (i.e. mannitol). Scale bars represent 10 µm.

3.1.5 Aerodynamic properties and lung compatibility

The pulmonary deposition of inhaled particles is significantly controlled by their aerodynamic properties. An aerodynamic diameter between 1 to 5 µm will help achieving higher particle deposition in the lung especially in the lower airways [55]. NiMps were characterized using NGI which is one the devices recommended by the European Pharmacopeia for aerodynamic assessment of fine particles (Chapter 2.9.18). NiMps exhibited good aerosolization behavior with MMAD of 3.02 ± 0.07 µm within the desirable range and high FPF (64.94 ± 3.47%) (**Figure 14**). GSD was found to be 1.74 ± 0.16 indicating a polydisperse powder which was also noticed in SEM micrographs. This GSD value, however, falls within the typical range for most pharmaceutical aerosols (1.5 - 2.5) [133]. NGI results proved the ability of NiMps to deliver the nanoparticles efficiently to the lungs omitting the need of additional excipients like coarse carrier particles (e.g. lactose) or aerosolization enhancer (e.g. amino acids).

Following deposition, NiMps will come in contact with lung fluids. Depending on their deposition site, the particles have to pass the mucus blanket within the airways or pulmonary surfactant layer lining the alveolar epithelium to reach their target [52]. In this regard, the interaction of NiMps with a monolayer of bovine lung surfactant (Alveofact®) was investigated using Langmuir film balance. Two different surface pressures were used to simulate the interaction of PLGA.CUR.NPs with pulmonary surfactant during the breathing process [134]. The pure monolayers were in continuous phase at those pressures. **Figure 15** shows the π-t isotherm of pure Alveofact® dynamically compressed up to a surface pressure of 25 mN/m (A) and 42 mN/m (B) at a velocity of 20 cm^2/min.

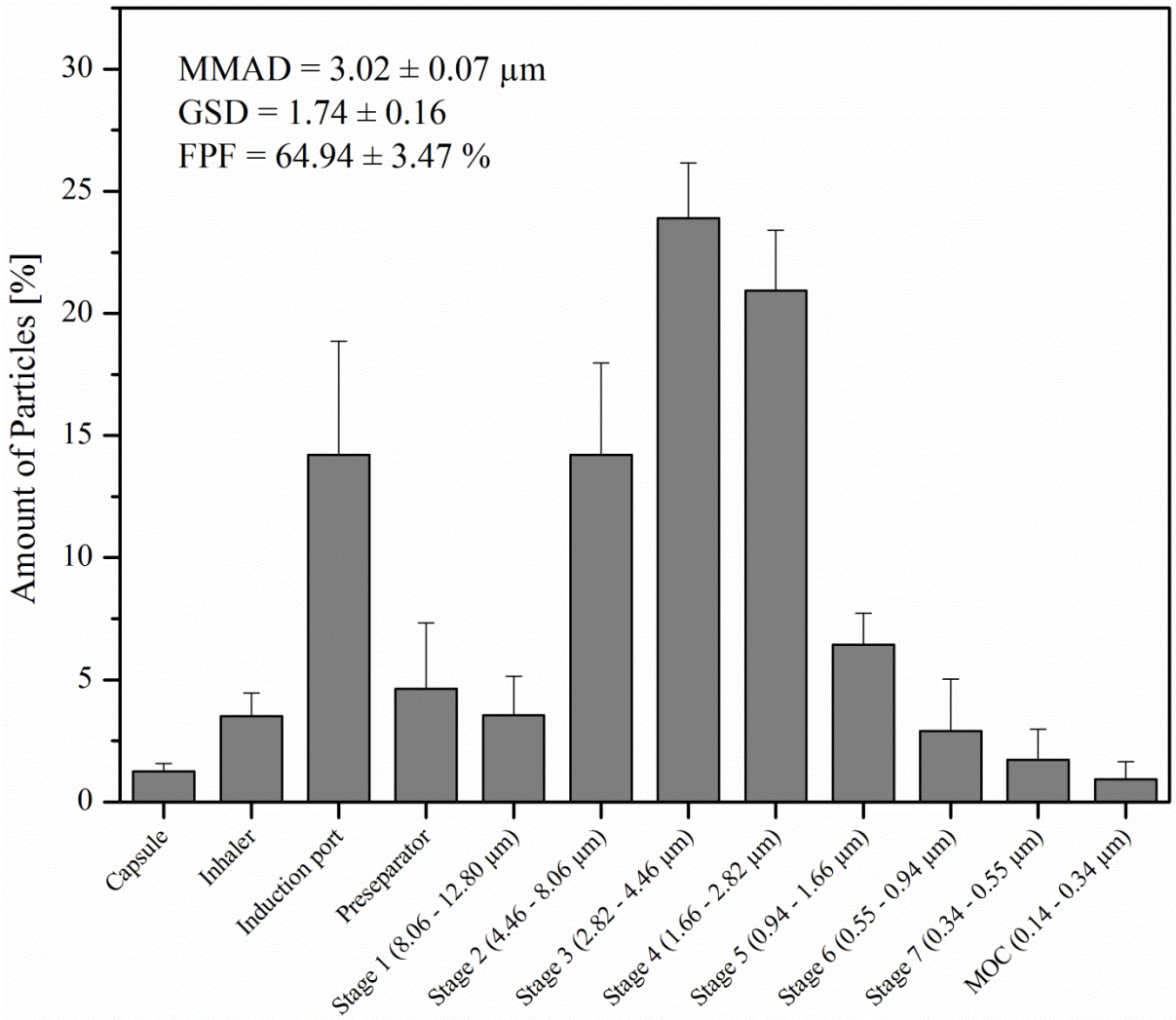

Figure 14 The distribution of Nano-in-Microparticles on different parts of the next generation impactor. Mass median aerodynamic diameter (MMAD), geometric standard deviation (GSD) and fine particle fraction (FPF) were also calculated. Values are presented as mean ± standard deviation.

After reaching the desired surface pressure, the barriers were stopped so that the Alveofact® monolayer could equilibrate. The properties of the Alveofact® monolayer were then monitored for 60 min. Directly after the barriers stopped, the π-t isotherms of pure Alveofact® decreased by 1–2 mN/m. This was caused by a new array of lipids in the monolayer after the dynamic compression or due to other processes like relaxation and desorption [135]. Subsequently, the monolayer equilibrated and the surface pressures stabilized. The gray curves represent the π-t isotherms where 20 µl of PLGA.CUR.NPs were added 15 min after the barriers were stopped. After the injection of the nanoparticles, no change in the π-t isotherm could be observed at both tested surface pressures, suggesting no substantial interaction between the nanoparticles and surfactant. In other words, integration of the nanoparticles into the surfactant monolayer would have caused an increase in the surface pressure over time, and vice versa, a decrease in the surface pressure would mean that the nanoparticles have either withdrawn the compounds out of the monolayer or destroyed it [102]. These outcomes confirmed that NiMps with all their components (nanoparticles and mannitol) are compatible with pulmonary surfactant at physiological pressures.

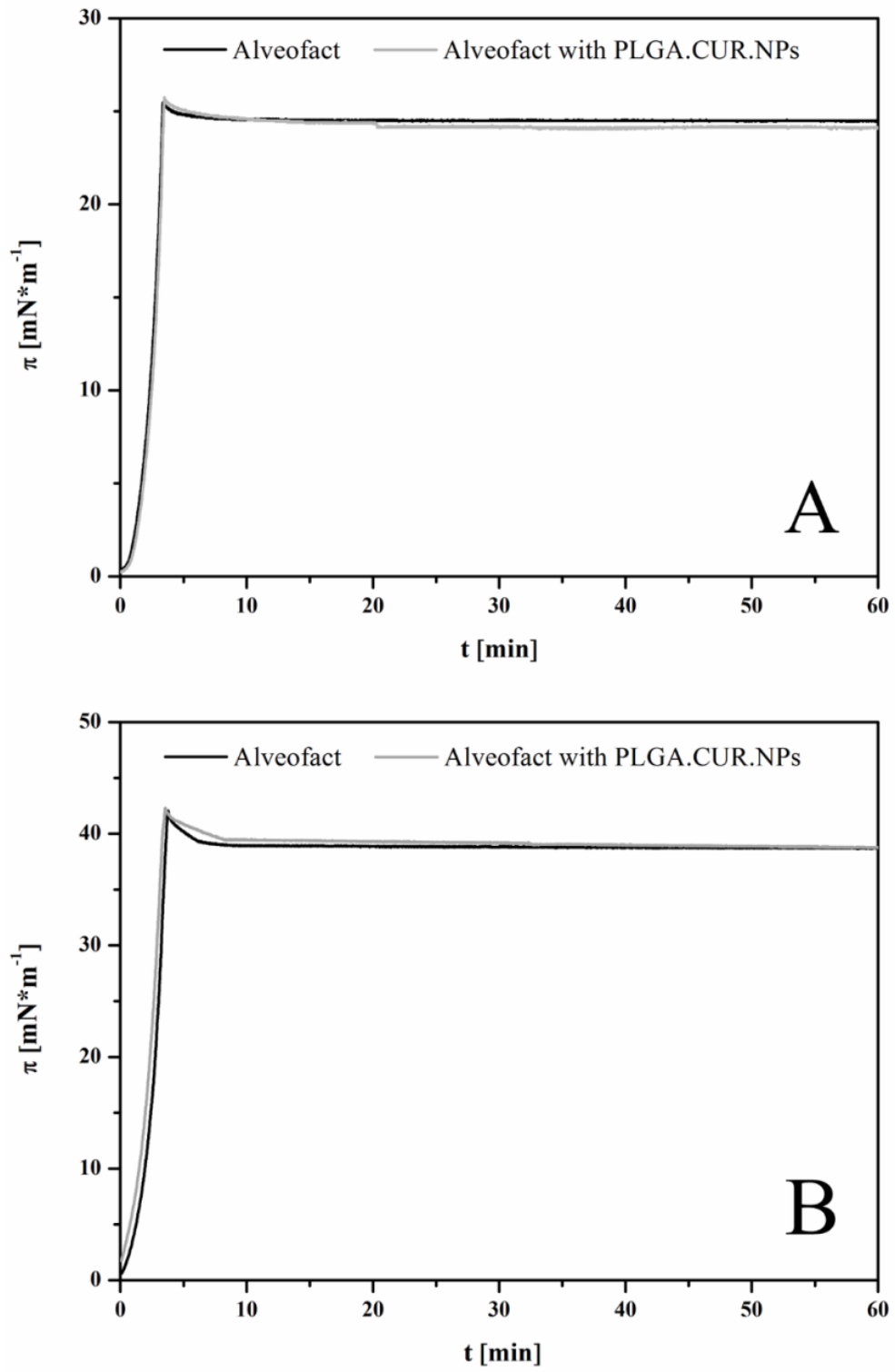

Figure 15 π-t (surface pressure-time) isotherms showing the interaction of curcumin loaded nanoparticles (PLGA.CUR.NPs) with a monolayer of bovine lung surfactant (Alveofact®) using Langmuir film balance. The surface pressures were increased up to 25 mN/m (A) and 42 mN/m (B). After an equilibration time of 15 min, PLGA.CUR.NPs were injected into the subphase.

3.2 Nano spray drying for coating of medical implants

3.2.1 Preliminary experiments

Coating and surface modification of medical implants with nanoparticles offers several advantages. Nanoparticulate systems can serve as a multifunctional coating which can act as drug depot with different release profiles. Moreover, nanoparticles can alter the surface morphology of the implants to prevent bacterial adhesion and even improve healing rate [136-138]. Nanoparticles have various forms and can be produced by several methods using natural or synthetic polymers. They have shown valuable utilizations in all aspects of life, especially as drug delivery systems. Nanoscale drug carriers have been employed to overcome numerous limitations and improve the efficiency of many active pharmaceutical ingredients, e.g. solubility enhancement, targeted drug delivery and controlled release [123, 139].

In this work, a novel approach for producing biocompatible nanoscale coatings using the Nano Spray dryer B-90 was introduced. Therefore, three model substances were chosen to represent three various categories of biomaterials; water soluble polymers, water insoluble polymers and pure drugs. For this purpose, chitosan, PLGA and curcumin were considered. The spray drying parameters were set to produce the smallest particle size possible taking into consideration the physicochemical properties of the chosen model substances (e.g. viscosity of chitosan solution, glass transition temperature of PLGA). Therefore, low solid concentration of the sprayed sample (0.1%) and the smallest available size of the spray mesh (4.0 µm) were used. Previous studies have confirmed that the solid concentration of the sprayed sample and the size of the spray mesh are the most critical parameters with the strongest influence on the particle size of the produced particles [60, 85, 140].

However, the effect of the implant position inside the particle collector and the required amount of the sprayed sample should also be optimized. Therefore, preliminary experiments were performed on titanium plates which were placed at three different positions inside the electrostatic particle collector. Initially, 15 ml samples were tested. This amount was found to be insufficient to get a complete coverage of the titanium plates. Subsequently, 50 ml samples were tried and found to be adequate. These findings indicated that only a small quantity of the sprayed substance (50 mg) was needed to achieve a successful coating even in the plates positioned at the bottom of the collector. This is one of the advantages of the Nano Spray Dryer B-90 that was originally developed for early stage research where larger amounts of the sample are hard to obtain [86, 140].

SEM micrographs revealed that the produced particles in all experiments were spherical and had a smooth surface. The titanium plates at the top part of the collector were covered with more particles which formed multilayer coating (**Figure 16 Top**). Moreover, the particle size analysis showed that the particle size distribution for all formulations on this level was heterogeneous and the mean particle size was around 600 nm in case of chitosan and around 900 nm in case of PLGA and curcumin (**Figure 17 Top**). On the other hand, the results of the bottom plates clearly showed that there is a significant decrease in the particle size distribution. It was also noticed that the plates on the bottom part of the collector had almost the same mean particle size but a narrower size distribution in comparison with the plates on the top part which correlated with previous studies [85]. Interestingly, in case of PLGA and curcumin the mean particle size decreased and a considerable number of smaller nanoparticles (around 300 nm) was also observed (**Figure 17 Bottom**). These results can be explained by the fact that larger particles have a higher surface charge and therefore get captured easily by the particle collector than smaller particles [85, 95, 141].

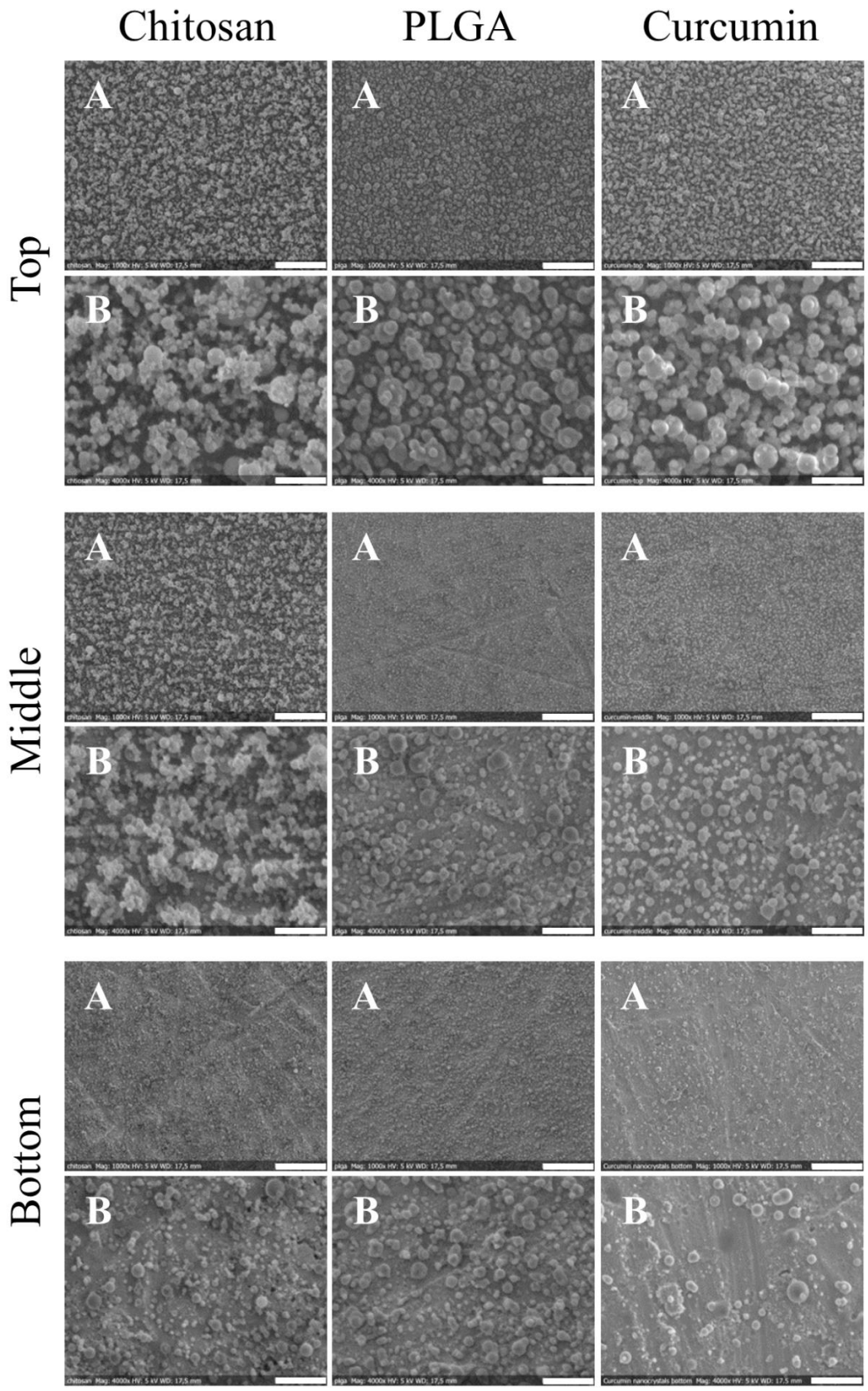

Figure 16 SEM micrographs showing the coating of titanium plates with three different substances; chitosan, PLGA and curcumin. The titanium plates were placed at three different positions inside the particle collector (i.e. Top, Middle and Bottom). Scale bars represent A: 20 µm and B: 5 µm.

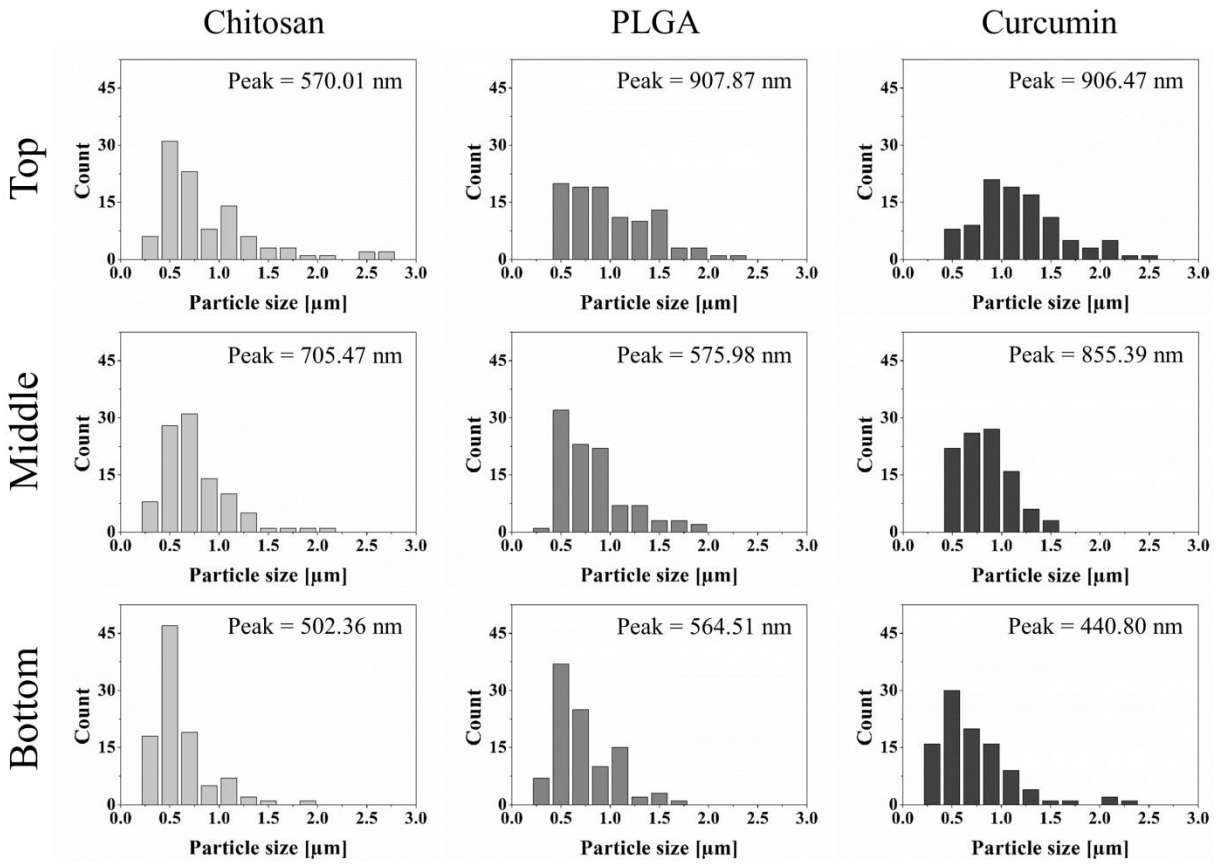

Figure 17 Particle size analysis of the SEM micrographs of titanium plates coated with chitosan, PLGA and curcumin respectively (**Figure 16**).

Finally, the optimized parameters were applied to dental implants which were used in this study as an example of small medical implants. The implants were positioned 12 cm towards the bottom of the particle collector as this position was found to be the best to completely coat the implant with the smallest particles. The visual inspections with stereomicroscope and CLSM provided a confirmation about a successful and homogenous coating by comparing the coated implant with unmodified one (**Figure 18**). SEM results of the implants were comparable with the titanium plates that were placed at the bottom part of the collector (**Figure 19**). According to particles size analysis, all implants were successfully coated with particles that were in the range of 300 nm – 1.5 µm with a mean particle size of 500 nm (**Figure 20**).

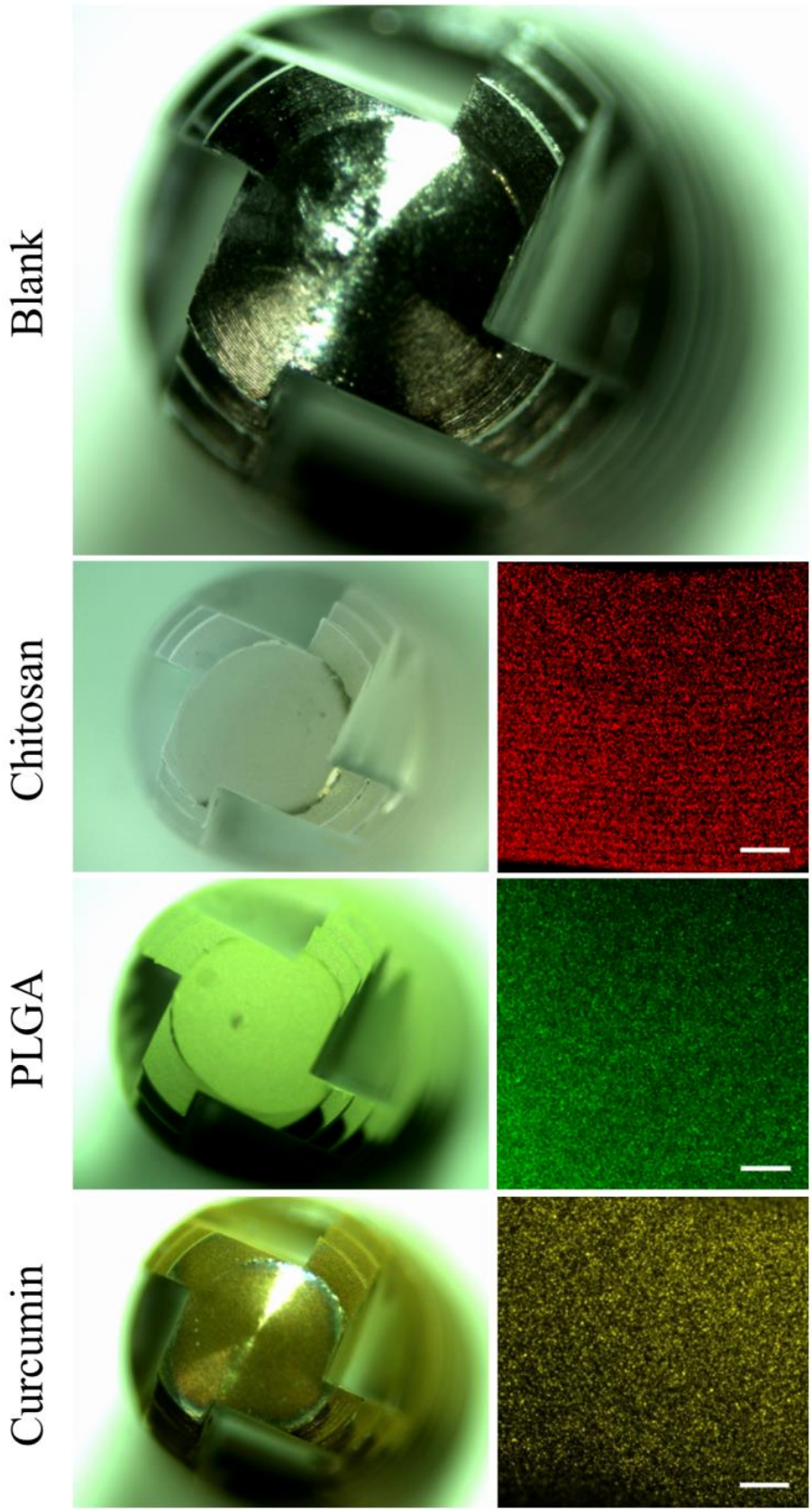

Figure 18 Stereomicroscope images (left) of the dental implants (apical view) before and after spray drying. Inset CLSM images (right) of the coated implants indicating coating uniformity. Scale bars represent 100 µm.

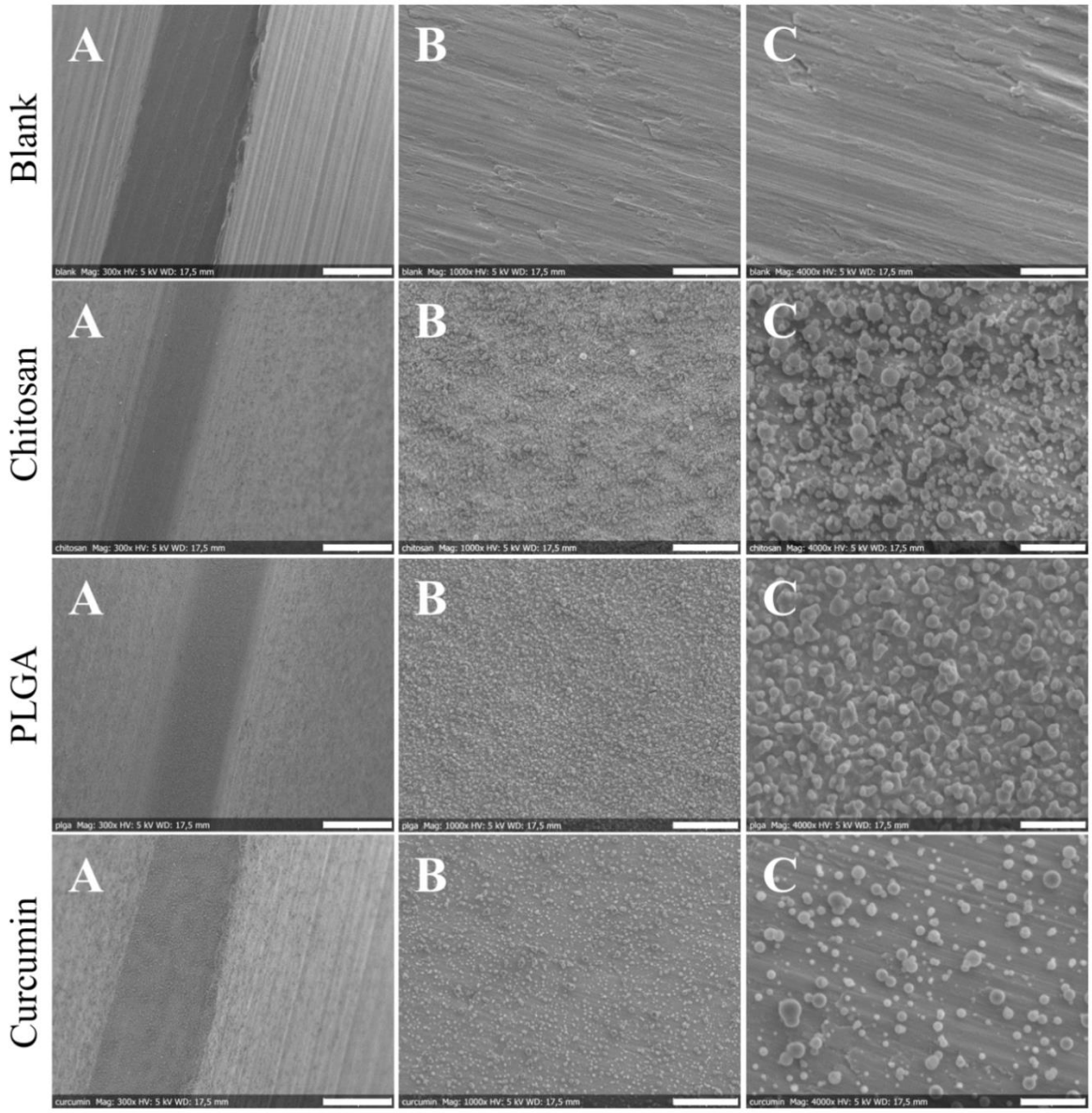

Figure 19 SEM micrographs showing successful coating of the dental implants with chitosan, PLGA and curcumin, respectively. A: shows the surface structure of one of the implant roots between two crests. B and C: show the surface morphology of the apical part of the implant. Scale bars represent A: 70 µm, B: 20 µm, C: 5µm

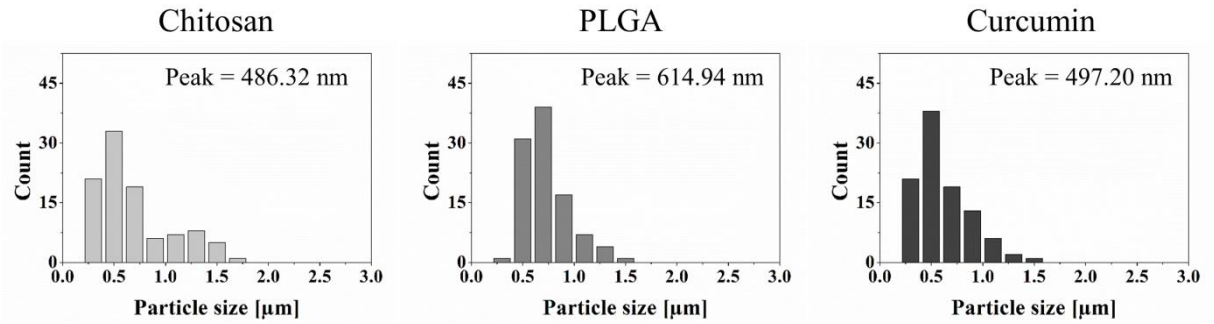

Figure 20 Particle size analysis of the SEM micrographs of dental implants coated with chitosan, PLGA and curcumin respectively (**Figure 19**).

3.2.2 Antibacterial and biocompatible nanocoatings

3.2.2.1 Morphology and surface properties

In the preliminary experiments, nano spray drying exhibited such promising potentials as a novel approach to prepare nanoscale coatings for dental implants. The wide range applicability of this technique was confirmed using three different model substances with different physicochemical properties, i.e. chitosan, PLGA and curcumin. The next step was to explore the capability of this coating technique to produce biocompatible nanocoatings with antibacterial activity. Therefore, PLGA-based nanocoatings were produced using norfloxacin as a model drug for broad-spectrum antibacterial agents [142-145]. The optimized spray drying process parameters from the preliminary experiments were applied on Ti-discs, taking into consideration previous studies, wherein the spray mesh size and the solid concentration of the feed solution had the most pronounced influence on the size of the produced particles [60, 86, 140]. Therefore, all formulations were prepared with low solid concentration (1 mg/ml) and the smallest spray mesh available (4.0 µm) was used, thereby achieving the smallest possible particle size. Due to its crucial role in controlling the properties of the produced nanocoatings, disc position inside the particle collector was investigated. Therefore, Ti-discs where fixed at three different positions (i.e. Top, Middle and Bottom).

SEM micrographs of the Ti-discs (**Figure 21**) were similar to those of the preliminary experiments (**Figure 16**). All produced particles were spherical and had a smooth surface. At the top part of the collector, the Ti-discs were covered with multilayered nanocoatings consisted of single particles and nanostructured microaggregates (**Figure 21 Top**). On the contrary, the Ti-discs at the bottom part were coated with a monolayer of single particles with no obvious presence of any aggregates (**Figure 21 Bottom**). Particle size analysis of the SEM micrographs revealed an average particle size around 600 nm for the nanocoatings at the top part of the collector with relatively broad particles size distribution and significant number of microparticles (**Figure 22 Top**). Interestingly, at the bottom part a substantial decrease in the particle size was observed (around 400 nm) with a more homogenous size distribution wherein most of the particles were in the submicron range (**Figure 22 Bottom**).

These results can be explained based on the fact that bigger particles carry higher surface charge; therefore, they get captured easily by the electrostatic particle collector [85, 95, 141]. Thus, as the dried particles moves downward, they will be fractionated along the electrostatic particle collector thereby having the smallest particles with the narrowest size distribution at the bottom part of the collector.

It is noteworthy that SEM results revealed no significant difference between unloaded nanocoatings (PLGA 0% NFX) and norfloxacin loaded nanocoatings (PLGA 5% NFX) in terms of morphology and particle size distribution.

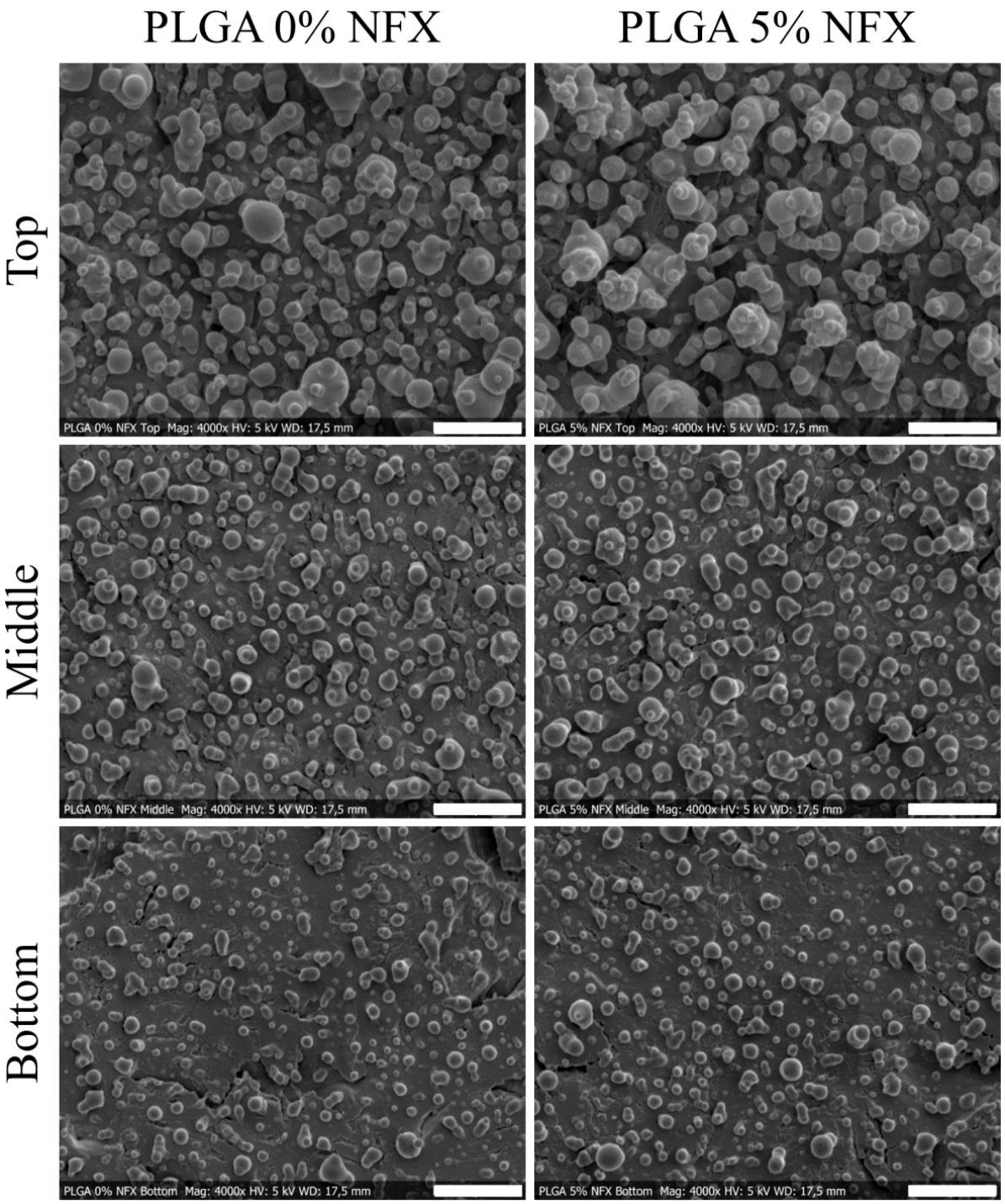

Figure 21 SEM micrographs of coated titanium discs showing the morphology and surface structure of unloaded nanocoatings (PLGA 0% NFX) and norfloxacin loaded nanocoatings (PLGA 5% NFX). The titanium discs were fixed at three different positions inside the electrostatic particle collector (i.e. Top, Middle and Bottom). Scale bars represent 5 µm.

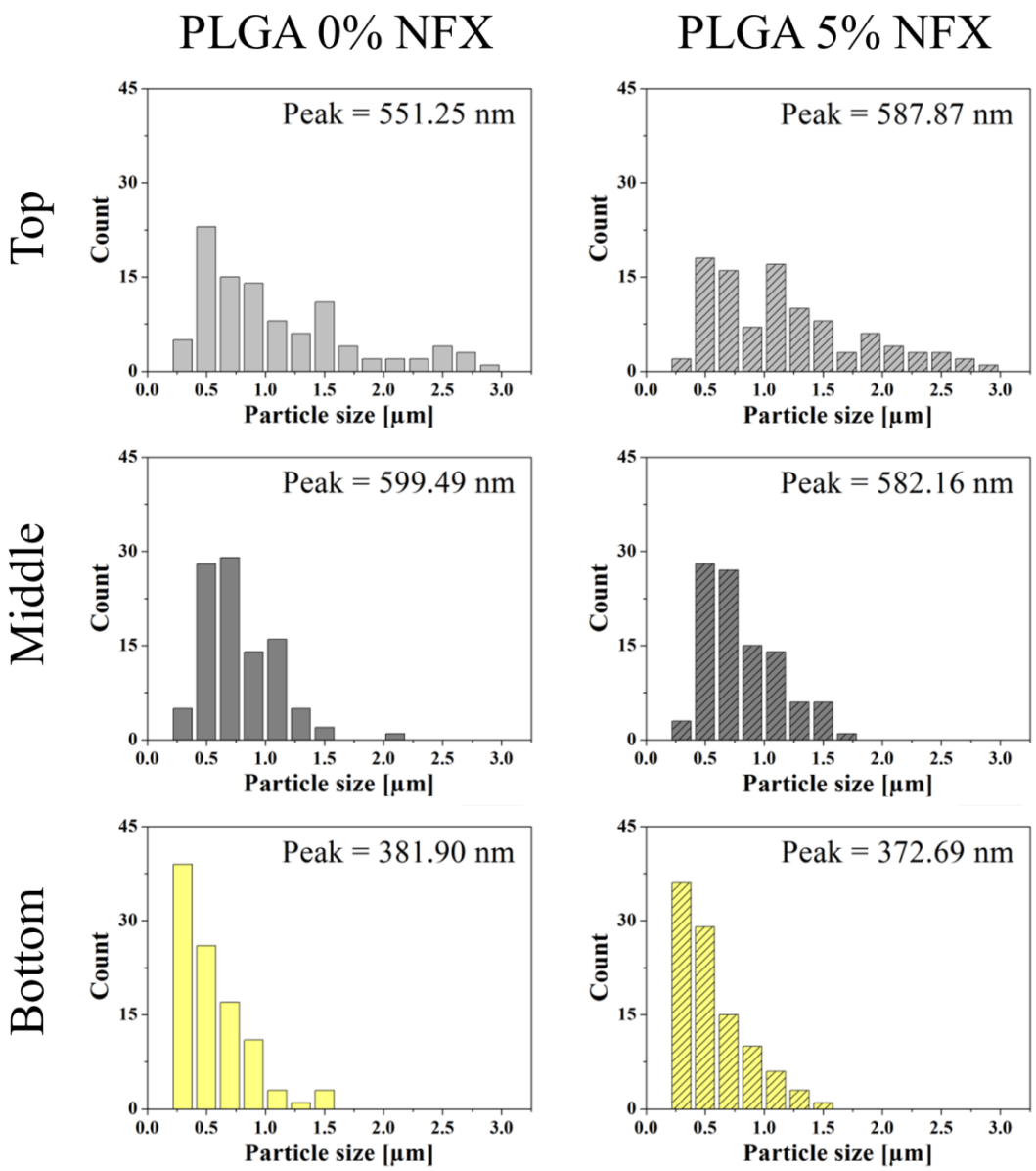

Figure 22 Particle size analysis based on the SEM micrographs of unloaded nanocoatings (PLGA 0% NFX) and norfloxacin loaded nanocoatings (PLGA 5% NFX) (**Figure 21**).

3.2.2.2 *In vitro* drug release studies

Nano spray drying has been successfully utilized in several studies for the preparation of PLGA submicroparticles that exhibited controlled drug release properties [60, 89, 92, 95].

Drug release rate was found to be influenced by several factors e.g. particle size [96], PLGA lactide:glycolide ratio and molecular weight [89].

In this work, the release profile of several nanocoatings was studied over a period of 15 days in PBS (pH 7.4) at 37 °C. To investigate the effect of theoretical drug loading on the release behavior, Ti-discs placed at the same level inside the particle collector (i.e. Top); however, with three different theoretical norfloxacin loadings (i.e. 2.5%, 5% and 10%) were examined (**Figure 23**). Furthermore, the influence of Ti-disc position inside the particle collector was also explored; therefore, Ti-discs with the same norfloxacin loading (i.e. 5%); however, placed at three different levels inside the particle collector (i.e. Top, Middle and Bottom) were tested (**Figure 24**). All nanocoatings exhibited similar release profiles that are typically observed with PLGA nano-/microparticles encapsulating hydrophobic drugs [136].

By observing the release graphs especially (**Figure 23 A**) and (**Figure 24 C**), the release profiles could be divided into two phases. In the first 48 h, an initial burst release was observed, which can be mainly due to drug desorption from the nanocoatings surface [146, 147]. Moreover, the sharp peak noticed in all graphs after 1 h incubation can be also attributed to the fast dissolution of free nonencapsulated drug [148]. This “burst phase” was found to be directly influenced by the theoretical norfloxacin loading and it was most obvious at the highest norfloxacin loading (i.e. 10%) which is in agreement with previous studies [147]. Starting from the third day until the end of experiment period, a second phase was noticed, wherein norfloxacin was released at low but constant rate. According to previous studies, drug diffusion is the main release mechanism at this phase, possibly through the matrix of PLGA particles or water-filled pores [147-149]. However, drug release from PLGA formulations is a very complex process; therefore, other mechanisms might be also controlling the release at this phase [148]. This sustained release phase did not seem to be influenced by theoretical norfloxacin loading or Ti-disc position inside the particle collector. It is worth mentioning that no secondary burst release was observed during the test period.

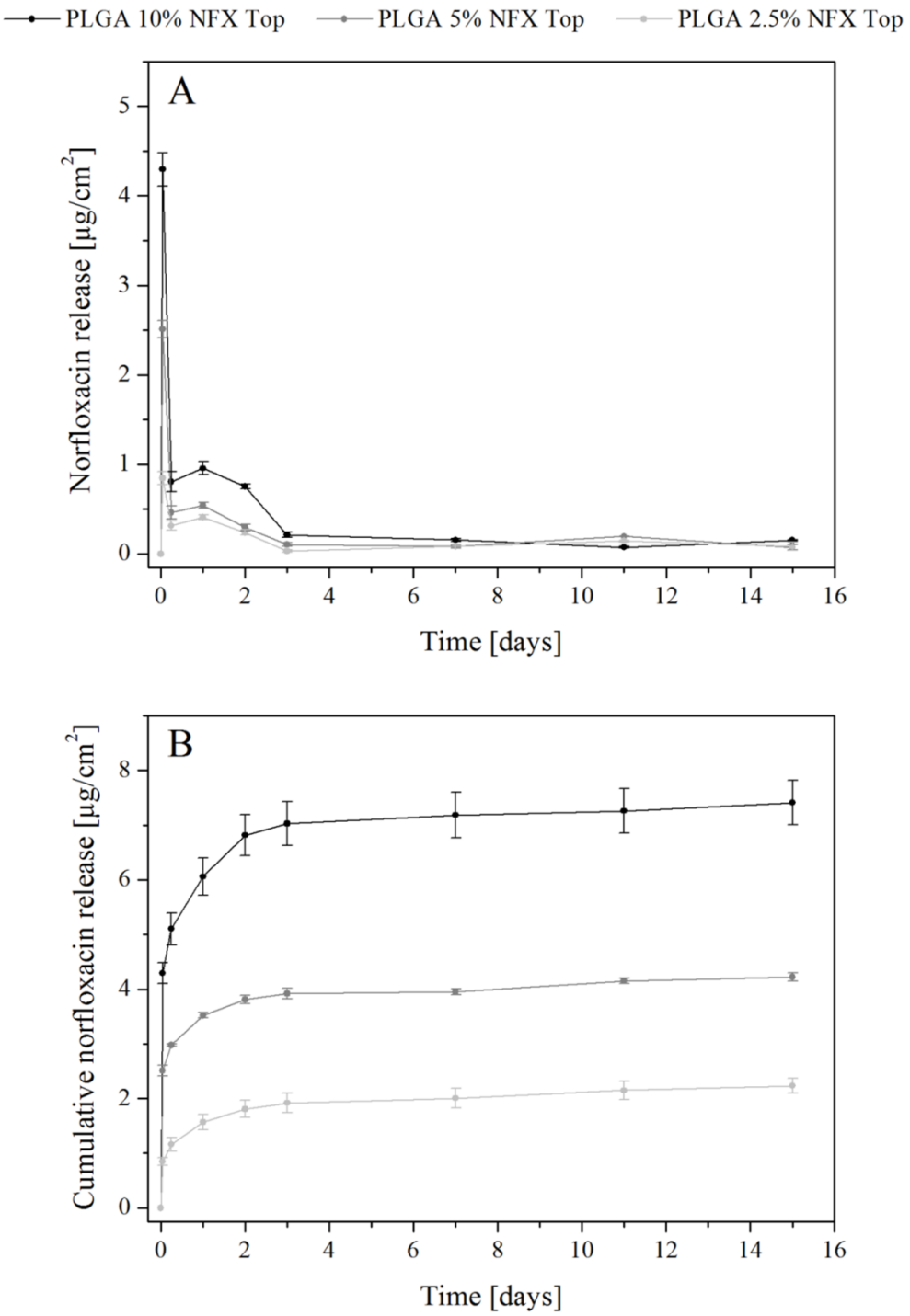

Figure 23 *In vitro* release profile of norfloxacin over a period of 15 days in PBS (pH 7.4) at 37 °C. In this experiment, the coated titanium discs were fixed at the same level inside the particle collector (i.e. Top); however, with three different theoretical norfloxacin loadings (i.e. 2.5%, 5% and 10%). A: The released amount of norfloxacin after different time intervals. B: Cumulative release profile of norfloxacin.

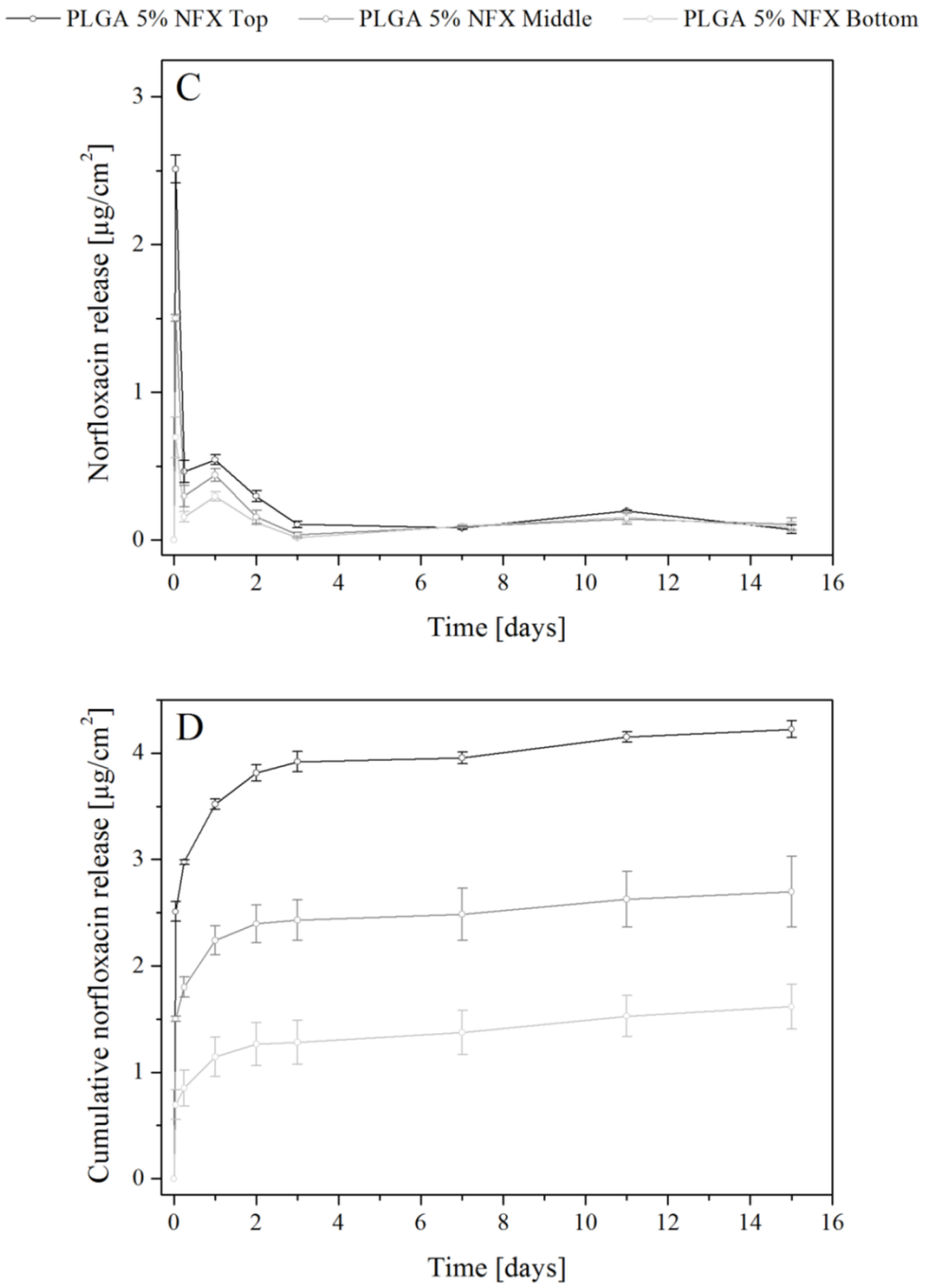

Figure 24 *In vitro* release profile of norfloxacin over a period of 15 days in PBS (pH 7.4) at 37 °C. In this experiment, the coated titanium discs had the same theoretical norfloxacin loading (i.e. 5%); however, they were fixed at three different levels inside the particle collector (i.e. Top, Middle and Bottom). A: The released amount of norfloxacin after different time intervals. B: Cumulative release profile of norfloxacin.

3.2.2.3 Nanocoating degradation

SEM was used to investigate the degradation of nanocoatings and the possible morphological changes they might experience after 15 days incubation in PBS (pH 7.4) at 37 °C. SEM micrographs showed that all examined nanocoatings (PLGA 0% NFX and PLGA 5% NFX) remained adhered to the surface of Ti-discs which was in agreement with previous studies [136]; however, substantial changes in the morphology and surface structure were observed (**Figure 25**). Most particles were deformed and had corrugated surface. Significant number of aggregates was noticeable even in the Bottom level which was not the case before incubation in PBS. Interestingly, some particles lost their structure completely and were merged together forming sort of porous film. This phenomenon was obvious in all levels, especially Top and Middle where it appeared as a net-like structure.

Previous studies have related the causes of PLGA particles aggregation and deformation to the fact that PLGA polymer starts to degrade by means of hydrolysis upon contact with the incubation medium (i.e. PBS). As the degradation process continues, the molecular weight decreases causing a drop in the glass transition temperature (T_g). When the T_g reaches a critical value below the temperature of incubation medium (i.e. 37 °C), PLGA polymer will be in the rubbery state and become more flexible. Consequently, PLGA particles start to aggregate and lose their spherical shape [150-152].

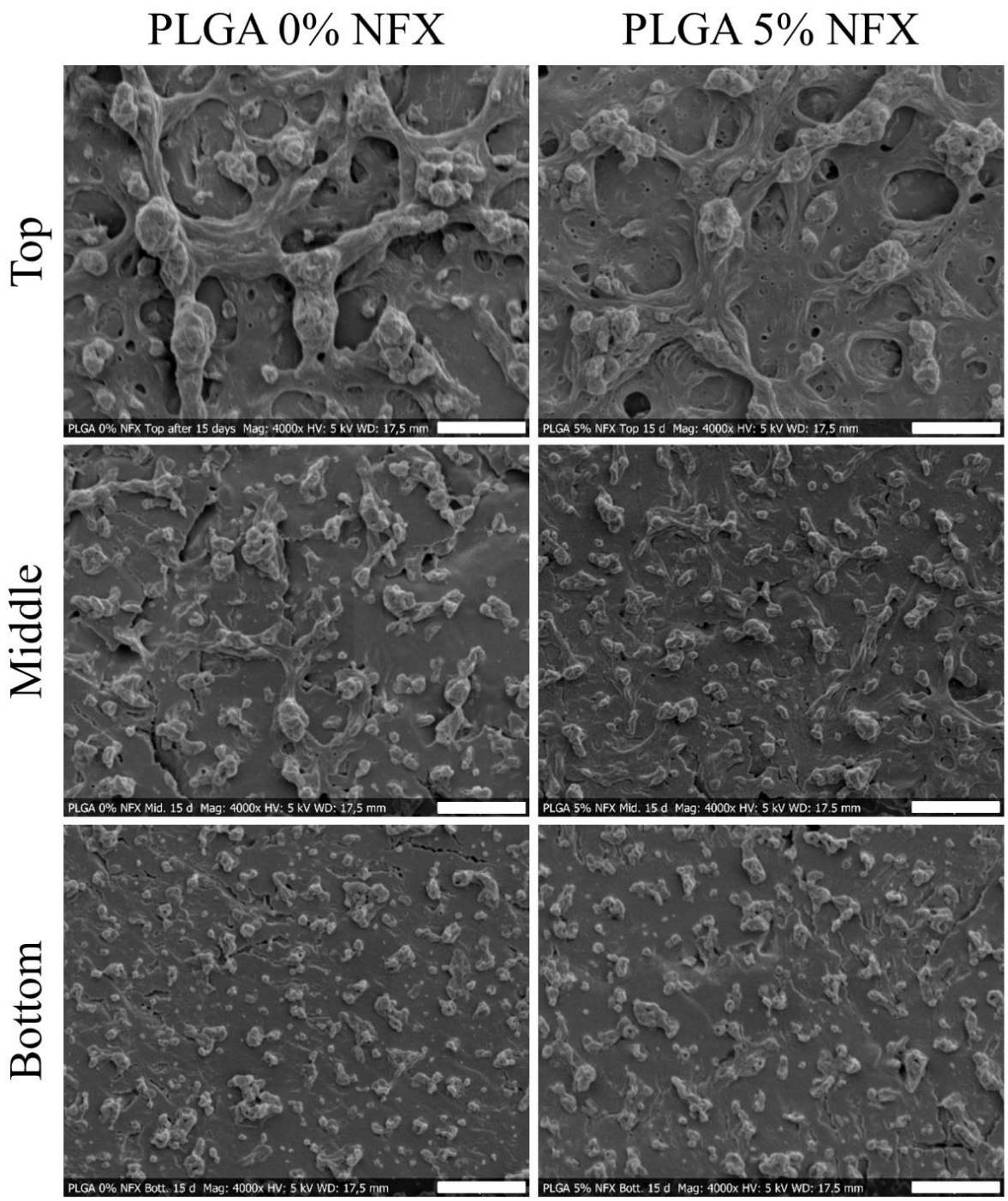

Figure 25 SEM micrographs of the unloaded nanocoatings (PLGA 0% NFX) and norfloxacin loaded nanocoatings (PLGA 5% NFX) after 15 days incubation at 37 °C in PBS (pH 7.4). The titanium discs were fixed at three positions inside the electrostatic particle collector (i.e. Top, Middle and Bottom). Scale bars represent 5 µm.

3.2.2.4 Antibacterial activity

Agar diffusion test is one of the standard methods commonly used for antimicrobial susceptibility testing [113]. In this study, *E. coli* was chosen as a model organism to evaluate antibacterial activity of the nanocoatings wherein the influence of the theoretical norfloxacin loading and Ti-disc position inside the particle collector were investigated (**Figure 26**). This approach served as a first step to explore the most suitable variant among different nanocoatings and reduce the number of samples. As expected, the largest zones of inhibition were observed in PLGA 10% NFX; however, they were comparable to those of PLGA 5% NFX. Moreover, at these loadings (i.e. 10% and 5%), Ti-disc position inside the particle collector did not have a pronounced influence on the zones of inhibition. A significant decrease in the zones of inhibition was noticed in PLGA 2.5% NFX, especially Middle and Bottom. PLGA 0% NFX were used as negative control and did not show any antibacterial activity. Since the bacterial growth inhibition is related to the amount of antibiotic diffused through the agar [113], a direct relationship between norfloxacin content in the nanocoatings and the size of the zones of inhibition could be seen. Spectrophotometric quantification showed that norfloxacin loading and Ti-disc position inside the particle collector significantly controlled the amount of norfloxacin per cm^2 of the nanocoating (**Figure 27**). This can be attributed to the particle fractionation effect along the particle collector previously observed in SEM micrographs (**Figure 21**), wherein Ti-discs at the top part were covered with more and larger particles in comparison to those at the bottom part. As a result, the produced nanocoatings had a norfloxacin content ranged between 10.33 $\mu g/cm^2$ (PLGA 10% NFX Top) and 0.73 $\mu g/cm^2$ (PLGA 2.5% NFX Bottom).

Based on the results of *in vitro* release studies and agar diffusion test, PLGA 5% NFX were chosen for further characterizations. They were found to be more efficient in comparison to other nanocoatings (i.e. 2.5% and 10%), exhibiting similar release profiles and sufficient antibacterial activity, yet without the need of higher norfloxacin loading.

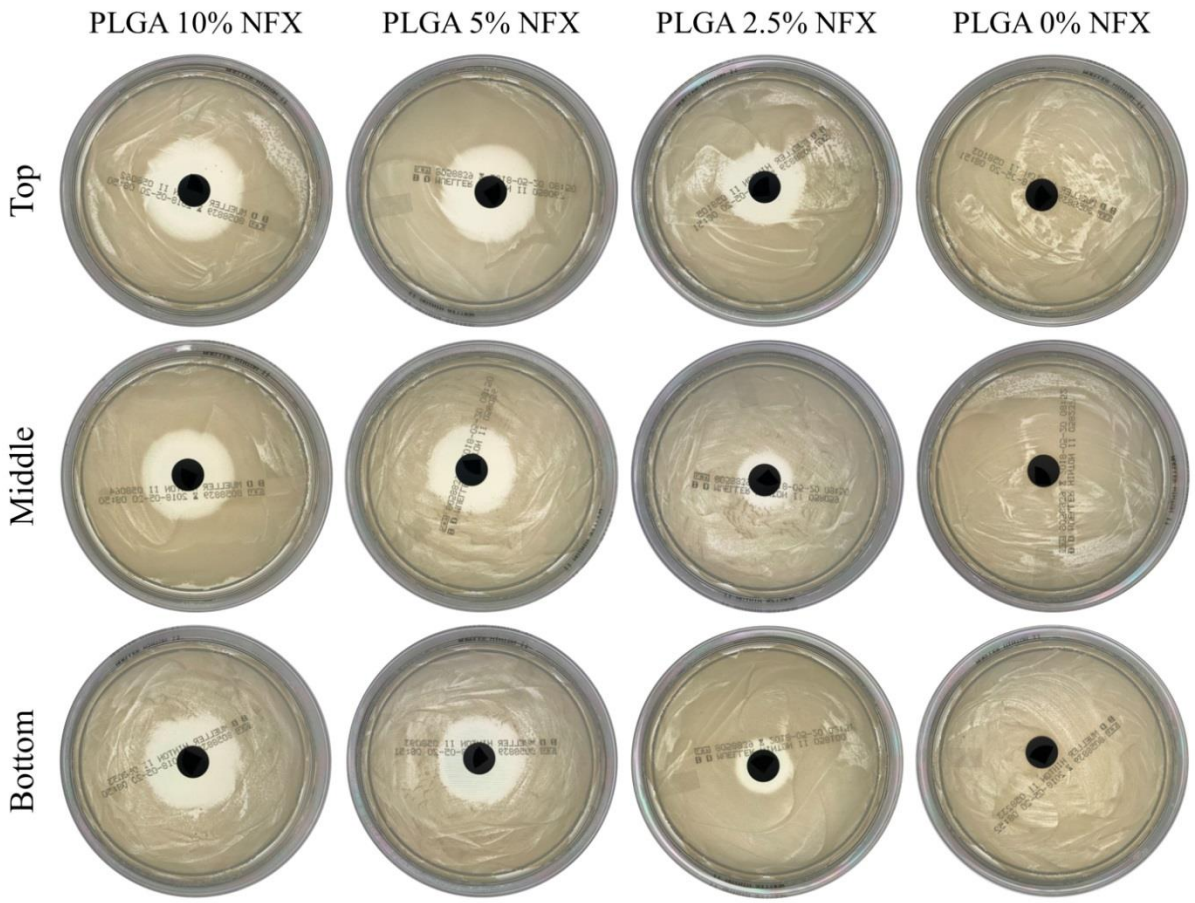

Figure 26 Summary of the results of agar diffusion test, wherein *E. coli* suspension was plated on Mueller Hinton agar plates and incubated with the coated titanium discs for 24 h at 37 °C. Nanocoatings with three different theoretical norfloxacin loadings (PLGA 2.5% NFX, PLGA 5% NFX and PLGA 10% NFX) were tested. Unloaded nanocoatings (PLGA 0% NFX) were used as a negative control. Top, Middle and Bottom indicate the position of the titanium discs inside the particle collector. The zones of inhibition formed around the titanium discs could be clearly observed, indicating the antibacterial activity of the nanocoatings.

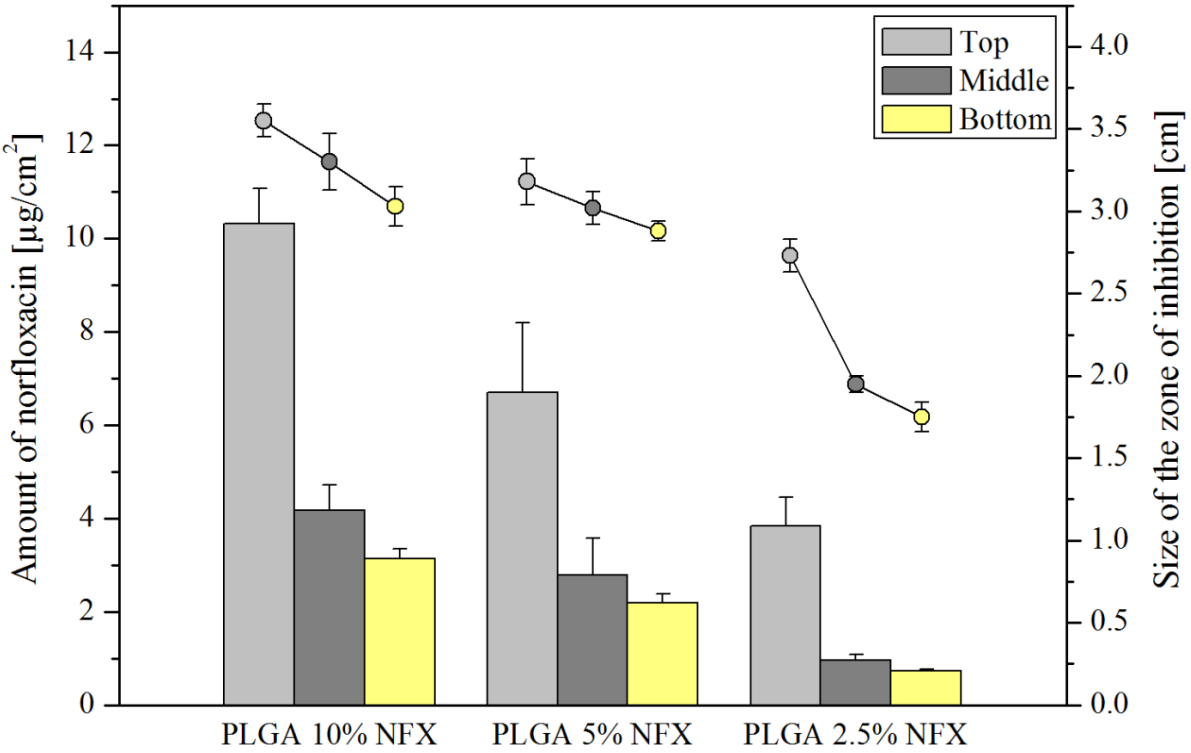

Figure 27 Graphical representation of the relationship between the amount of norfloxacin per cm^2 of the nanocoating (bars) and the diameter of the zone of inhibition (dots). Nanocoatings with three different theoretical norfloxacin loadings (PLGA 2.5% NFX, PLGA 5% NFX and PLGA 10% NFX) were tested. The titanium discs were fixed at three positions inside the electrostatic particle collector (i.e. Top, Middle and Bottom).

Since agar diffusion test deliver mainly qualitative results [153], further *in vitro* bacterial investigations with the chosen nanocoatings (i.e. PLGA 5% NFX) were performed to get a precise evidence about their antibacterial activity. Therefore, the coated Ti-discs were incubated with *E. coli* suspension for 24 h and the adhered bacteria were thereafter quantified. PLGA 5% NFX caused a significant reduction in the bacterial viability in comparison to uncoated Ti-discs ($p < 0.05$). This reduction ranged between 99.83% (PLGA 5% NFX Top) and 95.42% (PLGA 5% NFX Bottom) (**Figure 28**).

PLGA 0% NFX did not exhibit any considerable influence on the bacterial viability ($p > 0.05$) regardless of the Ti-disc position inside the particle collector. Hence, the antibacterial activity of PLGA 5% NFX can be attributed only to norfloxacin without any pronounced influence from the surface structure of the nanocoatings.

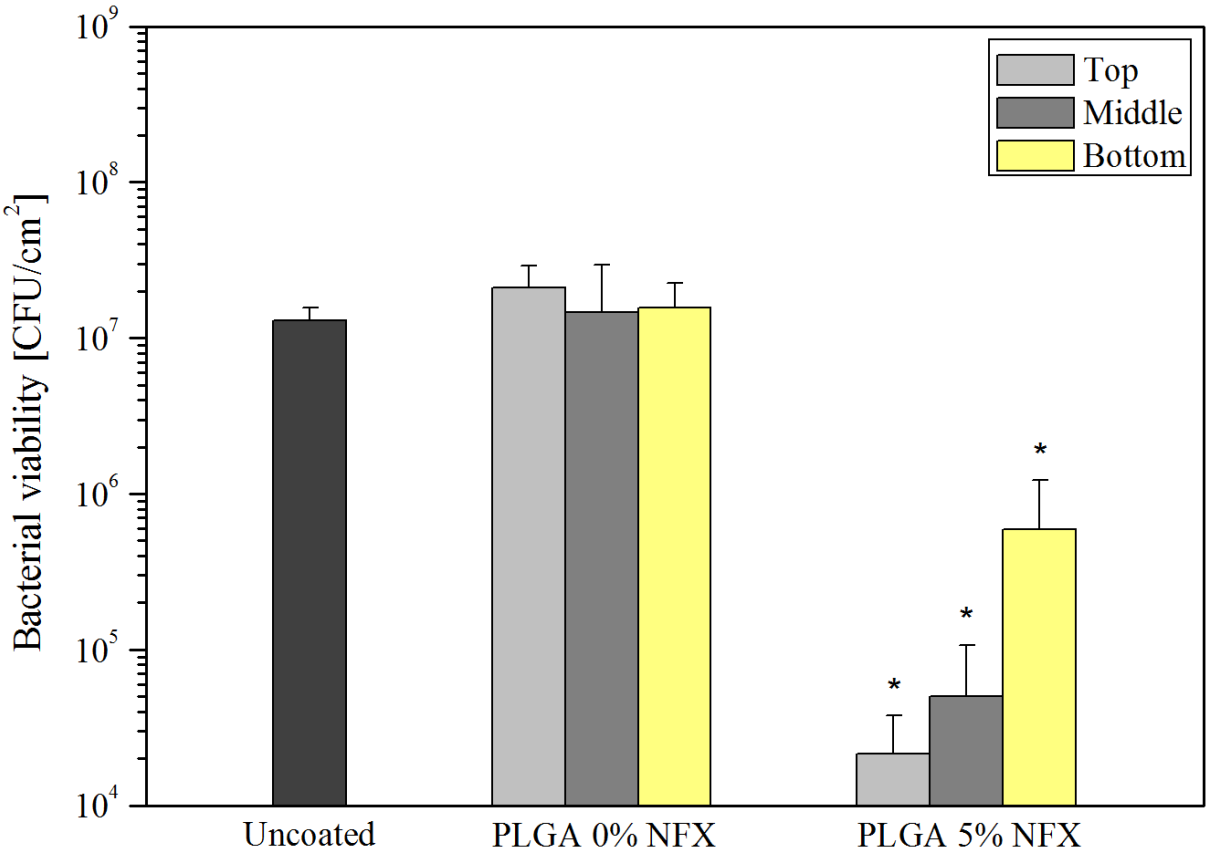

Figure 28 Evaluation of *in vitro* antibacterial activity of unloaded nanocoatings (PLGA 0% NFX) and norfloxacin loaded nanocoatings (PLGA 5% NFX). The titanium discs were fixed at three positions inside the electrostatic particle collector (i.e. Top, Middle and Bottom). Uncoated titanium discs were used as negative control. *E. coli* viability is presented as colony-forming unit per cm^2 of the titanium discs. The asterisk denotes probability values of $p < 0.05$ which were considered statistically significant.

3.2.2.5 *In vitro* biocompatibility

The nanocoating biocompatibility was evaluated using L929 cells as a standard sensitive cell line for assessing *in vitro* cytotoxicity [98, 154]. The cell growth on the surface of the Ti-discs was qualitatively and quantitatively studied over a period of 4 days.

First, the cells were visualized using fluorescence microscopy wherein the cell nucleus was counterstained with DAPI (**Figure 29**). All examined samples (i.e. uncoated Ti-discs, PLGA 0% NFX and PLGA 5% NFX) exhibited comparable results. A substantial increase in the cell number could be observed in the fluorescence micrographs of the Ti-discs after 96 h incubation where the cells covered most of the surface. These results gave only a visual confirmation of the nanocoating biocompatibility. Therefore, a quantitative assessment was still needed to understand the influence of norfloxacin loading and Ti-disc position inside the particle collector on the nanocoating cytotoxicity.

This was achieved by counting the number of cells adhered to the surface of Ti-discs after 24 h and 96 h incubation (**Figure 30**). Cell counting results of all samples after 24 h incubation were remarkably close with no significant difference between the coated (PLGA 0% NFX and PLGA 5% NFX) and the uncoated Ti-discs ($p > 0.05$). As seen previously in the visualization experiments, the cell number increased considerably in all samples after 96 h incubation. The number of the cells adhered to the coated (all nanocoatings except PLGA 5% NFX Top) and the uncoated Ti-discs was comparable ($p > 0.05$) indicating a good biocompatibility of the nanocoatings which did not exert any serious toxic effect that might influence the cell proliferation. These results are in agreement with previous studies which reported the use of PLGA nanoparticles as biocompatible coatings for medical implants [98, 115].

The only noticed cytotoxicity was with PLGA 5% NFX Top which resulted in suboptimal cell growth when compared to the uncoated Ti-discs ($p = 0.04$). This could be related to the high norfloxacin content in the nanocoating which might have adversely affected the cell proliferation. These findings indicated the importance of adjusting the drug content in the nanocoatings to achieve a balance between the desired therapeutic effect and the cytotoxicity.

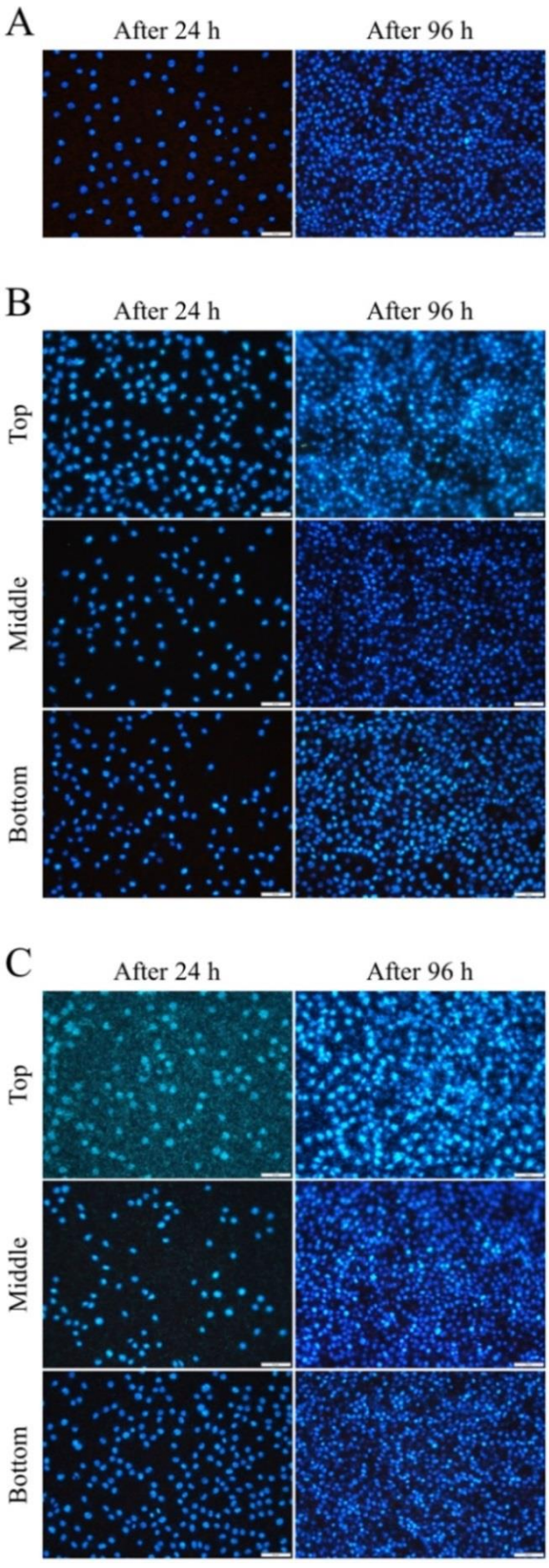

Figure 29 Fluorescence microscope images showing the growth of L929 cells on titanium discs after 24 h and 96 h incubation. A: uncoated discs, B: unloaded nanocoatings (PLGA 0% NFX), C: norfloxacin loaded nanocoatings (PLGA 5% NFX). The titanium discs were fixed at three positions inside the electrostatic particle collector (i.e. Top, Middle and Bottom). The cell nucleus (blue) was counterstained with DAPI. Scale bars represent 20 µm.

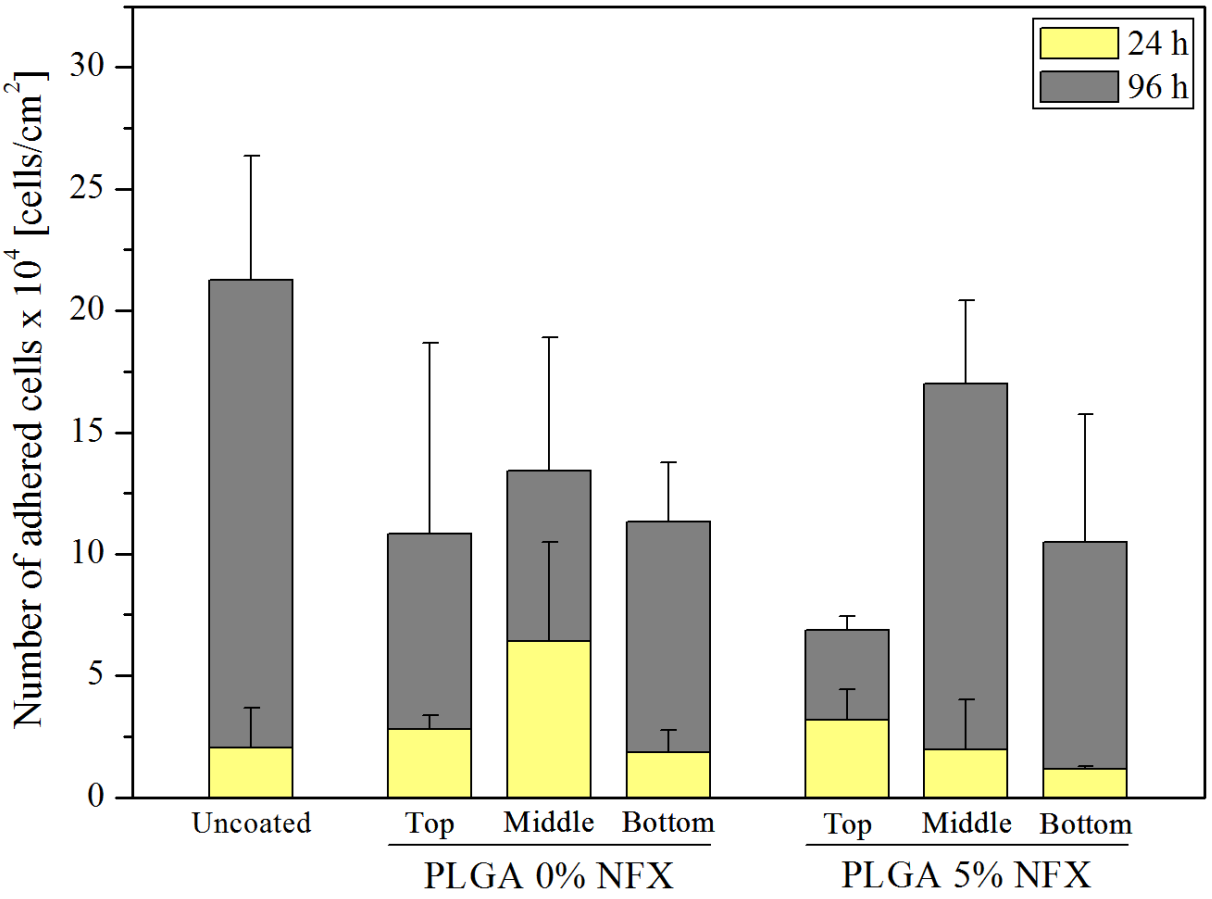

Figure 30 Number of cells adhered to the surface of the titanium discs after 24 h and 96 h incubation. Cell counting assay were performed using mouse fibroblasts (L929) where unloaded nanocoatings (i.e. PLGA 0% NFX) and norfloxacin loaded nanocoatings (PLGA 5% NFX) were tested. The titanium discs were fixed at three positions inside the electrostatic particle collector (i.e. Top, Middle and Bottom). Uncoated titanium discs were used as a negative control.

3.2.3 Coating of coronary stents

In the preliminary experiments, the preparation of nanoscale coatings using nano spray drying was developed on titanium plates which were used as a model material for dental implants. To investigate the potentials of this coating technique on a different type of medical implants, coronary stents made of stainless steel were used (Camouflage® coronary stent system, balloon diameter 2.5 mm, stent length 18 mm). The stent was fixed on the bottom part of the electrostatic particle collector (approx. 12 cm) and the nanocoatings were produced under the same conditions previously mentioned (**2.2.2.4**). PLGA was used as a model substance due to its interesting biodegradability and biocompatibility that made him one of the most commonly used polymers in the preparation of nanoparticle-eluting stents [155-157].

SEM micrographs of different parts of the coated stent showed a uniform coverage of the stent surface with PLGA nanocoatings even hard-to-reach areas (**Figure 31**). The produced particles formed a single layer and their morphology varied between spherical and irregular shape with a relatively wide particle size distribution.

These findings were to a great extent in agreement with those observed in dental implants, confirming the feasibility of utilizing nano spray drying as a promising approach for the coating and surface modification of different types of medical implants even those with challenging topography.

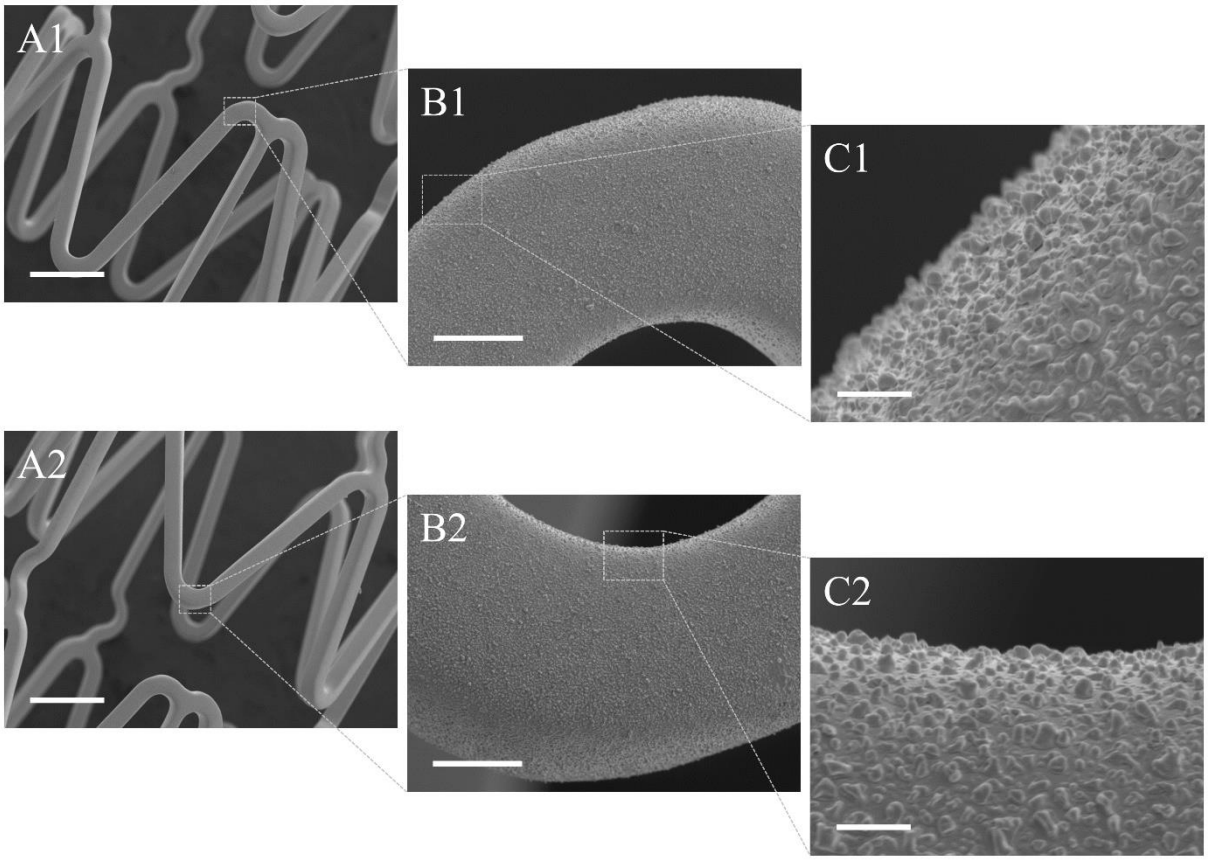

Figure 31 SEM micrographs of PLGA nanocoatings prepared using nano spray drying for the surface modification of coronary stent which was fixed approx. 12 cm towards the bottom part of the electrostatic particle collector. A: General view of the coated stent. B and C: Closer views showing detailed surface morphology of different parts of the coated stent. Scale bars represent A: 400 µm, B: 40 µm, C: 5 µm.

CHAPTER IV: Summary and outlook

4.1 Summary and outlook

Spray drying is a well-established method for the transformation of liquid formulations into dried particles. This technique is still gaining increasing interest due to its numerous advantages and wide range of applications. Furthermore, the emergence of nano spray drying in the last decade, took the capabilities of spray drying to the next level, especially in the field of nanoparticle production.

This thesis comprises detailed studies on the applications of spray drying in two important fields: pulmonary drug delivery and coating of medical implants.

The first objective was to employ spray drying in developing an inhalable photosensitizer loaded formulation for the bronchoscopic photodynamic therapy (**Figure 32**). Pulmonary administration of photosensitizers will help achieving both selective and completely non-invasive treatment against lung cancer. Thus, offering a promising alternative to the intravenous route and achieving better patient compliance.

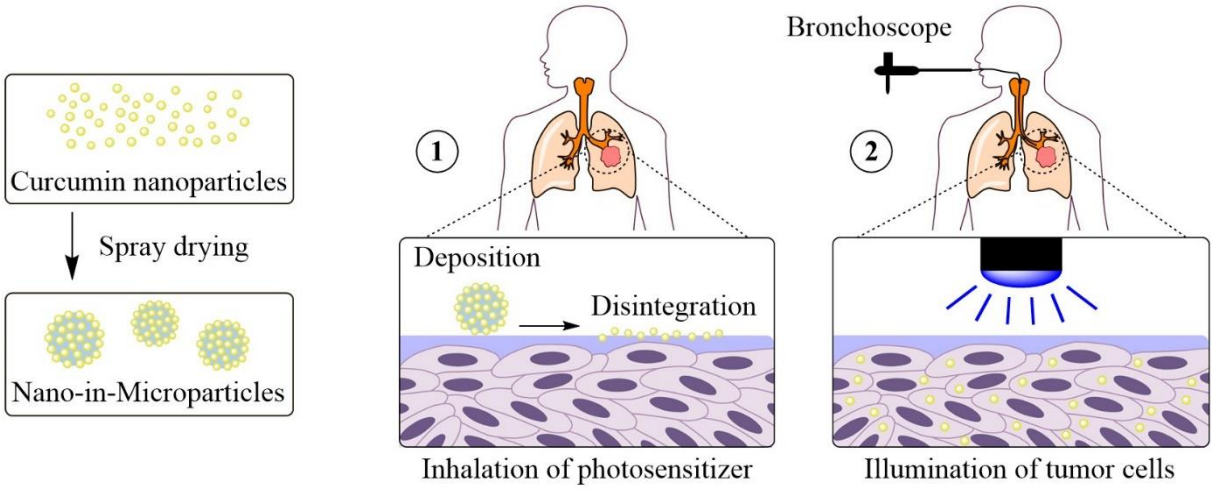

Figure 32 Graphical abstract summarizing the first objective of this thesis.

Curcumin was chosen as a naturally occurring photosensitizer; however, its low water solubility and poor bioavailability were the main drawbacks. Therefore, curcumin nanoparticles were prepared using the nanoprecipitation method to enhance its efficacy against tumor cells. According to dynamic light scattering measurements, curcumin nanoparticles had a homogenous size distribution and a particle size suitable for cellular uptake. The prepared nanoparticles exhibited a good hemocompatibility with minor hemolytic potential and no critical influence on coagulation time. *In vitro* irradiation experiments using

human lung epithelial carcinoma cells (A549) revealed an effective photoresponse of curcumin nanoparticles as they were able to destroy cancer cells upon activation with a light of specific wavelength using LED irradiating device. Moreover, curcumin nanoparticles exhibited a dose-dependent photocytotoxicity and the IC_{50} values of curcumin were directly dependent on the radiation fluence used.

Nano-in-Microparticles were produced by spray drying curcumin nanoparticles with mannitol, thereby transforming the nanoparticles into a dry powder for inhalation without experiencing drastic conditions. The aerodynamic properties of the Nano-in-Microparticles were investigated using the next generation impactor which revealed a large fine particle fraction and an appropriate mass median aerodynamic diameter for a sufficient deposition in the lungs. The Nano-in-Microparticles exhibited a good redispersibility and disintegrated into the original nanoparticles upon redispersion in aqueous medium. This can be attributed to mannitol which was used as the wall material embedding the nanoparticles to keep them intact during the drying process and facilitate their release from the microparticles. Langmuir monolayer experiments confirmed the compatibility of the Nano-in-Microparticles with the pulmonary surfactant which is an important prerequisite for the safe delivery of curcumin to its site of action in the lungs (i.e. tumor cells).

These results demonstrated the feasibility of spray drying for preparing inhalable drug carriers with promising potentials in the field of photodynamic therapy. *In vivo* studies should be the next step in order to evaluate the ability of these formulations to overcome the biological barriers of the lung. Furthermore, an accurate dosage assessment must be performed to achieve an effective therapy.

The second objective was to introduce nano spray drying as a novel technique for the preparation of nanoparticles of different biomaterials that are capable of modifying the surface structure of medical implants even those with a challenging topography (**Figure 33**)

The Nano Spray Dryer B-90 with its unique advanced features, facilitated particles production and implant coating in a single step omitting the need of additional drying or washing steps.

This newly developed coating technique will offer several advantages: a) the ability to produce particles in the submicron range from the pure substance solution without any additives (e.g. surfactants) or time-consuming complex modifications; b) very gentle process conditions that are suitable even for sensitive and thermolabile substances (e.g. enzymes, hormones and nucleic acids); c) this technique is highly efficient and cost-effective, since a small amount of the sample is needed to achieve the best results; d) the unique cylindrical

shape and functional principle of the particle collector enable a stable spatial surface coating, making upscaling easily applicable since it is possible to fix several implants on the particle collector to be coated simultaneously.

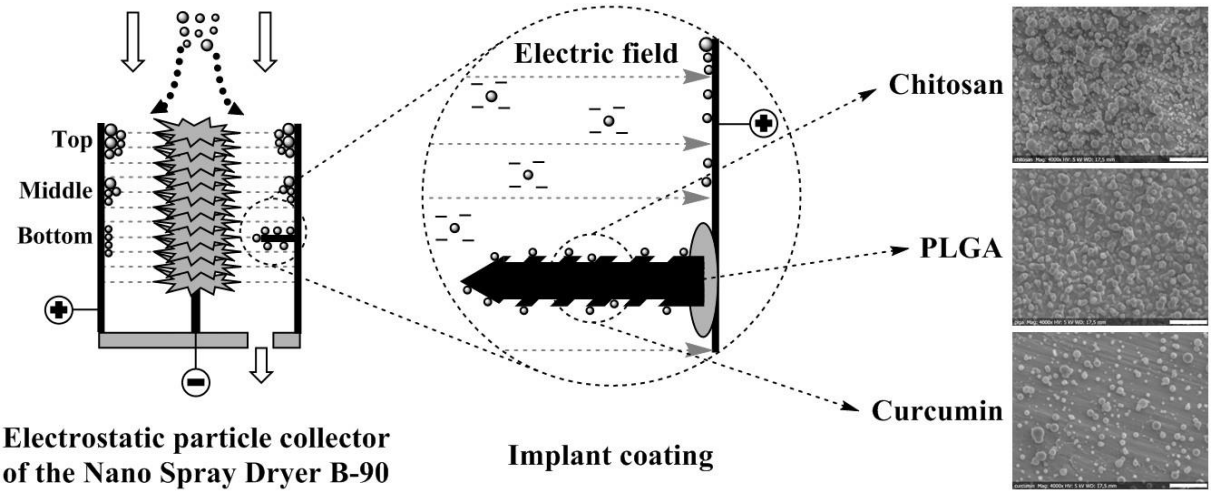

Figure 33 Graphical abstract summarizing the second objective of this thesis.

In this thesis, the wide range applicability of this coating technique has been demonstrated by testing three representative model substances, namely chitosan, poly(lactic-*co*-glycolic acid) and curcumin. Preliminary experiments were performed on titanium plates to optimize the process parameters, thereby achieving small particle size, narrow size distribution and complete coverage of the implants. The optimized parameters were thereafter successfully applied on dental implants and the coating homogeneity was confirmed using fluorescence microscopy. Scanning electron microscope images showed that most of the produced particles were in the submicron range and had a spherical shape with a smooth surface. Particle size analysis indicated the influence of the implant position inside the particle collector on the particle size distribution where the bottom part of the collector had the particles with the narrowest size distribution.

These findings paved the way for preparing biocompatible nanocoatings with antibacterial activity. The optimized process parameters from the preliminary experiments were applied on titanium discs, which were used as a model material for dental implants. The produced nanocoatings consisted of poly(lactic-*co*-glycolic acid) as a biodegradable polymer and norfloxacin as a model antibiotic. Scanning electron microscopy results of the nanocoatings were similar to those of preliminary experiments in terms of particle size distribution, morphology and surface structure which confirmed the reproducibility of this coating

technique. The nanocoatings exhibited a typical biphasic drug release profile with a burst release in the first 48 h, followed by sustained release phase until the end of experiment. Antibacterial activity of the nanocoatings was evaluated against *Escherichia coli* in two stages: first, qualitatively, using agar diffusion test which facilitated the examination of large number of samples, and then quantitatively, by counting the number of viable bacterial colonies adhered to the surface of the titanium discs. The antibacterial activity of the norfloxacin loaded nanocoatings was evident and could be observed either as zone of inhibitions (agar diffusion test) or as a significant reduction in the number of viable bacterial colonies (quantification experiments). This activity was directly dependent on the norfloxacin content in the nanocoatings which was influenced by the theoretical norfloxacin loading and the titanium disc position inside the particle collector. Finally, *in vitro* biocompatibility of the nanocoatings was investigated using mouse fibroblasts (L929) as a standard sensitive cell line for cytotoxicity assessment. Cell proliferation on the surface of the titanium discs was studied using fluorescence microscopy followed by cell counting assay. Both methods confirmed the biocompatibility of the examined nanocoatings which exhibited similar results when compared to the uncoated titanium discs.

Although nano spray drying has shown such interesting potentials for preparing novel nanocoatings, there is still room for improvement. This coating technique is still at its infancy and further optimization of the process parameters seems to be essential in order to produce nanocoatings capable of improving cell adhesion and exhibiting potent antibacterial activity even without the need of antibacterial agent.

4.2 Zusammenfassung und Ausblick

Die Sprühtrocknung ist eine gut etablierte Methode, um flüssige Formulierungen in getrocknete Partikel umzuwandeln und sie weckt aufgrund ihrer zahlreichen Vorteile und breiten Einsatzmöglichkeiten weiterhin großes Interesse. Zudem konnten innerhalb des letzten Jahrzehnts durch die Einführung der Nanosprühtrocknung die Anwendungsmöglichkeiten des Verfahrens der Sprühtrocknung auf eine ganz neue Ebene gehoben werden, vor allem die Herstellung von Nanopartikeln ist hier zu erwähnen.
Diese Doktorarbeit beinhaltet detaillierte Untersuchungen hinsichtlich der Anwendung der Sprühtrocknung in den beiden wichtigen Einsatzgebieten der pulmonalen Wirkstoffapplikation und der Beschichtung medizinischer Implantate.

Die erste Zielsetzung war die Entwicklung einer Photosensitizer beladenen inhalativen Formulierung mittels Sprühtrocknung, die für die bronchoskopische photodynamische Therapie eingesetzt werden soll. Die pulmonale Applikation eines Photosensitizers stellt hierbei sowohl eine selektive als auch eine nicht-invasive Behandlungsmöglichkeit für Lungenkrebs dar, wodurch eine intravenöse Gabe vermieden und eine bessere Komplianz des Patienten erzielt werden können.
Curcumin wurde als natürlich vorkommender Photosensitizer ausgewählt, obgleich dessen schlechte Wasserlöslichkeit und geringe Bioverfügbarkeit auf den ersten Blick große Nachteile darstellen. Aus diesem Grund erfolgte die Herstellung der Curcumin-Nanopartikel mithilfe der Nanopräzipitation, wodurch schlussendlich die Wirksamkeit des Photosensitizer gegenüber Tumorzellen erhöht werden konnte. Partikelgrößenmessungen, basierend auf dem Prinzip der dynamischen Lichtstreuung, zeigten eine für die zelluläre Aufnahme geeignete Partikelgröße mit homogener Größenverteilung. Darüber hinaus wiesen die Curcumin-Nanopartikel eine gute Hämokompatibilität mit geringem hämolytischen Potential und keinem nennenswerten Einfluss auf die Koagulationszeit auf. In vitro Bestrahlungsexperimente mit humanen Lungenepithelkarzinomzellen (A549) zeigten eine effektive Photoaktivierung der Curcumin-Nanopartikel, da eine Abtötung der Karzinomzellen bei Bestrahlung mit Licht einer spezifischen Wellenlänge mithilfe einer LED-Apparatur gezeigt werden konnte. Zum einen ergab sich für Curcumin-Nanopartikel eine dosisabhängige Phototoxizität und zum anderen zeigten die IC_{50}-Werte eine direkte Abhängigkeit von der aufgewendeten Fluenz.
Die Herstellung der Nano-in-Mikropartikel erfolgte, indem die Curcumin-Nanopartikel mit dem Trägerstoff Mannitol versprüht wurden, wodurch die Nanopartikel in ein zur Inhalation

geeignetes, trockenes Pulver übergingen, ohne dabei drastischen Bedingungen ausgesetzt zu werden. Die aerodynamischen Eigenschaften der Nano-in-Mikropartikel wurden mithilfe des Next Generation Impactors analysiert und offenbarten eine große Feinpartikelfraktion mit einem für die pulmonale Applikation geeigneten, massenbezogenen medianen aerodynamischen Durchmesser. Die Nano-in-Mikropartikel wiesen eine gute Redispergierbarkeit und eine geeignete Desintegration in die ursprüngliche nanopartikuläre Struktur nach Überführung in wässrige Medien auf. Diese Eigenschaft kann primär dem Mannitol zugeschrieben werden, welches als Wandmaterial die Nanopartikel umschließt, um sie während des Trocknungsprozesses gegenüber unterschiedlichen Prozessparametern zu schützen und ihre Freisetzung aus den Mikropartikeln weiterhin zu gewährleisten. Experimente mithilfe des Monoschicht-Membranmodells (Wilhelmy-Filmwaage) bestätigten die Kompatibilität der Nano-in-Mikropartikel mit dem pulmonalen Surfactant, was eine Grundvoraussetzung für den sicheren Transport von Curcumin zum Wirkort in der Lunge ist (z.B. Tumorzellen).

Diese Ergebnisse demonstrierten die Einsetzbarkeit der Sprühtrocknung zur der Herstellung inhalativer Arzneistoffträgersysteme mit erfolgversprechendem Potential im Bereich der photodynamischen Therapie. Als nächster Schritt sollten bei der Charakterisierung der Formulierungen bezüglich der Überwindung von biologischen Barrieren der Lunge in vivo Untersuchungen erfolgen. Darüber hinaus müsste eine Dosisanpassung für eine effektive Therapie durchgeführt werden.

Die zweite Zielsetzung war die Einführung der Nanosprühtrocknung als neue Methode zur Herstellung von Nanopartikeln aus unterschiedlichen Biomaterialien, die gleichzeitig in der Lage ist, Oberflächenstrukturen von medizinischen Implantaten selbst mit schwieriger Topographie erfolgreich zu modifizieren.

Der Nano-Sprühtrockner B-90, der sich durch eine fortschrittliche Funktionsweise und einen besonderen Aufbau auszeichnet, ermöglichte die Partikelproduktion und die Beschichtung von Implantaten in einem einzigen Schritt und machte zusätzliche Trocknungs- und Waschschritte überflüssig. Diese neue Beschichtungstechnik bietet viele Vorteile: a) Herstellung von Partikeln im Submikronbereich aus Lösungen von Reinsubstanzen ohne Zusatzstoffe (z.B. Surfactant) oder komplexe Modifikationen; b) sehr schonende Prozessbedingungen, die selbst für sensible und thermolabile Substanzen geeignet sind (z.B. Enzyme, Hormone und Nukleinsäuren); c) kostengünstiges und effizientes Verfahren, das nur eine geringe Probenmenge für ein gutes Resultat erfordert; d) einzigartiges

zylindrisches Design sowie außergewöhnliche Funktionsweise des Partikelkollektors ermöglichen ein erleichtertes Up-scaling des Verfahrens, da mehrere Implantate gleichzeitig auf dem Partikelkollektor aufgebracht werden können.

In dieser Doktorarbeit ist die breite Anwendbarkeit dieser Technik anhand von drei repräsentativen Modellsubstanzen, Chitosan, Poly(lactid-*co*-glycolid) und Curcumin belegt. Vorläufige Versuche wurden auf Titanplättchen durchgeführt, um die Prozessparameter so anzupassen, dass eine kleine Partikelgröße mit enger Größenverteilung sowie eine komplette Bedeckung der Implantatoberfläche erreicht werden konnten. Nachfolgend wurden die optimierten Prozessparameter auf Zahnimplantate übertragen und erzielten eine homogene, durch Fluoreszenzmikroskopie nachgewiesene Beschichtung. Aufnahmen mithilfe des Rasterelektronenmikroskops zeigten, dass die meisten hergestellten Partikel im Submikronbereich lagen und eine sphärische Form mit glatter Oberfläche aufwiesen. Die Partikelgrößenanalyse offenbarte den Einfluss der Implantatposition innerhalb des Partikelkollektors auf die Partikelgrößenverteilung, wobei der untere Abschnitt des Kollektors die engste Partikelgrößenverteilung aufwies.

Diese Ergebnisse stellten das Fundament für die Herstellung biokompatibler, antibakterieller Nanobeschichtungen dar. Die optimierten Prozessparameter aus den vorläufigen Versuchen fanden auf Titanplättchen Anwendung, die als Modellmaterial für Zahnimplantate dienten. Die hergestellten Nanobeschichtungen bestanden aus Poly(lactid-*co*-glycolid), einem bioabbaubaren Polymer, und Norfloxacin als Modellantibiotikum. Bildgebende Untersuchungen der Nanobeschichtungen mithilfe des Rasterelektronenmikroskops lieferten hinsichtlich der Partikelgrößenverteilung, Morphologie und Oberflächenstruktur Ergebnisse, wie sie bereits zuvor in den vorläufigen Versuchen festgestellt wurden, was die Reproduzierbarkeit der Beschichtungsmethode bestätigte. Die Nanobeschichtungen wiesen ein typisches zweiphasiges Freisetzungsprofil mit einer schnellen Freisetzung innerhalb der ersten 48 Stunden auf, der sich eine Freisetzung mit konstanter Geschwindigkeit bis zum Versuchsende anschloss. Die antibakterielle Wirkung der Nanobeschichtungen wurde gegen *Escherichia coli* in zwei Schritten evaluiert: Qualitativ durch den Agardiffusionstest, der es ermöglichte, eine große Probenanzahl zu analysieren, und quantitativ durch das Auszählen der Kolonie bildenden Einheiten, die auf der Oberfläche der Titanplättchen anhaften. Die antibakterielle Aktivität der mit Norfloxacin beladenen Nanobeschichtungen konnte als deutlich sichtbarer Hemmhof (Agardiffusionstest) sowie als signifikante Reduktion der Anzahl überlebender Bakterienkolonien identifiziert werden. Diese Aktivität war direkt vom Norfloxacin-Gehalt der Nanobeschichtung abhängig, der von der theoretischen Norfloxacin-

Beladung und der Position der Titanplättchen im Partikelkollektor beeinflusst wurde. Abschließend erfolgte die Untersuchung der in vitro Biokompatibilität der Nanobeschichtungen an Mausfibroblasten (L929), die als Standard für sensitive Zelllinien bei zytotoxischen Analysen gelten. Die Zellproliferation auf der Oberfläche der Titanplättchen wurde mithilfe eines Fluoreszenzmikroskops visualisiert und anschließend durch die Analyse der Zellzahl quantifiziert. Beide Methoden bestätigten die Biokompatibilität der untersuchten Nanobeschichtungen, welche ähnliche Ergebnisse wie die unbeschichteten Titanplättchen aufzeigten.

Obwohl die Nanosprühtrocknung ein solch vielversprechendes Potential bei der Herstellung neuer Nanobeschichtungen demonstrieren konnte, bleiben dennoch Verbesserungsmöglichkeiten offen. Diese Beschichtungsmethode befindet sich noch immer in ihrer Anfangsphase und benötigt daher eine fortwährende Optimierung der Prozessparameter. So sollen zukünftig Nanobeschichtungen entwickelt werden, die sowohl die Adhäsion körpereigener Zellen verbessern als auch eine potente antibakterielle Aktivität aufweisen. Die zugrundeliegende Wirkung sollte dabei lediglich auf die Struktur ihrer Oberfläche zurückzuführen sein und so den Einsatz antibiotisch wirksamer Substanzen überflüssig machen.

CHAPTER V: Appendix

5.1 References

[1] K. Masters, Spray drying handbook, 5th. ed., Longman Scientific & Technical, 1991.

[2] K. Cal, K. Sollohub, Spray drying technique. I: Hardware and process parameters, Journal of Pharmaceutical Sciences, 99 (2009) 575-586.

[3] A. Sosnik, K.P. Seremeta, Advantages and challenges of the spray-drying technology for the production of pure drug particles and drug-loaded polymeric carriers, Advances in Colloid and Interface Science, 223 (2015) 40-54.

[4] Training Papers Spray Drying, BÜCHI Labortechnik AG, Version B (2002) 1-19.

[5] J. Elversson, A. Millqvist-Fureby, G. Alderborn, U. Elofsson, Droplet and particle size relationship and shell thickness of inhalable lactose particles during spray drying, Journal of Pharmaceutical Sciences, 92 (2003) 900-910.

[6] A.L.R. Rattes, W.P. Oliveira, Spray drying conditions and encapsulating composition effects on formation and properties of sodium diclofenac microparticles, Powder Technology, 171 (2007) 7-14.

[7] A.B.D. Nandiyanto, K. Okuyama, Progress in developing spray-drying methods for the production of controlled morphology particles: From the nanometer to submicrometer size ranges, Advanced Powder Technology, 22 (2011) 1-19.

[8] J. Paluch Krzysztof, L. Tajber, I. Corrigan Owen, M. Healy Anne, Impact of process variables on the micromeritic and physicochemical properties of spray-dried porous microparticles, part I: introduction of a new morphology classification system, Journal of Pharmacy and Pharmacology, 64 (2012) 1570-1582.

[9] J. Paluch Krzysztof, L. Tajber, I. Amaro Maria, I. Corrigan Owen, M. Healy Anne, Impact of process variables on the micromeritic and physicochemical properties of spray-dried microparticles – Part II. Physicochemical characterisation of spray-dried materials, Journal of Pharmacy and Pharmacology, 64 (2012) 1583-1591.

[10] M. Maury, K. Murphy, S. Kumar, L. Shi, G. Lee, Effects of process variables on the powder yield of spray-dried trehalose on a laboratory spray-dryer, European Journal of Pharmaceutics and Biopharmaceutics, 59 (2005) 565-573.

[11] K. Ståhl, M. Claesson, P. Lilliehorn, H. Lindén, K. Bäckström, The effect of process variables on the degradation and physical properties of spray dried insulin intended for inhalation, International Journal of Pharmaceutics, 233 (2002) 227-237.

[12] L. Tajber, O.I. Corrigan, A.M. Healy, Spray drying of budesonide, formoterol fumarate and their composites—II. Statistical factorial design and in vitro deposition properties, International Journal of Pharmaceutics, 367 (2009) 86-96.

[13] M.I. Amaro, L. Tajber, O.I. Corrigan, A.M. Healy, Optimisation of spray drying process conditions for sugar nanoporous microparticles (NPMPs) intended for inhalation, International Journal of Pharmaceutics, 421 (2011) 99-109.

[14] P. Lebrun, F. Krier, J. Mantanus, H. Grohganz, M. Yang, E. Rozet, B. Boulanger, B. Evrard, J. Rantanen, P. Hubert, Design space approach in the optimization of the spray-drying process, European Journal of Pharmaceutics and Biopharmaceutics, 80 (2012) 226-234.

[15] C. Anish, A.K. Upadhyay, D. Sehgal, A.K. Panda, Influences of process and formulation parameters on powder flow properties and immunogenicity of spray dried polymer particles entrapping recombinant pneumococcal surface protein A, International Journal of Pharmaceutics, 466 (2014) 198-210.

[16] C. Bosquillon, P.G. Rouxhet, F. Ahimou, D. Simon, C. Culot, V. Préat, R. Vanbever, Aerosolization properties, surface composition and physical state of spray-dried protein powders, Journal of Controlled Release, 99 (2004) 357-367.

[17] N.R. Rabbani, P.C. Seville, The influence of formulation components on the aerosolisation properties of spray-dried powders, Journal of Controlled Release, 110 (2005) 130-140.

[18] R.P. Raffin, D.S. Jornada, M.I. Ré, A.R. Pohlmann, S.S. Guterres, Sodium pantoprazole-loaded enteric microparticles prepared by spray drying: Effect of the scale of production and process validation, International Journal of Pharmaceutics, 324 (2006) 10-18.

[19] T.P. Learoyd, J.L. Burrows, E. French, P.C. Seville, Chitosan-based spray-dried respirable powders for sustained delivery of terbutaline sulfate, European Journal of Pharmaceutics and Biopharmaceutics, 68 (2008) 224-234.

[20] H. Adi, P.M. Young, H.-K. Chan, H. Agus, D. Traini, Co-spray-dried mannitol–ciprofloxacin dry powder inhaler formulation for cystic fibrosis and chronic obstructive pulmonary disease, European Journal of Pharmaceutical Sciences, 40 (2010) 239-247.

[21] E.-Y. Xu, J. Guo, Y. Xu, H.-Y. Li, P.C. Seville, Influence of excipients on spray-dried powders for inhalation, Powder Technology, 256 (2014) 217-223.

[22] M.I. Amaro, L. Tajber, O.I. Corrigan, A.M. Healy, Co-Spray Dried Carbohydrate Microparticles: Crystallisation Delay/Inhibition and Improved Aerosolization Characteristics Through the Incorporation of Hydroxypropyl-β-cyclodextrin with Amorphous Raffinose or Trehalose, Pharmaceutical Research, 32 (2015) 180-195.

[23] M. Beck-Broichsitter, B. Strehlow, T. Kissel, Direct fractionation of spray-dried polymeric microparticles by inertial impaction, Powder Technology, 286 (2015) 311-317.

[24] B. Strehlow, U. Bakowsky, S.R. Pinnapireddy, J. Kusterer, G. Mielke, M. Keusgen, A Novel Microparticulate Formulation with Allicin In Situ Synthesis, Journal of Pharmaceutics & Drug Delivery Research, 5 (2016).

[25] F. Lyu, J.J. Liu, Y. Zhang, X.Z. Wang, Combined control of morphology and polymorph in spray drying of mannitol for dry powder inhalation, Journal of Crystal Growth, 467 (2017) 155-161.

[26] C. Bosquillon, C. Lombry, V. Préat, R. Vanbever, Influence of formulation excipients and physical characteristics of inhalation dry powders on their aerosolization performance, Journal of Controlled Release, 70 (2001) 329-339.

[27] A. Sommerwerk, J. Brüßler, J. Schäfer, L. Baginski, M. Bandulik, U. Bakowsky, Lipid coated chitosan microparticles as protein carriers, physica status solidi (c), 8 (2011) 1978-1984.

[28] S. Bianco, V. Caron, L. Tajber, O.I. Corrigan, L. Nolan, Y. Hu, A.M. Healy, Modification of the Solid-State Nature of Sulfathiazole and Sulfathiazole Sodium by Spray Drying, AAPS PharmSciTech, 13 (2012) 647-660.

[29] A. Gharsallaoui, G. Roudaut, O. Chambin, A. Voilley, R. Saurel, Applications of spray-drying in microencapsulation of food ingredients: An overview, Food Research International, 40 (2007) 1107-1121.

[30] K. Sollohub, K. Cal, Spray drying technique: II. Current applications in pharmaceutical technology, Journal of Pharmaceutical Sciences, 99 (2009) 587-597.

[31] M. Davis, G. Walker, Recent strategies in spray drying for the enhanced bioavailability of poorly water-soluble drugs, Journal of Controlled Release, 269 (2018) 110-127.

[32] J.S. Patton, P.R. Byron, Inhaling medicines: delivering drugs to the body through the lungs, Nature Reviews Drug Discovery, 6 (2007) 67-74.

[33] X. Murgia, C. de Souza Carvalho, C.-M. Lehr, Overcoming the pulmonary barrier: new insights to improve the efficiency of inhaled therapeutics, European Journal of Nanomedicine, 6 (2014) 157–169.

[34] Z. Liang, R. Ni, J. Zhou, S. Mao, Recent advances in controlled pulmonary drug delivery, Drug Discovery Today, 20 (2015) 380-389.

[35] J.S. Patton, C.S. Fishburn, J.G. Weers, The Lungs as a Portal of Entry for Systemic Drug Delivery, Proceedings of the American Thoracic Society, 1 (2004) 338-344.

[36] W. de Kruijf, C. Ehrhardt, Inhalation delivery of complex drugs—the next steps, Current Opinion in Pharmacology, 36 (2017) 52-57.

[37] J.S. Patton, J.D. Brain, L.A. Davies, J. Fiegel, M. Gumbleton, K.-J. Kim, M. Sakagami, R. Vanbever, C. Ehrhardt, The Particle has Landed—Characterizing the Fate of Inhaled Pharmaceuticals, Journal of Aerosol Medicine and Pulmonary Drug Delivery, 23 (2010) S-71-S-87.

[38] J. Kirch, M. Guenther, N. Doshi, U.F. Schaefer, M. Schneider, S. Mitragotri, C.-M. Lehr, Mucociliary clearance of micro- and nanoparticles is independent of size, shape and charge—an ex vivo and in silico approach, Journal of Controlled Release, 159 (2012) 128-134.

[39] J.G. Weers, T.E. Tarara, A.R. Clark, Design of fine particles for pulmonary drug delivery, Expert Opinion on Drug Delivery, 4 (2007) 297-313.

[40] G. Pilcer, K. Amighi, Formulation strategy and use of excipients in pulmonary drug delivery, International Journal of Pharmaceutics, 392 (2010) 1-19.

[41] P.C. Seville, T.P. Learoyd, H.Y. Li, I.J. Williamson, J.C. Birchall, Amino acid-modified spray-dried powders with enhanced aerosolisation properties for pulmonary drug delivery, Powder Technology, 178 (2007) 40-50.

[42] R. Vehring, Pharmaceutical Particle Engineering via Spray Drying, Pharmaceutical Research, 25 (2008) 999-1022.

[43] A.L. Feng, M.A. Boraey, M.A. Gwin, P.R. Finlay, P.J. Kuehl, R. Vehring, Mechanistic models facilitate efficient development of leucine containing microparticles for pulmonary drug delivery, International Journal of Pharmaceutics, 409 (2011) 156-163.

[44] O.N. Ógáin, J. Li, L. Tajber, O.I. Corrigan, A.M. Healy, Particle engineering of materials for oral inhalation by dry powder inhalers. I—Particles of sugar excipients (trehalose and raffinose) for protein delivery, International Journal of Pharmaceutics, 405 (2011) 23-35.

[45] F. Tewes, L. Tajber, O.I. Corrigan, C. Ehrhardt, A.M. Healy, Development and characterisation of soluble polymeric particles for pulmonary peptide delivery, European Journal of Pharmaceutical Sciences, 41 (2010) 337-352.

[46] L.M. Nolan, L. Tajber, B.F. McDonald, A.S. Barham, O.I. Corrigan, A.M. Healy, Excipient-free nanoporous microparticles of budesonide for pulmonary delivery, European Journal of Pharmaceutical Sciences, 37 (2009) 593-602.

[47] H.Y. Li, P.C. Seville, I.J. Williamson, J.C. Birchall, The use of amino acids to enhance the aerosolisation of spray-dried powders for pulmonary gene therapy, The Journal of Gene Medicine, 7 (2004) 343-353.

[48] J.C. Sung, B.L. Pulliam, D.A. Edwards, Nanoparticles for drug delivery to the lungs, Trends in Biotechnology, 25 (2007) 563-570.

[49] M. Paranjpe, C.C. Müller-Goymann, Nanoparticle-Mediated Pulmonary Drug Delivery: A Review, International Journal of Molecular Sciences, 15 (2014) 5852-5873.

[50] E. Rytting, J. Nguyen, X. Wang, T. Kissel, Biodegradable polymeric nanocarriers for pulmonary drug delivery, Expert Opinion on Drug Delivery, 5 (2008) 629-639.

[51] H.M. Mansour, Y.-S. Rhee, X. Wu, Nanomedicine in pulmonary delivery, International Journal of Nanomedicine, 4 (2009) 299-319.

[52] W. Yang, J.I. Peters, R.O. Williams, Inhaled nanoparticles—A current review, International Journal of Pharmaceutics, 356 (2008) 239-247.

[53] J. Zhang, L. Wu, H.-K. Chan, W. Watanabe, Formation, characterization, and fate of inhaled drug nanoparticles, Advanced Drug Delivery Reviews, 63 (2011) 441-455.

[54] P. Muralidharan, M. Malapit, E. Mallory, D. Hayes, H.M. Mansour, Inhalable nanoparticulate powders for respiratory delivery, Nanomedicine: Nanotechnology, Biology and Medicine, 11 (2015) 1189-1199.

[55] A. Bohr, C.A. Ruge, M. Beck-Broichsitter, Preparation of Nanoscale Pulmonary Drug Delivery Formulations by Spray Drying, in: D.G. Capco, Y. Chen (Eds.) Nanomaterial: Impacts on Cell Biology and Medicine, Springer Netherlands, Dordrecht, 2014, pp. 183-206.

[56] Y. Wang, M. Beck-Broichsitter, M. Yang, J. Rantanen, A. Bohr, Investigation of nanocarriers and excipients for preparation of nanoembedded microparticles, International Journal of Pharmaceutics, 526 (2017) 300-308.

[57] N. Anton, A. Jakhmola, T.F. Vandamme, Trojan Microparticles for Drug Delivery, Pharmaceutics, 4 (2012) 1-25.

[58] M.E. Ali, A. Lamprecht, Spray freeze drying for dry powder inhalation of nanoparticles, European Journal of Pharmaceutics and Biopharmaceutics, 87 (2014) 510-517.

[59] A.S. Silva, M.T. Tavares, A. Aguiar-Ricardo, Sustainable strategies for nano-in-micro particle engineering for pulmonary delivery, Journal of Nanoparticle Research, 16 (2014) 2602.

[60] M. Beck-Broichsitter, C. Schweiger, T. Schmehl, T. Gessler, W. Seeger, T. Kissel, Characterization of novel spray-dried polymeric particles for controlled pulmonary drug delivery, Journal of Controlled Release, 158 (2012) 329-335.

[61] T. Lebhardt, S. Roesler, H.P. Uusitalo, T. Kissel, Surfactant-free redispersible nanoparticles in fast-dissolving composite microcarriers for dry-powder inhalation, European Journal of Pharmaceutics and Biopharmaceutics, 78 (2011) 90-96.

[62] A. Grenha, B. Seijo, C. Serra, C. Remuñán-López, Chitosan Nanoparticle-Loaded Mannitol Microspheres: Structure and Surface Characterization, Biomacromolecules, 8 (2007) 2072-2079.

[63] R. Ni, J. Zhao, Q. Liu, Z. Liang, U. Muenster, S. Mao, Nanocrystals embedded in chitosan-based respirable swellable microparticles as dry powder for sustained pulmonary drug delivery, European Journal of Pharmaceutical Sciences, 99 (2017) 137-146.

[64] I. Takeuchi, Y. Tetsuka, T. Nii, M. Shinogase, K. Makino, Inhalable nanocomposite particles using amino acids with improved drug content and humidity resistance, Colloids and Surfaces A: Physicochemical and Engineering Aspects, 529 (2017) 387-393.

[65] I.M. El-Sherbiny, H.D.C. Smyth, Controlled Release Pulmonary Administration of Curcumin Using Swellable Biocompatible Microparticles, Molecular Pharmaceutics, 9 (2012) 269-280.

[66] P.H. Moghaddam, V. Ramezani, E. Esfandi, A. Vatanara, M. Nabi-Meibodi, M. Darabi, K. Gilani, A.R. Najafabadi, Development of a nano–micro carrier system for sustained pulmonary delivery of clarithromycin, Powder Technology, 239 (2013) 478-483.

[67] C. Gómez-Gaete, E. Fattal, L. Silva, M. Besnard, N. Tsapis, Dexamethasone acetate encapsulation into Trojan particles, Journal of Controlled Release, 128 (2008) 41-49.

[68] D.K. Jensen, L.B. Jensen, S. Koocheki, L. Bengtson, D. Cun, H.M. Nielsen, C. Foged, Design of an inhalable dry powder formulation of DOTAP-modified PLGA nanoparticles loaded with siRNA, Journal of Controlled Release, 157 (2012) 141-148.

[69] A. Grenha, B. Seijo, C. Remuñán-López, Microencapsulated chitosan nanoparticles for lung protein delivery, European Journal of Pharmaceutical Sciences, 25 (2005) 427-437.

[70] A. Grenha, C. Remuñán-López, E.L.S. Carvalho, B. Seijo, Microspheres containing lipid/chitosan nanoparticles complexes for pulmonary delivery of therapeutic proteins, European Journal of Pharmaceutics and Biopharmaceutics, 69 (2008) 83-93.

[71] C.A. Ruge, A. Bohr, M. Beck-Broichsitter, V. Nicolas, N. Tsapis, E. Fattal, Disintegration of nano-embedded microparticles after deposition on mucus: A mechanistic study, Colloids and Surfaces B: Biointerfaces, 139 (2016) 219-227.

[72] A. Torge, P. Grützmacher, F. Mücklich, M. Schneider, The influence of mannitol on morphology and disintegration of spray-dried nano-embedded microparticles, European Journal of Pharmaceutical Sciences, 104 (2017) 171-179.

[73] Z. Wang, J.L. Cuddigan, S.K. Gupta, S.A. Meenach, Nanocomposite microparticles (nCmP) for the delivery of tacrolimus in the treatment of pulmonary arterial hypertension, International Journal of Pharmaceutics, 512 (2016) 305-313.

[74] S. Al-Qadi, A. Grenha, D. Carrión-Recio, B. Seijo, C. Remuñán-López, Microencapsulated chitosan nanoparticles for pulmonary protein delivery: In vivo evaluation of insulin-loaded formulations, Journal of Controlled Release, 157 (2012) 383-390.

[75] A.A. McBride, D.N. Price, L.R. Lamoureux, A.A. Elmaoued, J.M. Vargas, N.L. Adolphi, P. Muttil, Preparation and Characterization of Novel Magnetic Nano-in-Microparticles for Site-Specific Pulmonary Drug Delivery, Molecular Pharmaceutics, 10 (2013) 3574-3581.

[76] N.M. Elbaz, I.A. Khalil, A.A. Abd-Rabou, I.M. El-Sherbiny, Chitosan-based nano-in-microparticle carriers for enhanced oral delivery and anticancer activity of propolis, International Journal of Biological Macromolecules, 92 (2016) 254-269.

[77] K. Kho, W.S. Cheow, R.H. Lie, K. Hadinoto, Aqueous re-dispersibility of spray-dried antibiotic-loaded polycaprolactone nanoparticle aggregates for inhaled anti-biofilm therapy, Powder Technology, 203 (2010) 432-439.

[78] M. Agnoletti, A. Bohr, K. Thanki, F. Wan, X. Zeng, J.P. Boetker, M. Yang, C. Foged, Inhalable siRNA-loaded nano-embedded microparticles engineered using microfluidics and spray drying, European Journal of Pharmaceutics and Biopharmaceutics, 120 (2017) 9-21.

[79] N. Tsapis, D. Bennett, B. Jackson, D.A. Weitz, D.A. Edwards, Trojan particles: Large porous carriers of nanoparticles for drug delivery, Proceedings of the National Academy of Sciences, 99 (2002) 12001–12005.

[80] K. Hadinoto, K. Zhu, R.B.H. Tan, Drug release study of large hollow nanoparticulate aggregates carrier particles for pulmonary delivery, International Journal of Pharmaceutics, 341 (2007) 195-206.

[81] F. Tewes, C. Ehrhardt, A.M. Healy, Superparamagnetic iron oxide nanoparticles (SPIONs)-loaded Trojan microparticles for targeted aerosol delivery to the lung, European Journal of Pharmaceutics and Biopharmaceutics, 86 (2014) 98-104.

[82] J.O.H. Sham, Y. Zhang, W.H. Finlay, W.H. Roa, R. Löbenberg, Formulation and characterization of spray-dried powders containing nanoparticles for aerosol delivery to the lung, International Journal of Pharmaceutics, 269 (2004) 457-467.

[83] C. Smith, Microscopy: Two microscopes are better than one, Nature, 492 (2012) 293-297.

[84] C. Tscheka, M. Hittinger, C.-M. Lehr, N. Schneider-Daum, M. Schneider, Macrophage uptake of cylindrical microparticles investigated with correlative microscopy, European Journal of Pharmaceutics and Biopharmaceutics, 95 (2015) 151-155.

[85] X. Li, N. Anton, C. Arpagaus, F. Belleteix, T.F. Vandamme, Nanoparticles by spray drying using innovative new technology: The Büchi Nano Spray Dryer B-90, Journal of Controlled Release, 147 (2010) 304-310.

[86] S.H. Lee, D. Heng, W.K. Ng, H.-K. Chan, R.B.H. Tan, Nano spray drying: A novel method for preparing protein nanoparticles for protein therapy, International Journal of Pharmaceutics, 403 (2011) 192-200.

[87] K. Bürki, I. Jeon, C. Arpagaus, G. Betz, New insights into respirable protein powder preparation using a nano spray dryer, International Journal of Pharmaceutics, 408 (2011) 248-256.

[88] D. Heng, S.H. Lee, W.K. Ng, R.B.H. Tan, The nano spray dryer B-90, Expert Opinion on Drug Delivery, 8 (2011) 965-972.

[89] N. Schafroth, C. Arpagaus, U.Y. Jadhav, S. Makne, D. Douroumis, Nano and microparticle engineering of water insoluble drugs using a novel spray-drying process, Colloids and Surfaces B: Biointerfaces, 90 (2012) 8-15.

[90] C. Arpagaus, A Novel Laboratory-Scale Spray Dryer to Produce Nanoparticles, Drying Technology, 30 (2012) 1113-1121.

[91] K. Baba, K. Nishida, Calpain inhibitor nanocrystals prepared using Nano Spray Dryer B-90, Nanoscale Research Letters, 7 (2012) 436.

[92] C. Arpagaus, A. Collenberg, D. Rütti, E. Assadpour, S.M. Jafari, Nano spray drying for encapsulation of pharmaceuticals, International Journal of Pharmaceutics, 546 (2018) 194-214.

[93] Nano Spray Dryer B-90, Technical data sheet, B-90 Data Sheet en 1311 A, BÜCHI Labortechnik AG, 1-9.

[94] C. Arpagaus, N. Schafroth, M. Meuri, Laboratory scale spray drying of lactose: a review, best@buchi Information Bulletin, Number 57/2010 (2010).

[95] C. Arpagaus, P. John, A. Collenberg, D. Rütti, 10 - Nanocapsules formation by nano spray drying A2 - Jafari, Seid Mahdi, in: Nanoencapsulation Technologies for the Food and Nutraceutical Industries, Academic Press, 2017, pp. 346-401.

[96] M. Beck-Broichsitter, I.E. Paulus, A. Greiner, T. Kissel, Modified vibrating-mesh nozzles for advanced spray-drying applications, European Journal of Pharmaceutics and Biopharmaceutics, 92 (2015) 96-101.

[97] M.M. Yallapu, B.K. Gupta, M. Jaggi, S.C. Chauhan, Fabrication of curcumin encapsulated PLGA nanoparticles for improved therapeutic effects in metastatic cancer cells, Journal of Colloid and Interface Science, 351 (2010) 19-29.

[98] B.M. Al Meslmani, G.F. Mahmoud, U. Bakowsky, Immobilization and characterization of PLGA nanoparticles on polyethylene terephthalate cardiovascular grafts for local drug

therapy of associated graft complications, Journal of Drug Delivery Science and Technology, 47 (2018) 144-150.

[99] S.R. Pinnapireddy, L. Duse, B. Strehlow, J. Schäfer, U. Bakowsky, Composite liposome-PEI/nucleic acid lipopolyplexes for safe and efficient gene delivery and gene knockdown, Colloids and Surfaces B: Biointerfaces, 158 (2017) 93-101.

[100] B.C. Evans, C.E. Nelson, S.S. Yu, K.R. Beavers, A.J. Kim, H. Li, H.M. Nelson, T.D. Giorgio, C.L. Duvall, Ex Vivo Red Blood Cell Hemolysis Assay for the Evaluation of pH-responsive Endosomolytic Agents for Cytosolic Delivery of Biomacromolecular Drugs, Journal of Visualized Experiments : JoVE, (2013) 50166.

[101] L. Duse, S.R. Pinnapireddy, B. Strehlow, J. Jedelská, U. Bakowsky, Low level LED photodynamic therapy using curcumin loaded tetraether liposomes, European Journal of Pharmaceutics and Biopharmaceutics, 126 (2018) 233-241.

[102] U. Bakowsky, W. Rettig, G. Bendas, J. Vogel, H. Bakowsky, C. Harnagea, U. Rothe, Characterization of the interactions between various hexadecylmannoside-phospholipid model membranes with the lectin Concanavalin A, Physical Chemistry Chemical Physics, 2 (2000) 4609-4614.

[103] M. Dash, F. Chiellini, R.M. Ottenbrite, E. Chiellini, Chitosan—A versatile semi-synthetic polymer in biomedical applications, Progress in Polymer Science, 36 (2011) 981-1014.

[104] E. Baghdan, S.R. Pinnapireddy, B. Strehlow, K.H. Engelhardt, J. Schäfer, U. Bakowsky, Lipid coated chitosan-DNA nanoparticles for enhanced gene delivery, International Journal of Pharmaceutics, 535 (2018) 473-479.

[105] F. Danhier, E. Ansorena, J.M. Silva, R. Coco, A. Le Breton, V. Préat, PLGA-based nanoparticles: An overview of biomedical applications, Journal of Controlled Release, 161 (2012) 505-522.

[106] F. Ungaro, I. d' Angelo, A. Miro, I. La Rotonda Maria, F. Quaglia, Engineered PLGA nano- and micro-carriers for pulmonary delivery: challenges and promises, Journal of Pharmacy and Pharmacology, 64 (2012) 1217-1235.

[107] F. Wan, M. Yang, Design of PLGA-based depot delivery systems for biopharmaceuticals prepared by spray drying, International Journal of Pharmaceutics, 498 (2016) 82-95.

[108] O. Naksuriya, S. Okonogi, R.M. Schiffelers, W.E. Hennink, Curcumin nanoformulations: A review of pharmaceutical properties and preclinical studies and clinical data related to cancer treatment, Biomaterials, 35 (2014) 3365-3383.

[109] S.R. Pinnapireddy, L. Duse, D. Akbari, U. Bakowsky, Photo-Enhanced Delivery of Genetic Material Using Curcumin Loaded Composite Nanocarriers, Clinics in Oncology, 2 (2017).

[110] L. Duse, E. Baghdan, S.R. Pinnapireddy, K.H. Engelhardt, J. Jedelská, J. Schaefer, P. Quendt, U. Bakowsky, Preparation and Characterization of Curcumin Loaded Chitosan Nanoparticles for Photodynamic Therapy, physica status solidi (a), 215 (2017) 1700709.

[111] A. Demont, Nano Spray Drying Booklet Theory & Applications, BÜCHI Labortechnik AG, (2017) 1-40.

[112] B.M. Al Meslmani, G.F. Mahmoud, F.O. Sommer, M.D. Lohoff, U. Bakowsky, Multifunctional network-structured film coating for woven and knitted polyethylene terephthalate against cardiovascular graft-associated infections, International Journal of Pharmaceutics, 485 (2015) 270-276.

[113] M. Balouiri, M. Sadiki, S.K. Ibnsouda, Methods for in vitro evaluating antimicrobial activity: A review, Journal of Pharmaceutical Analysis, 6 (2016) 71-79.

[114] B.M. Al Meslmani, G.F. Mahmoud, T. Leichtweiß, B. Strehlow, F.O. Sommer, M.D. Lohoff, U. Bakowsky, Covalent immobilization of lysozyme onto woven and knitted crimped polyethylene terephthalate grafts to minimize the adhesion of broad spectrum pathogens, Materials Science and Engineering: C, 58 (2016) 78-87.

[115] B.M. Al Meslmani, G.F. Mahmoud, U. Bakowsky, Development of expanded polytetrafluoroethylene cardiovascular graft platform based on immobilization of poly lactic-co-glycolic acid nanoparticles using a wet chemical modification technique, International Journal of Pharmaceutics, 529 (2017) 238-244.

[116] S.B. Brown, E.A. Brown, I. Walker, The present and future role of photodynamic therapy in cancer treatment, The Lancet Oncology, 5 (2004) 497-508.

[117] Á. Juarranz, P. Jaén, F. Sanz-Rodríguez, J. Cuevas, S. González, Photodynamic therapy of cancer. Basic principles and applications, Clinical and Translational Oncology, 10 (2008) 148-154.

[118] J.M. Vergnon, R.M. Huber, K. Moghissi, Place of cryotherapy, brachytherapy and photodynamic therapy in therapeutic bronchoscopy of lung cancers, European Respiratory Journal, 28 (2006) 200–218.

[119] E. Paszko, C. Ehrhardt, M.O. Senge, D.P. Kelleher, J.V. Reynolds, Nanodrug applications in photodynamic therapy, Photodiagnosis and Photodynamic Therapy, 8 (2011) 14-29.

[120] G. Mahmoud, J. Jedelská, B. Strehlow, U. Bakowsky, Bipolar tetraether lipids derived from thermoacidophilic archaeon Sulfolobus acidocaldarius for membrane stabilization of chlorin e6 based liposomes for photodynamic therapy, European Journal of Pharmaceutics and Biopharmaceutics, 95 (2015) 88-98.

[121] G. Mahmoud, J. Jedelská, B. Strehlow, S. Omar, M. Schneider, U. Bakowsky, Photo-responsive tetraether lipids based vesicles for prophyrin mediated vascular targeting and direct phototherapy, Colloids and Surfaces B: Biointerfaces, 159 (2017) 720-728.

[122] S. Zorofchian Moghadamtousi, H. Abdul Kadir, P. Hassandarvish, H. Tajik, S. Abubakar, K. Zandi, A Review on Antibacterial, Antiviral, and Antifungal Activity of Curcumin, BioMed Research International, 2014 (2014) 12.

[123] J.P. Rao, K.E. Geckeler, Polymer nanoparticles: Preparation techniques and size-control parameters, Progress in Polymer Science, 36 (2011) 887-913.

[124] M. Gaumet, A. Vargas, R. Gurny, F. Delie, Nanoparticles for drug delivery: The need for precision in reporting particle size parameters, European Journal of Pharmaceutics and Biopharmaceutics, 69 (2008) 1-9.

[125] K.D. Pagana, T.J. Pagana, Mosby's Manual of Diagnostic and Laboratory Tests-E-Book, Elsevier Health Sciences, 2013.

[126] G.J. Pillai, M.M. Greeshma, D. Menon, Impact of poly(lactic-co-glycolic acid) nanoparticle surface charge on protein, cellular and haematological interactions, Colloids and Surfaces B: Biointerfaces, 136 (2015) 1058-1066.

[127] D.E.J.G.J. Dolmans, D. Fukumura, R.K. Jain, Photodynamic therapy for cancer, Nature Reviews Cancer, 3 (2003) 380–387.

[128] K. Moghissi, Role of bronchoscopic photodynamic therapy in lung cancer management, Current Opinion in Pulmonary Medicine, 10 (2004) 256-260.

[129] D. van Straten, V. Mashayekhi, S.H. de Bruijn, S. Oliveira, J.D. Robinson, Oncologic Photodynamic Therapy: Basic Principles, Current Clinical Status and Future Directions, Cancers, 9 (2017) 19.

[130] A.M. Healy, M.I. Amaro, K.J. Paluch, L. Tajber, Dry powders for oral inhalation free of lactose carrier particles, Advanced Drug Delivery Reviews, 75 (2014) 32-52.

[131] Y.Y. Zuo, R.A.W. Veldhuizen, A.W. Neumann, N.O. Petersen, F. Possmayer, Current perspectives in pulmonary surfactant — Inhibition, enhancement and evaluation, Biochimica et Biophysica Acta (BBA) - Biomembranes, 1778 (2008) 1947-1977.

[132] N. Kang, Z. Policova, G. Bankian, M.L. Hair, Y.Y. Zuo, A.W. Neumann, E.J. Acosta, Interaction between chitosan and bovine lung extract surfactants, Biochimica et Biophysica Acta (BBA) - Biomembranes, 1778 (2008) 291-302.

[133] S. Newman, P. Anderson, P. Byron, R. Dalby, J. Peart, Respiratory Drug Delivery: Essential Theory and Practice, RDD Online / Virginia Commonwealth University, Richmond USA, 2009.

[134] R. Wüstneck, J. Perez-Gil, N. Wüstneck, A. Cruz, V.B. Fainerman, U. Pison, Interfacial properties of pulmonary surfactant layers, Advances in Colloid and Interface Science, 117 (2005) 33-58.

[135] M.R. Rodríguez Niño, A. Lucero, J.M. Rodríguez Patino, Relaxation phenomena in phospholipid monolayers at the air–water interface, Colloids and Surfaces A: Physicochemical and Engineering Aspects, 320 (2008) 260-270.

[136] E. Dayyoub, C. Hobler, P. Nonnweiler, M. Keusgen, U. Bakowsky, Nanostructured medical device coatings based on self-assembled poly(lactic-co-glycolic acid) nanoparticles, Materials Science and Engineering: C, 33 (2013) 3018-3024.

[137] S. Ferraris, S. Spriano, Antibacterial titanium surfaces for medical implants, Materials Science and Engineering: C, 61 (2016) 965-978.

[138] J. Raphel, M. Holodniy, S.B. Goodman, S.C. Heilshorn, Multifunctional coatings to simultaneously promote osseointegration and prevent infection of orthopaedic implants, Biomaterials, 84 (2016) 301-314.

[139] R. Singh, J.W. Lillard, Nanoparticle-based targeted drug delivery, Experimental and Molecular Pathology, 86 (2009) 215-223.

[140] K. Schmid, C. Arpagaus, W. Friess, Evaluation of the Nano Spray Dryer B-90 for pharmaceutical applications, Pharmaceutical Development and Technology, 16 (2011) 287-294.

[141] R.C. Suryaprakash, F.P. Lohmann, M. Wagner, B. Abel, A. Varga, Spray drying as a novel and scalable fabrication method for nanostructured CsH2PO4, Pt-thin-film composite electrodes for solid acid fuel cells, RSC Advances, 4 (2014) 60429-60436.

[142] E. Dayyoub, M. Frant, S.R. Pinnapireddy, K. Liefeith, U. Bakowsky, Antibacterial and anti-encrustation biodegradable polymer coating for urinary catheter, International Journal of Pharmaceutics, 531 (2017) 205-214.

[143] P.C. Appelbaum, P.A. Hunter, The fluoroquinolone antibacterials: past, present and future perspectives, International Journal of Antimicrobial Agents, 16 (2000) 5-15.

[144] B.S. Seitz, N. Plenagl, M. Raschpichler, H. Vögeling, M. Wojcik, S.R. Pinnapireddy, J. Brüßler, U. Bakowsky, Nanoparticles and Liposomes for the Surface Modification of Implants: A Comparative Study of Spraying and Dipping Techniques, physica status solidi (a), 215 (2018) 1700847.

[145] H. Vögeling, L. Duse, B.S. Seitz, N. Plenagl, M. Wojcik, S.R. Pinnapireddy, U. Bakowsky, Multilayer Bacteriostatic Coating for Surface Modified Titanium Implants, physica status solidi (a), 215 (2018) 1700844.

[146] A. Kumari, S.K. Yadav, S.C. Yadav, Biodegradable polymeric nanoparticles based drug delivery systems, Colloids and Surfaces B: Biointerfaces, 75 (2010) 1-18.

[147] H. Gasmi, F. Siepmann, M.C. Hamoudi, F. Danede, J. Verin, J.F. Willart, J. Siepmann, Towards a better understanding of the different release phases from PLGA microparticles: Dexamethasone-loaded systems, International Journal of Pharmaceutics, 514 (2016) 189-199.

[148] S. Fredenberg, M. Wahlgren, M. Reslow, A. Axelsson, The mechanisms of drug release in poly(lactic-co-glycolic acid)-based drug delivery systems—A review, International Journal of Pharmaceutics, 415 (2011) 34-52.

[149] C. Wischke, S.P. Schwendeman, Principles of encapsulating hydrophobic drugs in PLA/PLGA microparticles, International Journal of Pharmaceutics, 364 (2008) 298-327.

[150] N. Badri Viswanathan, S.S. Patil, J.K. Pandil, A.K. Lele, M.G. Kulkarni, R.A. Mashelkar, Morphological changes in degrading PLGA and P(DL)LA microspheres: implications for the design of controlled release systems, Journal of Microencapsulation, 18 (2001) 783-800.

[151] W. Friess, M. Schlapp, Release mechanisms from gentamicin loaded poly(lactic-co-glycolic acid) (PLGA) microparticles, Journal of Pharmaceutical Sciences, 91 (2002) 845-855.

[152] J. Panyam, M.M. Dali, S.K. Sahoo, W. Ma, S.S. Chakravarthi, G.L. Amidon, R.J. Levy, V. Labhasetwar, Polymer degradation and in vitro release of a model protein from poly(d,l-lactide-co-glycolide) nano- and microparticles, Journal of Controlled Release, 92 (2003) 173-187.

[153] L.B. Reller, M. Weinstein, J.H. Jorgensen, M.J. Ferraro, Antimicrobial Susceptibility Testing: A Review of General Principles and Contemporary Practices, Clinical Infectious Diseases, 49 (2009) 1749-1755.

[154] ISO 10993-5:2009(en) Biological evaluation of medical devices — Part 5: Tests for in vitro cytotoxicity, (2009).

[155] J.-M. Lü, X. Wang, C. Marin-Muller, H. Wang, P.H. Lin, Q. Yao, C. Chen, Current advances in research and clinical applications of PLGA-based nanotechnology, Expert Review of Molecular Diagnostics, 9 (2009) 325-341.

[156] K. Nakano, K. Egashira, S. Masuda, K. Funakoshi, G. Zhao, S. Kimura, T. Matoba, K. Sueishi, Y. Endo, Y. Kawashima, K. Hara, H. Tsujimoto, R. Tominaga, K. Sunagawa, Formulation of Nanoparticle-Eluting Stents by a Cationic Electrodeposition Coating Technology, JACC: Cardiovascular Interventions, 2 (2009) 277-283.

[157] A.S. Puranik, E.R. Dawson, N.A. Peppas, Recent advances in drug eluting stents, International Journal of Pharmaceutics, 441 (2013) 665-679.

5.2 Lists

5.2.1 List of abbreviations

ACE	Acetone
ACN	Acetonitrile
aPTT	Activated partial thromboplastin time
ATCC®	American Type Culture Collection
CFU	Colony-forming unit
CLEM	Correlative light and electron microscope
CLSM	Confocal laser scanning microscope
DAPI	4',6-diamidino-2-phenylindole
DLS	Dynamic light scattering
DMEM	Dulbecco's modified Eagle's medium
DMSO	Dimethyl sulfoxide
DPBS	Dulbecco's phosphate-buffered saline
DSMZ	Deutsche Sammlung von Mikroorganismen und Zellkulturen
EBSS	Earle's balanced salt solution
EE	Encapsulation efficiency
ETOH	Ethanol
FDA	Food and Drug Administration
FPF	Fine particle fraction
GSD	Geometric standard deviation
LDV	Laser Doppler velocimetry
LED	Light-emitting diode
MHB	Mueller Hinton Broth
MMAD	Mass median aerodynamic diameter
MTT	3-(4,5-dimethylthiazol-2-yl)-2,5-diphenyltetrazolium bromide
NaOAc	Sodium acetate
NFX	Norfloxacin
NGI	Next generation impactor
NiMps	Nano-in-Microparticles
PBS	Phosphate-buffered saline
PdI	Polydispersity index
PDT	Photodynamic therapy

PLGA	Poly(lactic-*co*-glycolic acid)
PLGA.CUR.NPs	Curcumin loaded nanoparticles
PLGA.NPs	Unloaded nanoparticles
PVA	Poly(vinyl alcohol)
RH	Relative humidity
SEM	Scanning electron microscope
siRNA	Small interfering ribonucleic acid
T_g	Glass transition temperature

5.2.2 List of figures

Figure 1 SEM micrographs showing the influence of nanoparticles:matrix mass ratio on the morphology of NiMps 10
Figure 2 The Nano Spray Dryer B-90 11
Figure 3 Diagram showing the difference in the functional principle between the Nano Spray Dryer B-90 (left) and the Mini Spray Dryer B-290 (right) 12
Figure 4 Scheme of preparation of curcumin loaded PLGA nanoparticles 22
Figure 5 Illustration of the functional principle of the Nano Spray Dryer B-90 29
Figure 6 Close-up images from inside the electrostatic particle collector 31
Figure 7 Illustration of the agar diffusion test 33
Figure 8 Hemocompatibility experiments 38
Figure 9 Evaluation of the photocytotoxicity 39
Figure 10 Fitted dose-response photocytotoxicity curves 40
Figure 11 CLSM images of A549 cells 41
Figure 12 SEM micrographs showing the morphology 43
Figure 13 CLSM images showing the morphology of the Nano-in-Microparticles 44
Figure 14 The distribution of Nano-in-Microparticles on different parts of the next generation impactor 45
Figure 15 π-t (surface pressure-time) isotherms 47
Figure 16 SEM micrographs showing the coating of titanium plates 50
Figure 17 Particle size analysis of the SEM micrographs of titanium plates 51
Figure 18 Stereomicroscope images (left) of the dental implants (apical view) 52
Figure 19 SEM micrographs showing successful coating of the dental implants 53
Figure 20 Particle size analysis of the SEM micrographs of dental implants 53
Figure 21 SEM micrographs of coated titanium discs showing the morphology 55
Figure 22 Particle size analysis based on the SEM micrographs 56
Figure 23 *In vitro* release profile of norfloxacin over a period of 15 days in PBS 58
Figure 24 *In vitro* release profile of norfloxacin over a period of 15 days in PBS 59
Figure 25 SEM micrographs of the unloaded nanocoatings (PLGA 0% NFX) and norfloxacin loaded nanocoatings (PLGA 5% NFX) after 15 days incubation at 37 °C in PBS (pH 7.4) ... 61
Figure 26 Summary of the results of agar diffusion test 63
Figure 27 Graphical representation of the relationship between the amount of norfloxacin per cm^2 of the nanocoating (bars) and the diameter of the zone of inhibition (dots) 64
Figure 28 Evaluation of *in vitro* antibacterial activity 65

Figure 29 Fluorescence microscope images showing the growth of L929 cells 67
Figure 30 Number of cells adhered to the surface of the titanium discs 68
Figure 31 SEM micrographs of PLGA nanocoatings prepared using nano spray drying 70
Figure 32 Graphical abstract summarizing the first objective of this thesis. 72
Figure 33 Graphical abstract summarizing the second objective of this thesis. 74

5.2.3 List of tables

Table 1 Spray drying process parameters 3
Table 2 Literature review of the most common characterizations of spray dried particles 5
Table 3 Comparison between the Nano Spray Dryer B-90 and the Mini Spray Dryer B-290 12
Table 4 Summary of spray drying parameters 29
Table 5 Particle size distribution, ζ-potential and encapsulation efficiency (EE). 37

5.3 Research output

1. **E. Baghdan**, M. Raschpichler, W. Lutfi, S.R. Pinnapireddy, M. Pourasghar, B.S. Seitz, J. Schäfer, M. Schneider, U. Bakowsky, Antibacterial coating and surface modification of dental implants using nano spray drying. *Manuscript in preparation*
   Equally contributing author

2. **E. Baghdan**, L. Duse, J.J. Schüer, S.R. Pinnapireddy, M. Pourasghar, J. Schäfer, M. Schneider, U. Bakowsky, Development of an inhalable curcumin loaded Nano-in-Microparticles for bronchoscopic photodynamic therapy. *Submitted Manuscript*

3. **E. Baghdan**, S.R. Pinnapireddy, H. Vögeling, J. Schäfer, A.W. Eckert, U. Bakowsky, Nano spray drying: A novel technique to prepare well-defined surface coatings for medical implants, Journal of Drug Delivery Science and Technology, (2018).

4. **E. Baghdan**, S.R. Pinnapireddy, B. Strehlow, K.H. Engelhardt, J. Schäfer, U. Bakowsky, Lipid coated chitosan-DNA nanoparticles for enhanced gene delivery, International Journal of Pharmaceutics, 535 (2018) 473-479.
   Equally contributing author

5. L. Duse, **E. Baghdan**, S.R. Pinnapireddy, K.H. Engelhardt, J. Jedelská, J. Schaefer, P. Quendt, U. Bakowsky, Preparation and Characterization of Curcumin Loaded Chitosan Nanoparticles for Photodynamic Therapy, physica status solidi (a), 215 (2017) 1700709.
   Equally contributing author

6. K.H. Engelhardt, S.R. Pinnapireddy, **E. Baghdan**, J. Jedelská , U. Bakowsky, Transfection Studies with Colloidal Systems Containing Highly Purified Bipolar Tetraether Lipids from Sulfolobus acidocaldarius, Archaea, 2017 (2017) 12.

5.4 Presentations

5.4.1 Oral presentations

07/2016	**Novel drug delivery systems based on biodegradable nanoparticles and liposomes** Evonik Nutrition & Care GmbH, Darmstadt, Germany

5.4.2 Poster presentations

03/2018	**Nano-Sprühtrocknung: Neuartige Methode zur Beschichtung von medizinischen Implantaten** 13. Thementage Grenz- und Oberflächentechnik & 11. Biomaterial-Kolloquium, Zeulenroda, Germany
03/2018	**Nano spray drying: a novel technique to prepare well-defined surface coatings for medical implants** CRS Germany Local Chapter 2018, Halle, Germany
08/2017	**Preparation and characterization of curcumin loaded chitosan nanoparticles for photodynamic therapy** Engineering of functional interfaces - EnFI 2017, Marburg, Germany
03/2017	**Preparation and characterization of curcumin loaded Nano-in-Micro particles** CRS Germany Local Chapter 2017, Marburg, Germany

5.5 Awards

06/2013 – 11/2017	**Academic scholarship** Brot für die Welt – Evangelischer Entwicklungsdienst
03/2018	**Best poster award** 11. Biomaterial-Kolloquium, Zeulenroda, Germany

5.6 Curriculum Vitae

PERSONAL DETAILS

Name	Elias Baghdan
Date of birth	30.01.1988
Place of birth	Damascus, Syria
Marital status	Married (1 child)
Nationality	Syrian

EDUCATION AND WORK EXPERIENCE

04/2013 – Present	**PhD student** Philipps-Universität Marburg, Department of pharmaceutics and biopharmaceutics Marburg, Germany
10/2010 – 08/2012	**Graduate teaching assistant** Syrian international private university for science and technology Damascus, Syria
10/2005 – 06/2010	**Bachelor of pharmacy** Syrian international private university for science and technology Damascus, Syria
09/2002 – 06/2005	**Secondary education** Alassyea private school Damascus, Syria

5.7 Danksagung

Die Entstehung dieser Arbeit wäre ohne eine Vielzahl von Personen, die mich während meiner Promotionszeit begleitet haben, nicht möglich gewesen.

Mein besonderer Dank gilt meinem Doktorvater Prof. Dr. Udo Bakowsky für die hervorragende Betreuung und die zahlreichen konstruktiven Diskussionen, welche mich immer wieder auf ein Neues motivierten und neue Ideen entstehen ließen. Ich hätte mir keinen besseren Mentor für diesen Lebensabschnitt wünschen können. Ich danke dir von Herzen.

Weiterhin danke ich Prof. Dr. Frank Runkel für die Erstellung des Zweitgutachtens, Prof. Dr. Maike Petersen für die Leitung der Prüfungskommission und Prof. Dr. Cornelius Krasel für die Begutachtung meiner Dissertation als Nebenfachprüfer.

Der Organisation Brot für die Welt bin ich zum einen für die finanzielle Unterstützung in Form eines Promotionsstipendiums und zum andern für die vielen schönen Erfahrungen im Rahmen vielfältiger Veranstaltungen zu besonderem Dank verpflichtet. Insbesondere möchte ich hierbei Nadine Ebinghaus, Christin Goldschmidt, Fanny Kamptz, Ulrike Küstner, Andrea Mögle, Kathleen Schneider Murandu, Carolin Rölle, Susanne Werner und Florence Zeller erwähnen.

Ich danke der Evangelischen Kirche von Kurhessen-Waldeck, vor allem Dr. Ruth Gütter, Bischof Prof. Dr. Martin Hein, Petra Hilger, Schwester Renate Lippe und Dr. Martin Lückhoff, dass sie mir bei den Schwierigkeiten, die nach meiner Ankunft in Marburg auf mich zu kamen, geholfen haben. Außerdem haben sie wesentlich dazu beigetragen, dass ich mich für das Stipendium bei Brot für die Welt beworben und dadurch diese einzigartige Chance genutzt habe.

Ein großer Dank gilt auch meinem Betreuer Dr. Jens Schäfer, der mir während meiner gesamten Promotionszeit stets mit Rat und Tat zur Seite stand.

Dr. Jana Brüßler und Dr. Jarmila Jedelská danke ich für die administrative Unterstützung und ständige Hilfsbereitschaft.

Ich danke meinen Kollegen aus dem Arbeitskreis Bakowsky herzlich für ihre Hilfe und Unterstützung, besonders Michael Agel für die zahlreichen wissenschaftlichen Diskussionen und seine nützlichen Ratschläge, Thomas Breunig für die Zusammenarbeit während seines Pharmaziepraktikums, Dr. Eyas Dayyoub für seine freundliche Einführung in den Arbeitskreis, Lili Duse für die Zellkultur- und Hämokompatibilitätsversuche sowie für ihre ständige Hilfsbereitschaft und Geduld, Dr. Konrad Engelhardt für die Durchführung rasterkraftmikroskopischer Untersuchungen und die lustige, gemeinsame Zeit am alten Institut, Nathalie Goergen für die Versuche an der Chorioallantoismembran, Jennifer

Lehmann für die nette Zusammenarbeit im Praktikum, Eva Mohr für die Bereitstellung und Pflege der Zelllinien, Dr. Shashank Reddy Pinnapireddy für das Korrekturlesen meiner Publikationen und das Erstellen von Bildern mit dem Rasterelektronen- und dem Konfokalmikroskop, Eduard Preis für die Unterstützung bei der Auswertung der Freisetzungsversuche wie auch für das Korrekturlesen der deutschen Fassung dieser Arbeit, Michael Raschpichler für die mikrobiologischen Untersuchungen und die enge, freundschaftliche Zusammenarbeit, Julia Schüer für die Experimente mit der Filmwaage, Benjamin Seitz für seine Bemühungen am Rasterkraftmikroskop, Boris Strehlow für die Einweisung in das Fachgebiet der Sprühtrocknung, des Next Generation Impactors und der Rasterelektronenmikroskopie, Hendrik Vögeling für die Hilfe bei der Vorbereitung der Titanplättchen. Sascha Hubing, Nikola Plenagl und Dr. Matthias Wojcik danke ich ebenfalls für die tolle Zusammenarbeit und die stets freundliche und angenehme Atmosphäre im Büro.

Bei Susanne Lüttebrandt, Julia Michaelis und Doris Reißenweber bleibt mir lediglich zu sagen: Ihr seid die Besten. Ihr tragt wesentlich dazu bei, dass an unserem Institut vieles so reibungslos funktioniert und habt stets ein offenes Ohr für die verschiedensten Belange. Vielen herzlichen Dank.

Ich danke Prof. Dr. Cornelia M. Keck sowie ihren Mitarbeitern für die nette Zeit am Institut.

Außerdem bedanke ich mich bei Prof. Dr. Marc Schneider vom Institut für Biopharmazie und Pharmazeutische Technologie der Universität des Saarlandes für die gute und konstruktive Kooperation, sowie besonders seinen Mitarbeitern Aljoscha Könneke für die Unterstützung bei der Datenanalyse der Experimente mit dem Next Generation Impactor und Marcel Pourasghar für das Erstellen von Bildern mittels der Rasterelektronenmikroskopie und der Korrelative Licht- und Elektronenmikroskopie.

Des Weiteren danke ich Michael Hellwig vom wissenschaftlichen Zentrum für Materialwissenschaften der Philipps-Universität Marburg für seine technische Unterstützung bei der Rasterelektronenmikroskopie.

Ich bedanke mich herzlich bei Dr. Marco Kleine sowie Dr. Gabriele Wendt von der Büchi Labortechnik AG sowohl für die wissenschaftlichen Diskussionen als auch für die technische Unterstützung bei der Sprühtrocknung.

Abschließend möchte ich mich von tiefstem Herzen bei meinen Eltern bedanken, ohne deren Unterstützung und Motivation ich nicht dort angelangt wäre, wo ich heute stehe. Meiner Liebe, Walaa Lutfi, danke ich, dass du immer für mich da bist, sowohl bei der gemeinsamen Arbeit im Labor als auch an meiner Seite im alltäglichen Leben. Danke, dass es dich und Elena gibt. Danke, dass ihr jeden Tag aufs Neue mein Leben bereichert.